

III

BETA-RAY SPECTROMETER THEORY AND DESIGN, MAGNETIC ALPHA-RAY SPECTROSCOPY, HIGH RESOLUTION SPECTROSCOPY

K. SIEGBAHN

§ 1. Introduction. General discussion of spectrometers

Parallel to the experimental work on the study of nuclear decay schemes and other problems in nuclear spectroscopy, continuous work has been devoted to the perfection of the spectroscopic instruments. Much of the earlier experimental investigations could be performed with rather simple and sometimes even crude techniques but such cases are becoming increasingly rare. The remaining problems generally require very advanced and differentiated techniques. A great number of various approaches to the design of spectrometers have been suggested and tried out. In this chapter we will present most of these ideas. but it will become evident that not all of them have turned out to be equally useful. During the past years a few types of instruments have gradually proved to have special advantages and have therefore been more extensively developed and come into greater use. In spite of this, some of the less used types of arrangements might in special cases have very attractive properties and it is still hard to exclude the possibility of unexpected future developments.

In other chapters of this book the application of a number of energy or momentum resolving devices, in which the *ionisation* property of nuclear radiation in matter is utilized in different ways, is discussed in detail. Generally, such spectrometers simultaneously act as particle detectors. They frequently have high efficiencies and they can conveniently be incorporated into electronic arrangements of different kinds, such as coincidence circuits. Still, it is increasingly evident that magnetic (or electric) fields of various shapes combined with suitable particle detectors can resolve complex nuclear spectra of particles or quanta (as secondary produced particles) in considerably more detail and in a more clear-cut way. High resolution crystal diffraction γ -spectrometry (Chapter IV) is a field with great potentialities for the study of γ -radiation, but even here one usually has to supplement the data with magnetic studies of the corresponding electron spectra in order to reach decisive conclusions as to the properties of the nuclear levels. Also in the field of *coincidence* spectroscopy one can achieve the most powerful devices regarding energy and time resolution by combining magnetic spectrometers with suitable detectors. Considering the energy resolution alone it is furthermore shown that some magnetic spectrometers under favourable source conditions can reach the limits set by the inherent widths of atomic levels (see § 11 and Chapter XVIIIB). In view of these circumstances,

spectrometers are the basic instruments in nuclear spectroscopy and therefore deserve some special emphasis.

Broadly speaking, the problem in -spectrometr theory and design is twofold: to collect as much as possible of the nuclear radiation into the spectrometer and to attain a maximum of energy resolution. Since all electron-optical systems possess aberrations, e.g. spherical, it is evident that one cannot find an instrument which is perfect in both respects. The problem is still more complicated since one has to take into account a great number of other important features such as the maximum size of the emitting source, the problem of designing and shielding the detector in order to get low background, the practical difficulties of realizing a particular fieldform and of measuring the field, the power consumption and the cooling problem, the economical and workshop aspects of the construction, the flexibility of the instrument, the problem of accurate adjustments, etc. It is also important to consider what type of detector can be used with a particular instrument, e.g. a photographic plate, a GM counter of small size with a very thin window, a scintillation counter, an array of semiconductor detectors, etc. It may also be interesting to know whether a certain focusing principle permits ironfree construction, or if permanent magnets can be used. Some types of spectrometer can be handled conveniently only in the low energy range (this is generally true for electrical spectrometers), and other types may be impracticable or even unreliable for high precision work in the low energy region (certain magnetic spectrometers of shaped field, containing iron). Some focusing principles which mathematically would give excellent properties as to collecting power and resolution may not be suitable.

Besides the two main characteristics of a spectrometer, namely collecting power and resolution, there are a number of other features which determine the potentialities of a particular spectrometer type. Several of these are very difficult or even impossible to formulate in mathematical language, and it is therefore understandable that one cannot select a certain spectrometer as being superior to any other type because of a more advantageous 'figure of merit' based upon purely theoretical considerations. Nevertheless, such considerations have proved to be useful and, though not always decisive in the choice of a certain spectrometer type, they certainly are of importance in a number of cases.

The large variety of spectrometers may, for convenience, be classified into magnetic and electric spectrometers, the first group being by far in greater use. According to accepted nomenclature one further distinguishes between flat and helical spectrometers in the first group. By a 'flat' spectrometer one means one in which the magnetic lines of force are mainly in the direction perpendicular to the electron paths, whereas 'helical' stands for all types of lens fields, i.e. where the lines of force are mainly in the direction of the electron paths.

The two basic types of focusing are those obtained by means of a homogeneous field which is either perpendicular to the rays, in which case the electrons describe circles, or nearly parallel to the rays, when they describe helical paths. These two extreme cases are quite simple to treat theoretically and the focusing properties can

generally be given in exact and simple forms. Historically these two types of focusing were also the first to be developed, and in particular the first mentioned type was, except for a few preliminary trials of the helical method, the only one in use before the beginning of the forties. All work on classical radioactivity was consequently made with homogeneous flat spectrometers. It is particularly illuminating to study the electron image formation in these two special cases, since many of the basic features found there are qualitatively in common with more complicated types of focusing.

The transverse homogeneous field focuses electrons in only one plane, whereas the longitudinal field is space-focusing. From this point of view the two focusing systems would correspond in optics to cylindrical and spherical lenses, respectively. By shaping the transverse field so as to vary as $1/\sqrt{\rho}$, ρ being the distance to the axis of symmetry, the transverse field also becomes space-focusing. This so-called 'double focusing' spectrometer yields an extraordinarily good theoretical figure of merit and is furthermore relatively easy to construct, both with and without iron, and to adjust to very high resolutions. The collecting power can be made very high and the source and detection problems are easy to master. The double focusing spectrometer has therefore come into wide use.

The electron-optical spherical aberrations of both flat and helical spectrometers can be reduced by shaping the fields in different ways. The collecting power can be increased for flat spectrometers by using sector magnets, i.e. having the source and detector outside the field. One then introduces one more degree of freedom into the electron-optical system by shaping the boundaries of the magnetic pole pieces to accept more radiation. Several such sector magnets can be used simultaneously in order to further increase the collecting power. In particular, the so called 'orange' spectrometer should be mentioned in this connection, the collecting power of which is very high. The properties of lens spectrometers with or without shaped fields can be improved by using suitably placed ring focus baffles.

The electron-optical image formation can generally be described analytically by means of expressions containing terms that are functions of source dimensions and 'opening angles' φ and ψ . If the width of the image is proportional to φ there is no focusing, if it is proportional to the second power, the device is 'first-order' focusing and if it is proportional to the fourth power, there is 'third-order' focusing, etc. The double focusing spectrometer, for instance, can be made first-order focusing in φ and third-order focusing in ψ .

In the following paragraphs of this chapter the various types of spectrometers will be presented and the fundamental theoretical problems discussed. There exist some previous survey articles in this field¹⁻¹⁰. For work prior to 1940 the reader is referred to books by Philipp¹¹ and by Rutherford *et al.*¹²

¹ E. Persico and C. Geoffrion, Rev. Sci. Instr. 21 (1950) 945.

² P. Grivet J. Phys. Radium 11 (1950) 582; 12 (1952) 1.

³ P. Cavanagh, Progress in Nuclear Physics 1 (London, 1950) 140.

⁴ N. F. Verster, Progress in Nuclear Physics 1 (London, 1952) 1.

⁵ R. Hayward, Advance in Electronics 5 (New York, 1953) 97.

§ 2. Some basic relations in & spectroscopy

An electron (charge e , velocity v) moving in a homogeneous magnetic field B in a plane perpendicular to the lines of force describes a circular path with a radius of curvature ρ . The motion is given by the equation:

$$Bev = \frac{mv^2}{\rho} \quad (1)$$

where $m = m_0/\sqrt{1 - (v^2/c^2)}$. The momentum is:

$$p = mv = eB \quad (2)$$

In B-ray spectroscopy it has been found convenient to express the momentum of an electron by means of its B -value, since this value immediately will tell what magnitude of magnetic field and apparatus dimensions are required to handle the electrons in a given experiment. The use of coordinates of momentum instead of energy in γ -ray spectroscopy is partly due to the simple fact that it is the momentum of the focused electrons that is proportional to the magnetic field of the spectrometer or (approximately, if iron is used) to the exciting electric current, and not the energy. For electrostatic spectrometers, however, the situation is different, as the energy of the electron is proportional to the deflecting voltage, but since such spectrometers are fairly uncommon, the BP-coordinates have been generally accepted.

Suppose that we investigate a distribution of electrons in a magnetic spectrometer, the momentum distribution being $N(p)dp$. If instead we wish to plot the spectrum as an energy distribution $n(E)dE$, it is obvious that the widths dE and dp are different, which will influence the form of the spectrum. Since $E = p^2/2m$ we get $dE = (p/m)dp$ and consequently, using E instead of p as abscissa axis, the corresponding intensities in the momentum distribution should be multiplied by m/p .

In a magnetic spectrometer with fixed geometry and variable B the quantity $R = (B)/B$ is constant, where (B) is a measure of the accepted momentum band. When plotting the momentum distribution it is therefore necessary to divide the number of counts P at each magnetic field setting by the corresponding field in order to get the correct form of the spectrum. Table 1 summarizes¹³ how the number of

⁶ K. Siegbahn, Beta- and Gamma-Ray Spectroscopy (North-Holl. Publ. Co., Amsterdam, 1955) p. 52.

⁷ T. R. Gerholm, Handbuch der Physik 33 (ed. S. Flugge; Springer-Verlag, Berlin, 1956) p. 609.

⁸ M. Deutsch and O. Kofoed-Hansen, Experimental Nuclear Physics 3 (ed. E. Segré; J. Wiley & Sons, New York, 1959) p. 427.

⁹ M. Mladjenovic, Nucl. Instr. and Methods 7 (1960) 11.

¹⁰ C. S. Wu and C. Geffron, Nuclear Spectroscopy A (ed. F. Ajzenberg-Selove; Academic Press, New York, 1960) p. 70.

¹¹ K. Philipp, Kernspektren, Hand- und Jahrbuch der Chemischen Physik 9 (Leipzig, 1937) p. 186.

¹² E. Rutherford, J. Chadwick and C. D. Ellis, Radiations from Radioactive Substances (Cambridge, 1930).

¹³ Quoted from: O. Klemperer, Electron Optics (Cambridge University Press,

TABLE I

	<i>Magnetic spectrometer</i>	<i>Electric spectrometer</i>
	<i>B = const.</i>	<i>B = variable</i>
<i>Values measured directly</i>		
Abscissa	Radius	Magnetic field <i>B</i>
Ordinate	Number of counts <i>P</i>	Number of counts <i>P</i>
<i>Plotted as momentum distr. curve:</i>		
Abscissa	ρ	B
Ordinate	P	P/B
<i>Plotted as energy distr. curve:</i>		
Abscissa	ρ^2	B^2
Ordinate	P/ρ	P/B^2
		Voltage V
		Number of counts P
		\sqrt{V}
		P/\sqrt{V}
		V
		P/V

counts *P* should be handled in the case of a magnetic spectrometer of constant field or constant radius and also for a transverse electric field spectrometer. Both momentum and energy spectra are considered.

Conversion lines having *B*-values extending from ≈ 1000 to 3000 are particularly easy to observe. 50 keV corresponds to *B* ≈ 800 and 500 keV to *B* ≈ 3000 . The relation between momentum and energy *E* is obtained by combining (2) with

$$E = mc^2 - m_0c^2 \quad (3)$$

which yields

$$E = \{(m_0c^2)^2 + e^2c^2(B\rho)^2\}^{1/2} - m_0c^2. \quad (4)$$

If we express *E* in keV and *B* in gauss · cm we get (using DuMond and Cohen's 1955 adjusted values of elementary constants¹⁴; see Appendix 2) very accurately:

$$E(\text{keV}) = (510.976 \pm 0.007) \{[3442.2 \pm 0.1] \times 10^{-10}(B\rho)^2 + 1\}^{1/2} - 1 \quad (5)$$

where 510.976 is the rest mass energy of the electron expressed in keV. If we denote this quantity by μ we can also write down another useful relationship, namely that between the fractional changes of energy and momentum:

$$\frac{\Delta E}{E} = \left(1 + \frac{\mu}{\mu + E}\right) \frac{\Delta(B\rho)}{B\rho}. \quad (6)$$

This equation may be used when an accurate interpolation in *E-B* tables (see Appen-

¹⁴ E. R. Cohen, J. W. M. DuMond, T. W. Layton and J. S. Rollett, Rev. Mod. Phys. 27 (1955) 363.

dix 2) is needed. Furthermore, since the resolution R of magnetic spectrometers is obtained as the relative line width on the momentum scale, i.e. $R = (B_p)/B$, eq. (6) may be used to obtain the corresponding energy resolution.

Frequently, momentum and energy are expressed in relativistic units, i.e.:

$$= \frac{p}{m_0 c} = \frac{B}{1704.43}, \quad (7)$$

$$\epsilon = \frac{E}{m_0 c^2} = \frac{E}{510.976}. \quad (8)$$

If we consider the rest mass energy also, we then have the simple relationship:

$$\epsilon^2 = \eta^2 + 1. \quad (9)$$

The relation between E (in keV) and B_p (in gauss · cm) according to (5) is given in the diagram of Fig. 1 (for more accurate work, see Appendix 2). Inserted in Fig. 1 is the relation between $\beta = v/c$ and E (in keV) for electrons. One can notice that already at 100 keV the electron velocity is one-half that of light. For α -particles at 5 MeV, β is only 0.05. The high β -values of electrons in radioactive radiations intro-

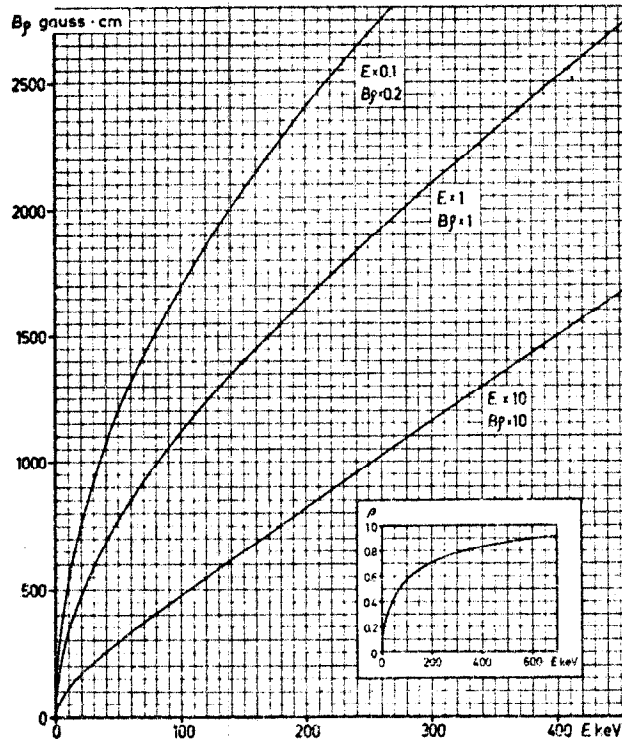


Fig. 1. The relation between E and B_p for electrons. Inserted: $\beta = v/c$ as a function of E .

duce a great complication in the design of electrostatic spectrometers because of changing focusing properties due to the relativistic effects (see § 10).

Fig. 2 shows the relation (6) between the energy and momentum resolution.

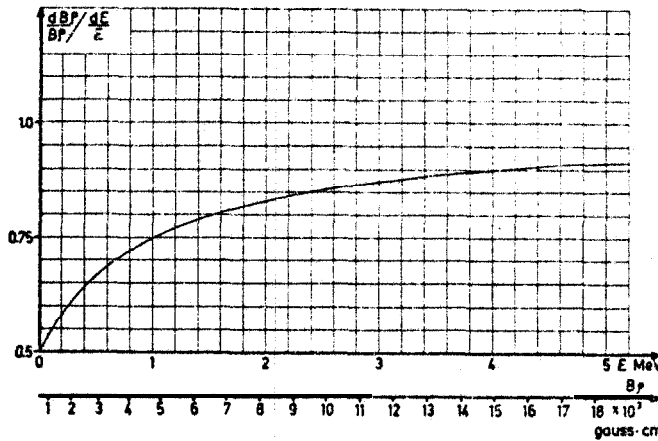


Fig. 2. Relation between energy and momentum resolution according to eq. (6).

§ 3. Nomenclature

In the following theoretical treatment we need a few definitions of some basic concepts.

A radioactive source generally consists of a number of radioactive atoms distributed in a much larger quantity of inactive material, for instance the carrier used in the radiochemical procedure. The number of electrons leaving the source per unit time divided by the weight of the inactive source material is a measure of the *specific activity* of the source (expressed as mCur/g). In many cases it is this quantity that sets the ultimate limit on the obtainable energy resolution, rather than the spectrometer data themselves. The *total* available activity is usually not of the same importance as the specific activity*.

In certain cases we may speak of an almost infinitely good specific activity, for instance in the case of an active deposit of Rutherfordium (i.e. Th(B+C+C'') or Ra(B+C+C'')). In such cases an electron emitted from the radioactive source leaves the source without energy straggling and an electron line may serve as a strictly monokinetic electron source (concerning the natural line widths of conversion lines: see § 11 and Chapter XVIIIB). These electrons are emitted in all directions but only a certain fraction of them will pass through the defining entrance baffles (or slits) of the spectrometer. This *solid angle* of the spectrometer is usually expressed directly in per cent of the total sphere. Some spectrometers have a solid angle of the order of 20% or even more.

Not all of the monokinetic electrons passing through the entrance slit will necessarily be counted by the detector. If the detector slit is wide enough they will be, but

* The problem of getting the source homogeneously distributed on the backing is treated in Chapter VIIA.

it may also happen that the detector is adjusted to only accept a certain fraction of the monokinetic electrons. The fraction of all monokinetic electrons leaving the source which is actually counted *in the detector* we may call the spectrometer *transmission* T .

Due to the spherical aberration of the system (and other possible image errors) the electron line, when registered in the spectrometer, will appear as a line of a certain width $\Delta(B\rho)$. For convenience $\Delta(B\rho)$ refers to the full width at half the height of the line ('half width'). This entity is experimentally well defined, whereas theoretical calculations usually yield with better definition the width at the bottom of the line $\Delta^0(B\rho)$ ('base width'). $\Delta^0(B\rho)$ is approximately equal to $2\Delta(B\rho)$. The relative line width $R = \Delta(B\rho)/B\rho$ is a constant for a spectrometer with fixed geometry of the rays. R is often a good measure of the *resolution* or resolving power and is usually given in per cent. The best resolution so far obtained in β -ray spectroscopy is $\approx 0.01\%$. For most high transmission spectrometers the resolution is around 1% or worse.

If the electron-optical image formation results in very asymmetrically shaped lines, having a steep edge at one side, the resolving power towards *that* side may be appreciably better than indicated by the half width. The so called Hubert baffle for magnetic lenses yields asymmetric lines with a steep edge at the low energy side (see § 8) and the semicircular focusing for narrow sources gives steep edges at the *high* energy side (see next §).

The ratio between the transmission T and the resolving power R (for many spectrometers ≈ 1) is generally a good measure of the electron-optical quality of a spectrometer. Since this quantity does not take into account the ability of the spectrometer to handle extended sources, which is of importance as soon as the specific activity is not infinitely good, a better figure of merit of a spectrometer is to substitute in place of the transmission in the above ratio the '*luminosity*' A defined as $A = Q\sigma$, where σ is the source area. The luminosity is expressed in cm^2 . The so called '*over-all luminosity*' L is correspondingly defined as $L = T\sigma$.

Strictly speaking one would need still another quantity expressing the *information* which is actually afforded by a certain instrument. A multigap instrument or a ring-focus lens may have a large solid angle compared to a semicircular instrument or another 'flat' instrument. The former types however, do not possess a *focal plane* which can be used for either a photographic or a multidetector system (which can be connected to a multichannel storage unit). It is difficult to numerically evaluate the figure of merit connected with the existence of a focal plane. If one disregards the possibilities of photographic recording and considers only electrical counting, a reasonable factor with which to multiply the luminosity in order to obtain a better measure of the information, I , would be the number n of detectors which can be used together in the focal plane. We thus have $Z = nL$. Since the number n for some instruments such as the semicircular or the double focusing type may be quite high (for instance 100) the above discussion shows how the figures of merit can change quite drastically if properties other than transmission, resolution and source size are considered.

A further quantity, which is closely connected to the resolution and the

dimensions of the spectrometer and the source, is the dispersion γ . It gives the change in position of the electron-optical image if the $B\rho$ of the electrons is slightly changed, i.e. $\gamma = dx/d(B\rho)$. It is found for instance (see § 5) that the double focusing spectrometer has twice the dispersion of the homogeneous field spectrometer, which means that sources which are twice as wide can be used if the resolution and dimensions of the instruments are the same. The dispersion can also be defined in slightly different ways, and some of these will be used in the following theoretical treatments.

S4. The semicircular spectrometer

In 1910 the first determinations of the energies of β -particles by their deflection in a magnetic field were carried out by von Baeyer and Hahn¹⁵. They employed the so called 'direct deflection method'. β -rays emitted from a radioactive wire were allowed to pass through a narrow slit and then, after an arbitrarily chosen distance, recorded on a photographic plate placed with its surface facing the wire and the slit. The deflecting magnetic field was perpendicular to the rays. With the aid of this simple arrangement von Baeyer et al.¹⁶ discovered the occurrence of definite lines in the energy spectrum of P-radiation. However, the transmission and resolving power were very poor, since the rays were not focused. The first magnetic focusing device is due to Danysz¹⁷ who in 1912 suggested the so-called semicircular focusing principle, which still is of great use in β -ray spectroscopy.

Let us consider a point source which is emitting monochromatic electrons (e.g. a conversion line) in all directions. We investigate¹⁸ the electron paths in a plane perpendicular to an applied magnetic field (See Fig. 3.) A defining slit selects a diverging pencil of electrons, all having the same radius of curvature ρ . It is easily seen that the pencil after half a revolution will reach a minimum width. The focusing is not perfect, i.e. there is a certain spherical aberration causing a finite width Δx of

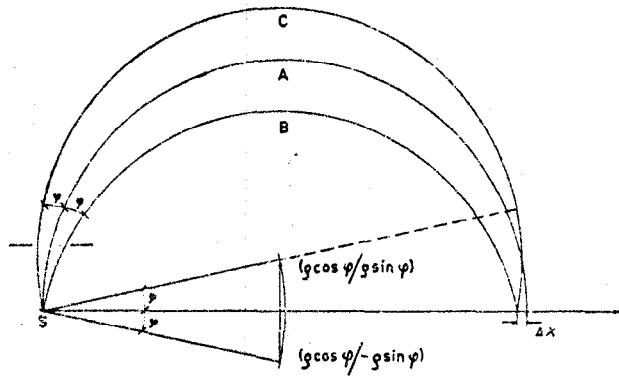


Fig. 3. The semicircular focusing principle.

¹⁵ O. V. Raeuer and O. Hahn, Phys. Zeitschr., 11 (1910) 488.

¹⁶ O. V. Baeyer, O. Hahn and L. Meitner, Phys. Zeitschr. 12 (1911) 373, 378; 13 (1912) 264.

¹⁷ J. Danysz, Le Radium 9 (1912) 1: 10 (1913) 4.

¹⁸ K. Siegbahn, Ark. f. Mat. Astr. Fys. 30A (1944) No. 20.

the image. From the figure we notice that $x = 2\rho - 2\rho \cos \varphi$, 2ρ being the aperture. If we had started with a source the width of which was S , the full image width would be

$$x = s + 2\rho(1 - \cos \varphi). \quad (10)$$

From this expression we obtain the relative line width, e.g. the base resolving power R^0 , considering that $x = 42\rho$ and that φ is small:

$$R^0 = \frac{4\rho}{\rho} = \frac{s}{2\rho} + \frac{\varphi^2}{2}. \quad (11)$$

The resolving power is thus made up of two terms, the first of which is dependent upon the width of the source and the radius of curvature, and the second upon the angular aperture. Only for infinitely thin sources is the resolving power independent of the spectrometer size. For sources that have a certain specific activity and consequently must have a certain width, the first term by necessity contributes to the resolving power. For *optimum conditions* the two terms should give about equal contributions to the resolving power, which yields the condition:

$$\varphi = \sqrt{(s/\rho)}. \quad (12)$$

So far we have only discussed the total width of the line at the base. It is very instructive to study the intensity distribution within the line profile. The intensity at each point on the plate, situated along the x-axis, is proportional to the number of particles per unit area that strike the plate. We first study the intensity distribution from a point source. We may then write:

$$I \propto \frac{d\varphi}{dx}. \quad (13)$$

Since $x = 2\rho \cos \varphi$ we obtain

$$I \propto \frac{1}{2\rho \sin \varphi} \propto \frac{1}{\sqrt{(4\rho^2 - x^2)}}. \quad (14)$$

As a new variable we introduce the distance from the 'edge' $z = 2\rho - x$. We are only interested in the intensity distribution near the edge where $p \gg z$. We thus get

$$I \propto \frac{1}{\sqrt{z}} \quad (15)$$

which is the intensity distribution from a point source. It should be observed that the curve shows points of discontinuity at $z = 0$ and $z = 2\rho(1 - \cos \varphi)$.

If we now consider the case where the source has a width s , we must integrate over the source, i.e.

$$I \propto \int_0^s \frac{ds}{\sqrt{z - s}}. \quad (16)$$

Because of the discontinuities the integral has to be separated into three different parts :

$$I_1 = \int_0^z \frac{ds}{\sqrt{(z-s)}} \propto \sqrt{z} \quad \text{for } 0 < z < s \quad (17a)$$

$$I_2 = \int_0^s \frac{ds}{\sqrt{(z-s)}} \propto \sqrt{z} - \sqrt{z-s} \quad \text{for } s < z < 2\rho(1 - \cos \varphi) \quad (17b)$$

$$I_3 = \int_{z-2\rho(1-\cos\varphi)}^s \frac{ds}{\sqrt{(z-s)}} \propto \sqrt{2(1-\cos\varphi)} - \sqrt{z-s} \quad \text{for } 2\rho(1-\cos\varphi) < z < 2\rho(1-\cos\varphi) + s \quad (17c)$$

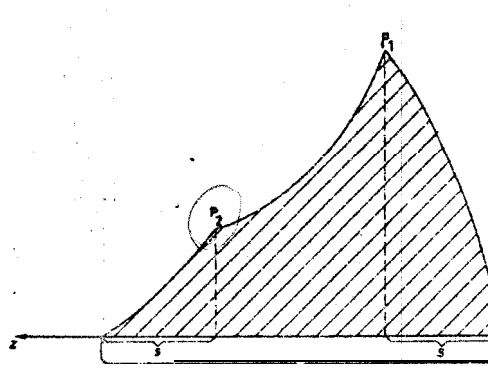


Fig. 4. Intensity distribution of a β -line.

The intensity distribution so obtained is plotted in Fig. 4. The profile of the 'line' has a sharp maximum (singular point) P_1 at $z = s$ and a further singular point P_2 at $z = 2\rho(1 - \cos \varphi)$. Obviously the edge of the line at $z = 0$ corresponds to the edge of the source nearest to the plate, whereas the top P_1 of the line corresponds to the other edge of the source. Either of these two distances corresponds to 2ρ , which is governed by the momentum of the electron for a given magnetic field B .

In the above discussion we have made some simplifying assumptions for the sake of lucidity. In practice the active wire has a certain height and in some particular cases it may not be flat but round. Actually it turns out that the essential features of the curve given in Fig. 4 are retained while the calculations are greatly complicated.^{19, 20}

¹⁹ W. Wostc., Proc. Roy. Soc. A114 (1927) 729.

²⁰ K. Li, Proc. Cambridge Phil. Soc. 33 (1937) 164.

By decreasing φ the point P_2 approaches P_1 , thus making the line sharper without affecting the intensity at P_1 , until they coincide. A further reduction of φ will result in an intensity loss at the line peak. in accordance with our previous statement optimum conditions occur, therefore, when $2s = 2\rho(1 - \cos\varphi) + s$ i.e. $\varphi = \sqrt{(s/\rho)}$.

Let us further examine the optimum condition for the height h of the source. An electron emitted at a distance $\frac{1}{2}h$ will form an angle ψ with the medium plane if it strikes the plate at $-\frac{1}{2}h$. Its radius of curvature in the plane perpendicular to B will be $\rho \cos \psi$. The electron will then obviously strike the plate closer to the source than the central ray. The distance along x between these two points on the image will be:

$$x = 2p - 2\rho \cos \psi. \quad (18)$$

Since ψ is small we get

$$\psi = h/\pi\rho \quad (19)$$

which combined with (18) yields

$$x = h^2/\pi^2\rho. \quad (20)$$

In analogy with the foregoing, the total height of the source should not be so great that the width of the image arising from the height exceeds that governed by the width s of the source and the finite angular aperture φ , i.e.

$$h^2/\pi^2\rho \leq s. \quad (21)$$

As the optimum condition we thus get

$$h \leq \pi\sqrt{s\rho}. \quad (22)$$

In many practical cases h has to be made shorter than that given by (22).

If the field B is changed and the line is registered by means of a detector, the slit of which is w , the line becomes correspondingly broader. We may then write down the complete expression for the base resolving power (which is about twice the experimentally defined relative half-width, see § 3)

$$R^0 = \frac{1}{2}\rho^{-1} \{s + w + \rho(\varphi^2 + \psi^2)\}. \quad (23)$$

The dispersion is

$$\gamma = 2/B. \quad (24)$$

The solid angle is given by

$$\Omega = \varphi\psi/2\pi \quad (25)$$

and the luminosity by

$$A = sh \frac{\varphi\psi}{2\pi}. \quad (26)$$

For an *approximate* treatment of the optimum conditions we may put the different contributions to the line width equal in (23) and obtain $R^0 \approx 2\varphi^2$. The solid angle is then

$$\Omega \approx R^0/4\pi. \quad (27)$$

The transmission T cannot be given without more elaborate calculations taking into consideration the exact form of the image. A very reasonable assumption is, however, that T is approximately equal to $\frac{1}{2}\Omega$ and that the relative half width R of the Dine is approximately $\frac{1}{2}R^0$. Then $T \approx 0.1 R$.

Geoffrion²¹ has made a more detailed study of the optimum conditions when a very long source and a correspondingly sized GM counter slit are used with fixed geometry. The conditions are:

- (i) $s = w = \frac{4}{3}\rho R$.
- (ii) The width of the diaphragm at 90° is $2\rho(\frac{2}{3})^{\frac{1}{2}}R^{\frac{1}{2}}$.
- (iii) The heights of the source, the diaphragm and GM slit arc $h = 2\pi\rho(\frac{1}{3})^{\frac{1}{2}}R^{\frac{1}{2}}$.

Under these conditions, the relation between the maximum intensity of a line I_{\max} and the resolution is:

$$I_{\max} = 0.457 K\rho^2 R^{\frac{1}{2}} \quad (29)$$

where K is the number of monoenergetic electrons emitted by the source in all directions per unit area, per unit time.

An instrument was later designed according to these conditions by Geoffrion and Giroux²². The radius of curvature was 30.5 cm. For normal operation the resolution was 0.25% at a transmission of 0.07%. The source and GM slit heights were 5 cm, and both widths 1 mm. The detector was equipped with an electrostatic accelerator allowing detection of very slow electrons down to zero energy with some transmission corrections²³.

There are two possibilities for arranging the source, the defining entrance slit, and the photographic plate. These are illustrated in Figs. 5 and 6. In the first alternative (Fig. 5), which is the more usual, the entrance slit is situated in the plane of the photo-

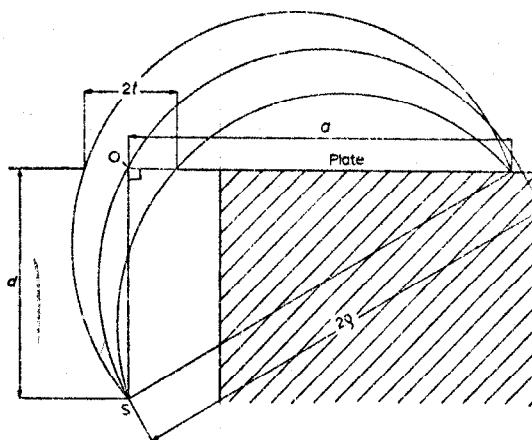


Fig. 5. Source and plate not in the same plane.

²¹ C. Geoffrion, Rev. Sci. Instr. 20 (1949) 638.

²² C. Geoffrion and G. Giroux, Can. J. Phys. 34 (1956) 920.

²³ G. Giroux and C. Geoffrion, Can. J. Phys. 34 (1956) 153.

graphic plate, the source being situated on a perpendicular to the plane of the photographic plate passing through the middle of the slit. With this mounting the ray which corresponds to the 'edge' of the line ('central' ray) will pass through O, independently of ρ . Thus the whole plate can be utilized without risking that the ray forming the sharp edge of the line will be screened off at the defining slit.

In the second alternative, shown in Fig. 6, the source is situated in the plane of the photographic plate and the slit is situated rather near the source and adjusted so that

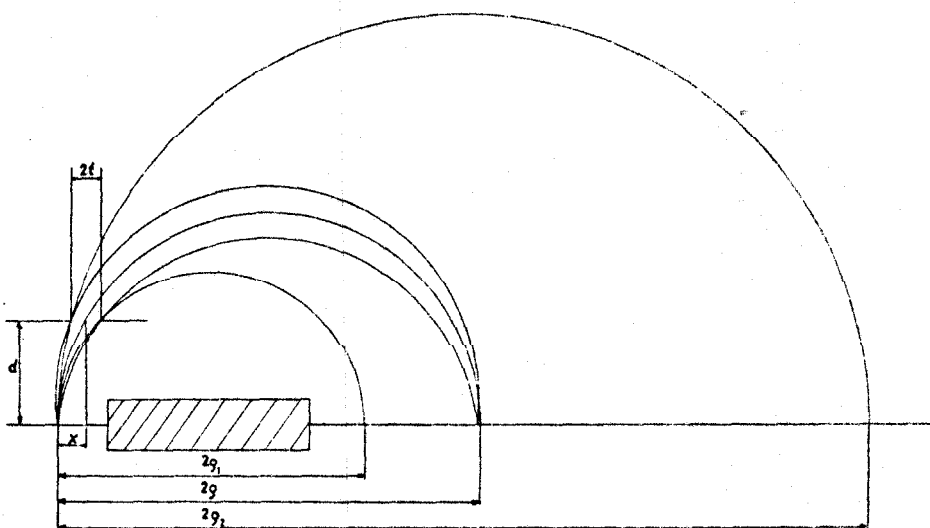


Fig. 6. Source and plate in the same plane.

the central ray for a certain value of ρ will pass through the middle of the slit. For too large or too small ρ the 'central' rays will be screened off at the defining slit. It is easy to show that this will happen when

$$\rho_1 < \frac{\rho d^2}{d^2 + 2tp}, \quad \rho_2 > \frac{\rho d^2}{d^2 - 2tp}. \quad (30)$$

If d is made small enough it is found that there is a fairly large range in ρ that can be utilized without loss of the central rays, even at high resolution. This mounting has the advantage that the values of ρ , and consequently the $B\rho$ -values of the lines, can be accurately and simply measured, since the sources as well as all the lines are situated in the same plane. Furthermore the electrons all strike the plate perpendicular to the plate surface. The more intricate problem of measuring the p -values in the mounting of Fig. 5 is amply discussed by Släts²⁴ in connection with the description of his high-resolution permanent-magnet spectrograph. In a design due to

²⁴ H. Släts, Ark. f. Fysik 6 (1953) 415; Nucl. Instr. and Methods 2 (1958) 332.

Siegbahn¹⁸, the second alternative of mounting was used. The source, slit and plate were mounted on the same holder and could be adjusted and measured in a simple way with a comparator. The magnetic field was measured by means of a flip coil in this design. In another design due to Lindstrom²⁵ the accurate proton resonance method was used for the field-measurement. GM counters in coincidence were used as a detector in order to reduce the background.

Though the semicircular method is very inferior to many other recently developed spectrometer types in regard to transmission (because of the lack of space-focusing), it has some very important advantages: (a) It is a simple and cheap instrument to build; (b) The magnetic field can easily be measured with great accuracy; (c) It is particularly well suited to photographic registering of a large part of the spectrum. The latter is probably the most important, since the low transmission is in this way partly compensated for, because of the fact that a great number of unknown conversion lines can be surveyed simultaneously which, if the resolution is set to be high, may take a long time to do with other types of spectrometers having much higher transmissions. The photographic method is rather difficult to use, however, when accurate intensity measurements are required. One then has to convert photographic blackening into true intensity, which is a delicate problem. This has been discussed by several investigators and is treated in this book by Slatis (Chapter VII).

Some advantages of the photographic method of registering may be mentioned here, apart from the above mentioned fact that a large part of the spectrum can be simultaneously recorded. When dealing with very low activities, one can make extremely long exposures, say several weeks, in order to obtain detectable lines. As a thumb rule for the sensitivity, a line from a radioactive source emitting totally 1000 β -particles per minute within that line can be detected after one month's exposure²⁶. A ten times more sensitive method^{27,28} is to use nuclear emulsion plates (Ilford G5 or K5) and to count each electron track microscopically, although this technique is a very tedious one. The lower energy limit of detection is around 7 keV. By using 10 kV pre-, or even better post-, acceleration of the electrons (i.e. acceleration at the source or before the photographic plate, respectively) electrons down to zero energy can be recorded. Fig. 7 shows 40 keV conversion lines registered by Sevier with the track counting method**.

In Fig. 8 is given an illustrative example of photographically recorded spectra. It is the complex conversion spectrum of $Au(p(65 MeV), xn)Hg$ taken at successive intervals of time²⁹. In this investigation, performed by Mihelich and co-workers, 175 spectrograms were taken and 250 electron lines analysed. In § 11 is also reproduced the spectrum of $Th(B+C+C'')$ recorded with Slatis' high-resolution permanent-magnet spectrograph.

²⁵ G. Lindstrom, Ark. f. Fysik 4 (1951) 1.

²⁶ F. Asaro, private communication.

²⁷ 2. Kleinheinz, Z. Naturforsch. 11a (1956) 252.

²⁸ K. D. Sevier, Nucl. Instr. and Methods 22 (1963) 345: Ark. f. Fysik 25 (1963) 87.

²⁹ L. P. Gillon, K. Gopalakrishnan A. de-Shalit and J. W. Mihelich, Phys. Rev. 93 (1954) 124.

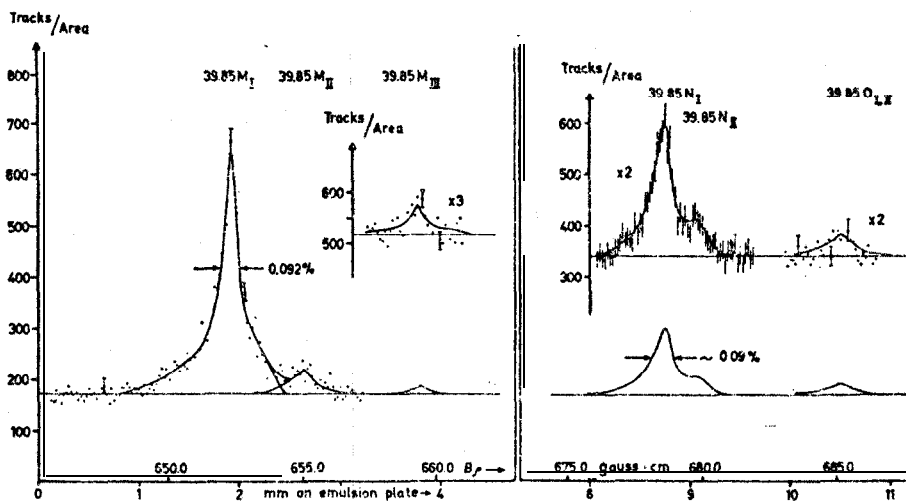
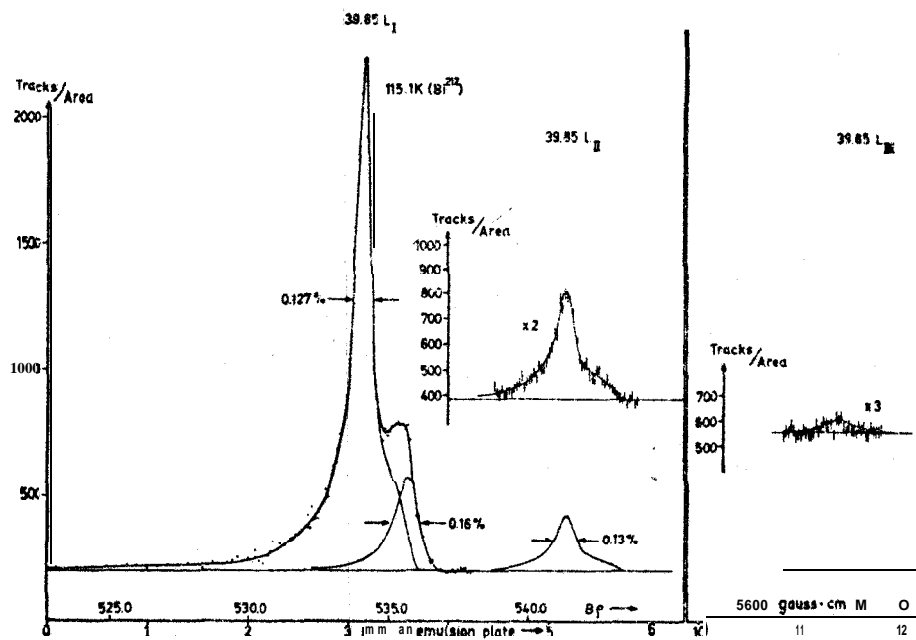


Fig. 7. The conversion lines of the 40 keV transition in Tl^{208} using the electron track counting technique (Ilford K5 emulsion) according to Sevier. The high, and to some extent the low energy tails, are caused by Doppler broadening due to u-recoil.

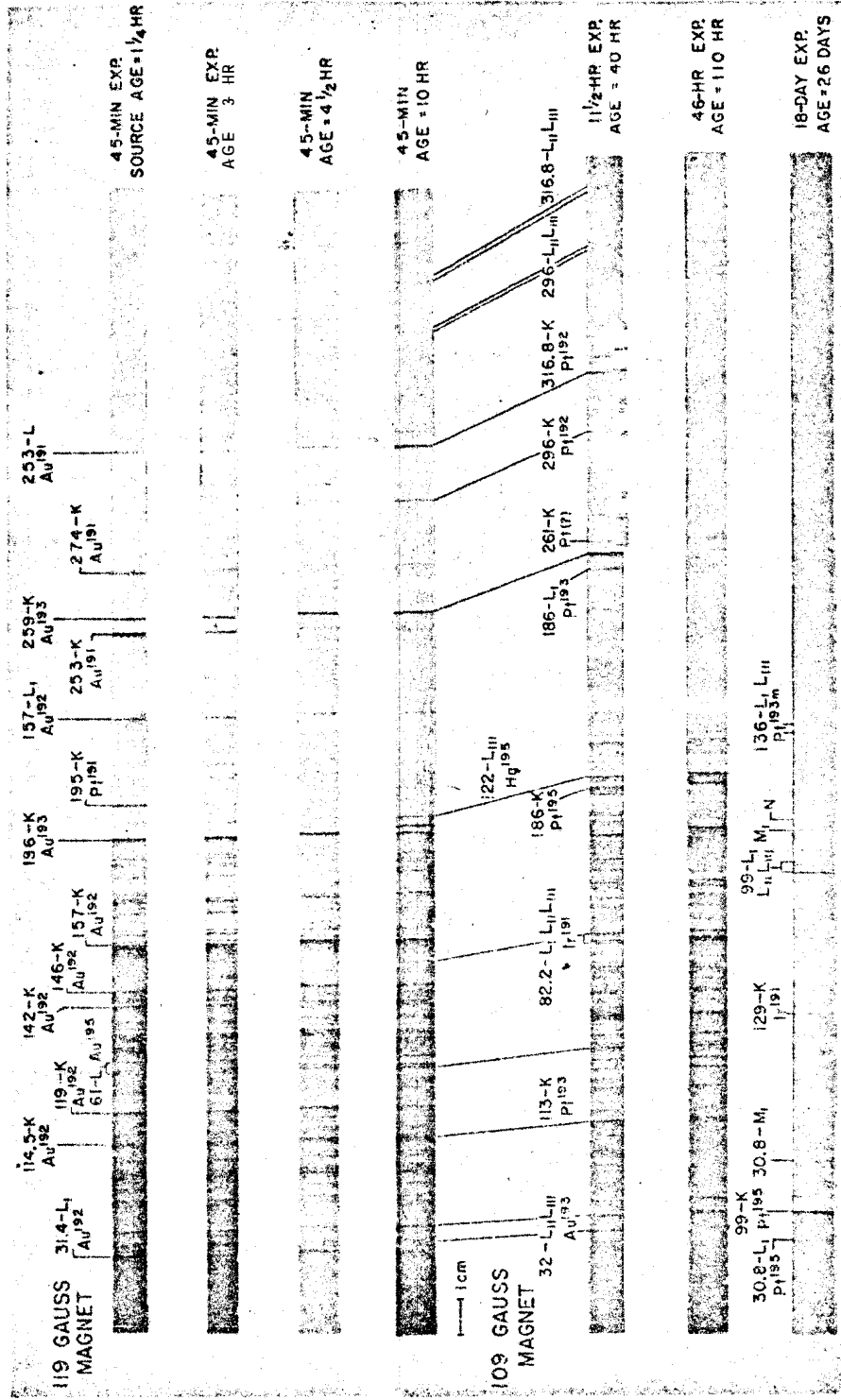
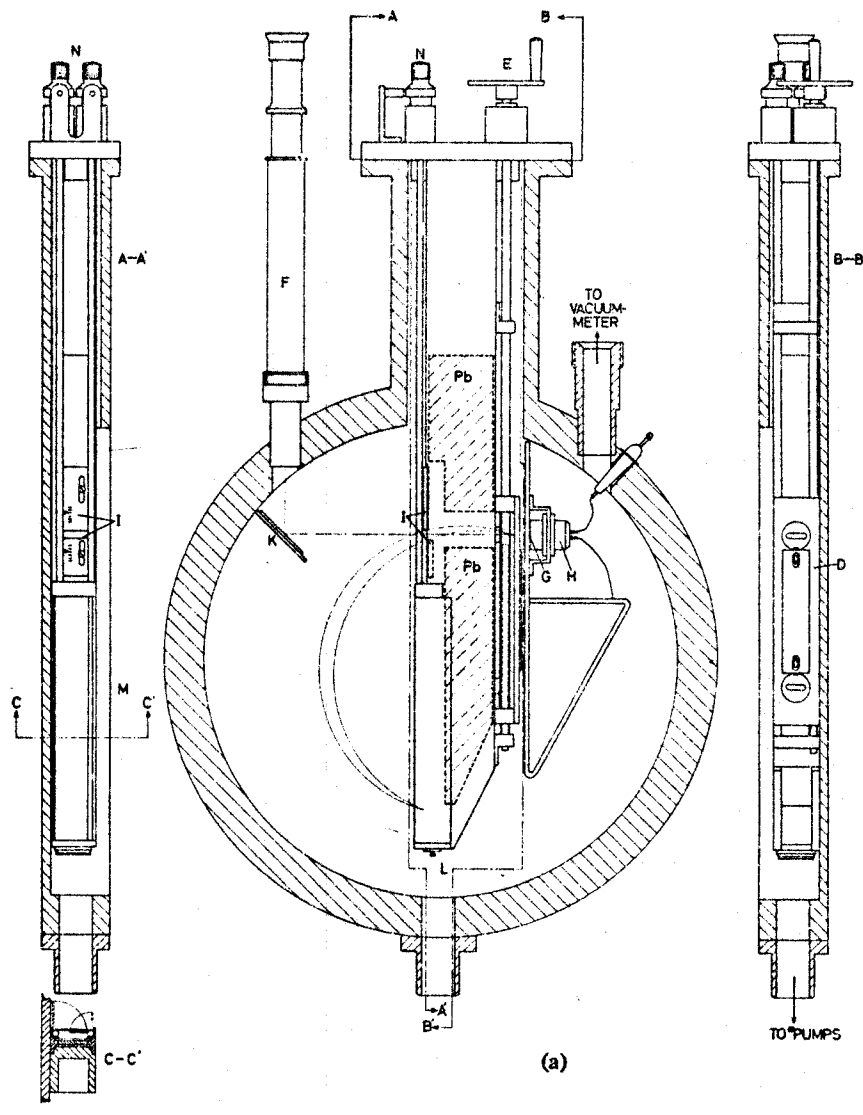
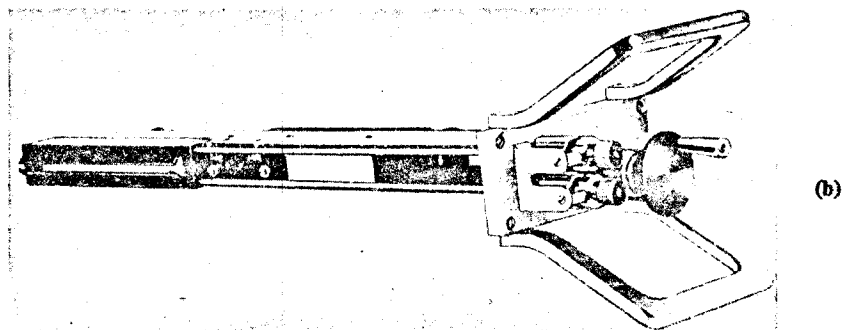


Fig. 8. β -spectra from different Hg isotopes obtained by Au(p(65 MeV), xn)Hg, registered by means of a permanent magnet semicircular spectrograph, according to Mihelich *et al.*



(a)



(b)

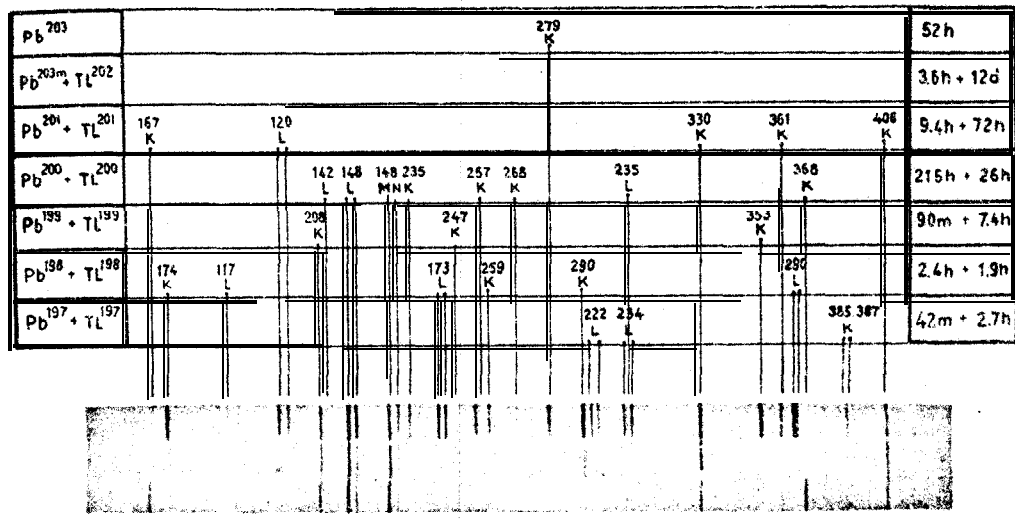


Fig. 10. Spectrum of Pb isotopes (with daughters) produced in the reaction $Tl(p(75 \text{ MeV}), xn) Pb$. The three spectra are recorded at the following intervals after the irradiation: 1.30-3.30 hours. 10.30-13.30 hours and 22.30-26.30 hours.

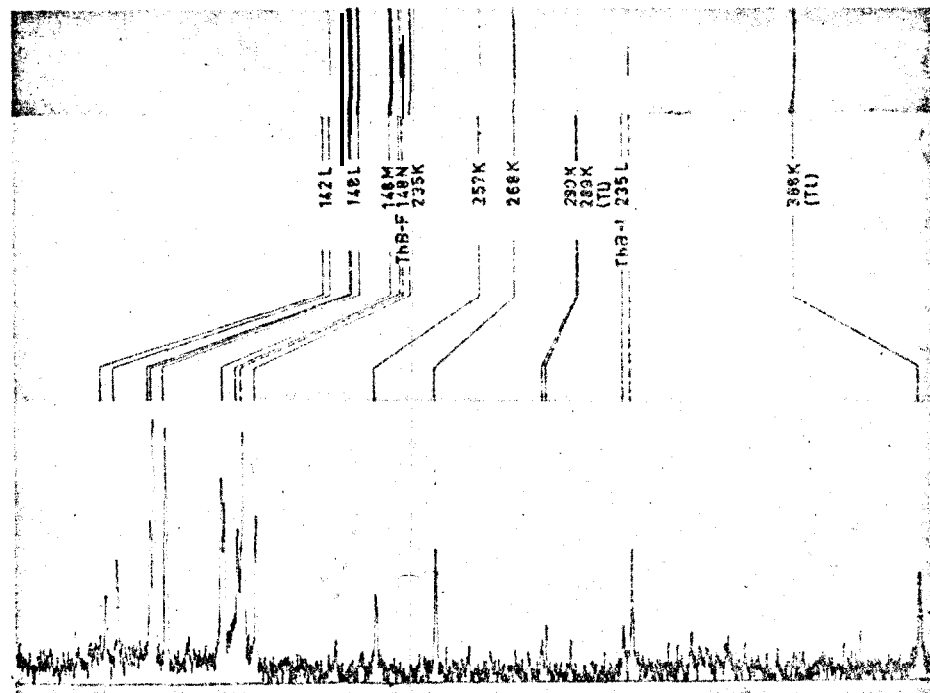


Fig. 11. (a) Spectrum of mass separated $Pb^{200} + Tl^{200}$, with ThB reference lines in central section.
(b) Microphotogram of the same spectrum.

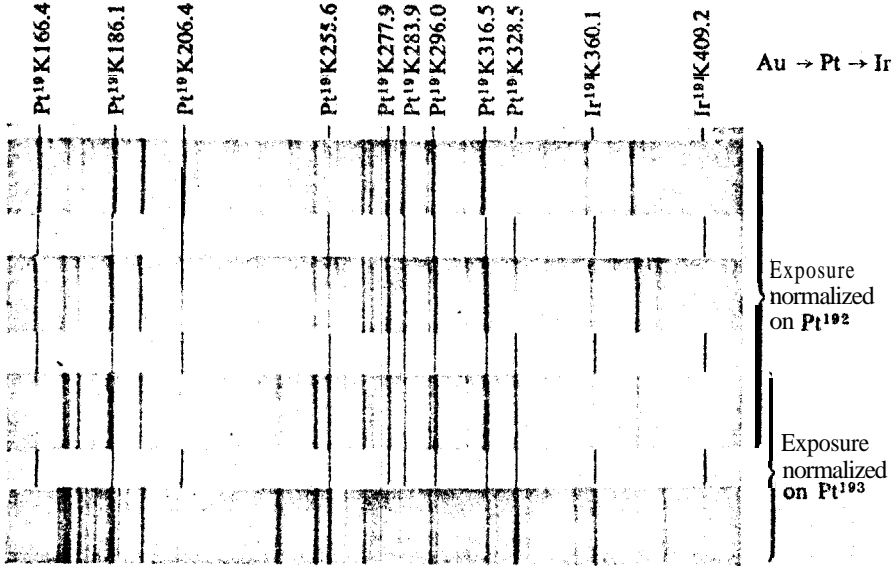


Fig. 12. Spectrum of $\text{Au} \rightarrow \text{Pt} \rightarrow \text{Ir}$ obtained in the reaction $\text{Pt}(p,xn)\text{Au}$, acc. to Marklund et. al.

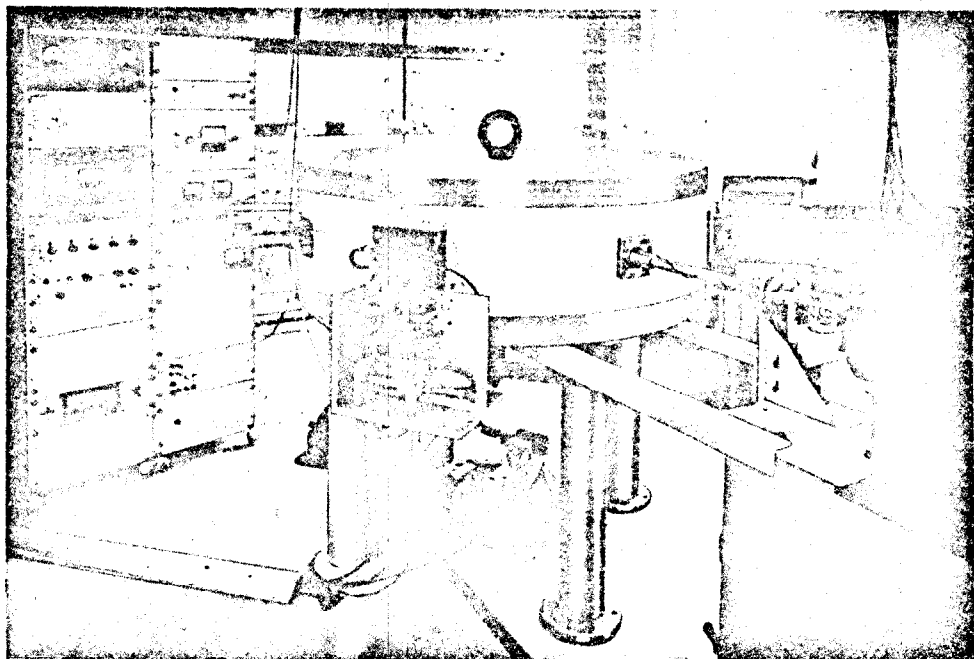


Fig. 20. 50 cm iron yoke double focusing spectrometer

Several new designs of semicircular spectrographs have been made. In many extensive investigations in the heavy element region, Hollander and colleagues at Berkeley ³⁰ have made use of a set of photographic permanent-magnet spectrographs of a fairly large and simple construction. Mladjenovid ³¹ has a similar design with a larger diameter in order to get high dispersion. Large-sized, permanent-magnet instruments have also been investigated by a Hungarian group ³² with an 'operating' radius $\rho = 75$ cm. Only a limited momentum band can be recorded simultaneously in this design, however.

A spectrograph for precise relative measurements ³³ is shown in Fig. 9. By means of an electromagnet a very homogeneous field can be achieved which is constant in time within $1 : 10^6$ as a result of recent developments in transistorized electronics ³⁴. Two sources can be brought simultaneously into the spectrograph, one of which is for calibration purposes. The position of the line sources can be observed through a telescopic arrangement, providing for an exact interchange of the two sources by means of an externally operated screw. The film holder is provided with a two 'door' shutter system which is also operated from outside. This permits the exposure of three separate spectra adjacent to each other, or a calibration spectrum superimposed upon an unknown spectrum (see Figs. 10, 11 and 12).

It is interesting to study the different parameters of the above instrument in order to be able to adjust them to each other. The resolution and transmission as a function of slit width was plotted (for $\rho = 7$ cm) for different source widths (see Fig. 13). From the diagram it is seen that a reduction in source width below 50μ is of little influence on the resolution unless ψ (i.e. the source height) is not also decreased.

Fig. 14 shows a new design due to the author for a permanent magnet spectrograph for photographic registering or, alternatively, for electrical counting by means of a semiconductor detector (or an array of such detectors). For low energy studies, the plate holder is provided with an isolated metal plate at a potential of ≈ 10 kV located immediately behind the photoplate. Since the limit for the photographic method is 7 keV such a 'post'-accelerating system can register electrons down to zero

- ³⁰ W. G. Smith and J. M. Hollander, Phys. Rev. 101 (1956) 746;
J. M. Hollander, W. G. Smith and J. W. Mihelich, Phys. Rev. 102 (1956) 740;
J. M. Hollander, Phys. Rev. 103 (1956) 1590;
J. M. Hollander, W. G. Smith and J. O. Rasmussen, Phys. Rev. 102 (1956) 1372;
J. O. Rasmussen, F. L. Canavan and J. M. Hollander, Phys. Rev. 107 (1957) 141;
R. W. Hoff and J. M. Hollander, Phys. Rev. 109 (1958) 447;
R. G. Albridge, J. M. Hollander, C. J. Gallagher and J. H. Hamilton;
Nucl. Phys. 27 (1961) 529;
F. Asato, F. S. Stephens, J. M. Hollander and I. Perlman, Phys. Rev. 117 (1960) 492;
J. Valentin, D. J. Horen and J. M. Hollander, Nucl. Phys. 31 (1962) 353, 373.
³¹ M. Mladjenovic, Bull. Inst. Nuclear Sci. 'Boris Kidrich' 6 (1956) 53.
³² S. Janos, B. Denes and Ferenc, Atomki Kozlemenek 3 (1961) 105.
³³ E. Karlsson and K. Siegbahn, Nucl. Instr. and Methods 7 (1960) 113.
³⁴ R. L. Garwin, Rev. Sci. 29 (1958) 223.

energy. A post-accelerating system has previously been designed by Delesalle³⁵ and more recently by Mehlhorn and Albridge³⁶.

The semiconductor detector is particularly useful because of its extremely small size and correspondingly low background. The low energy limit for its use is presently set at around 50 keV.

The evaluation of complicated conversion line spectra from several isotopes and many different nuclear and atomic levels might be very time consuming. It is therefore very valuable to set up a program for automatic data processing.

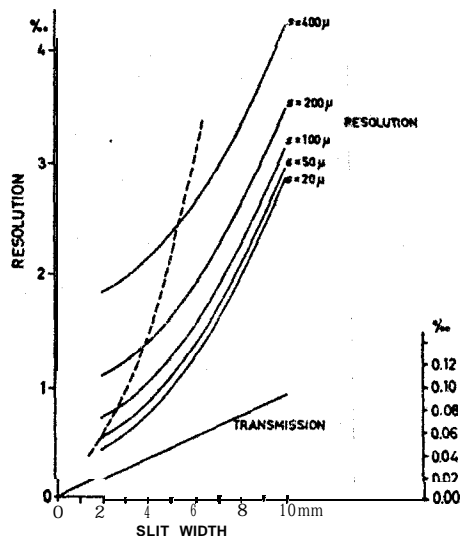


Fig. 13. Transmission and resolution of the spectrograph according to Fig. 9. Dashed line shows the best choices of source and slit widths.

This has been done by Schneider and Lindqvist³⁷. The input values are the measured line coordinates on the plate, a list of atomic binding energies ($K, L_I, L_{II}, L_{III}, M_I$ etc.) in the Z-region concerned and also some calibration line coordinates. The computer can then make the analysis in a very short time, presenting the corresponding γ -energies and ascribing them to the different isotopes and also showing from which atomic levels the conversion lines originate.

§ 5. The double focusing spectrometer

The main disadvantage of the semicircular focusing principle is the absence of space-focusing. In 1946 a device was developed^{38,39} which combines many of the features of one-dimensional semicircular focusing and two-dimensional helical or lens focusing.

³⁵ J. Delessalle, J. Phys. Radium 19 (1958) 111.

³⁶ W. Mehlhorn and R. G. Albridge, Nucl. Instr. and Methods 26 (1964) 37.

³⁷ W. Schneider and T. Lindqvist, Nucl. Instr. and Methods 13 (1961) 21.

³⁸ N. Svartholm and K. Siegbahn, Ark. Mat. Astr. Fys. 33A (1946) No. 21.

³⁹ K. Siegbahn and N. Svartholm, Nature 157 (1946) 872.

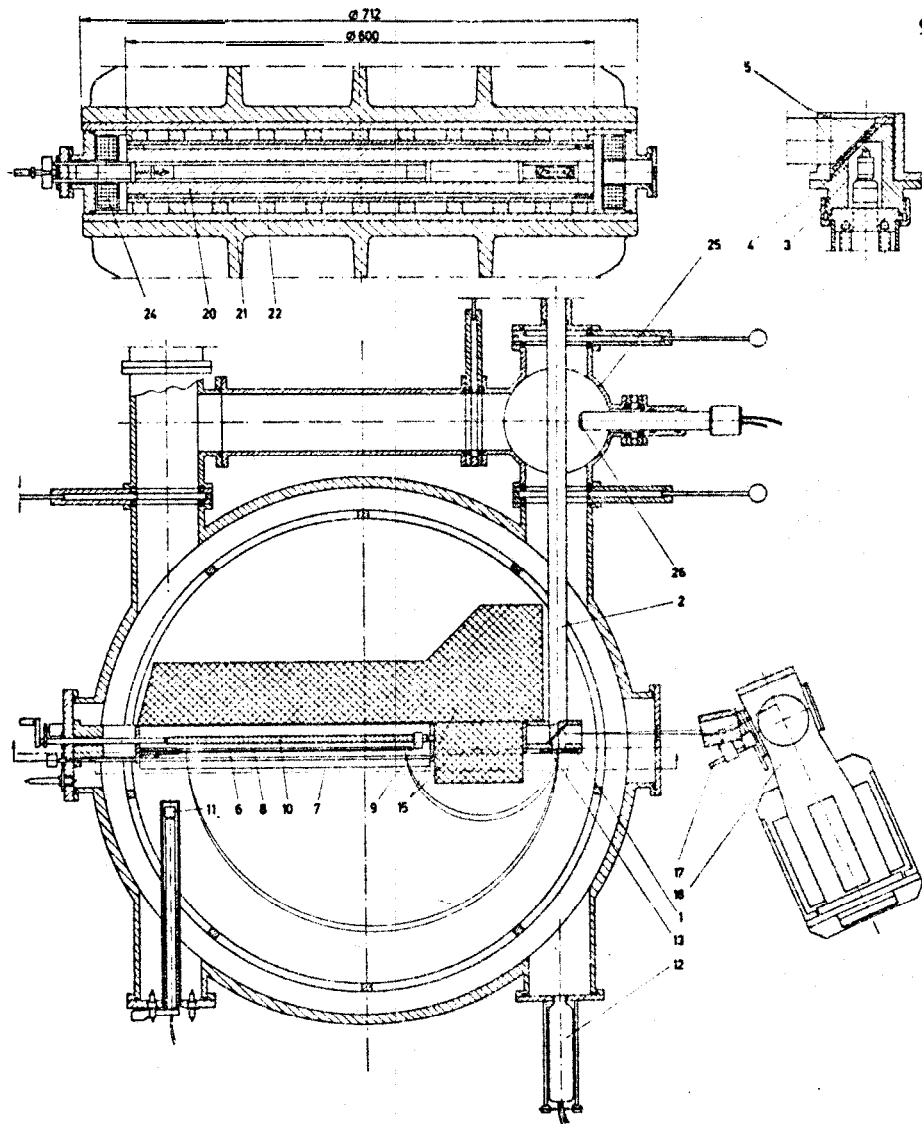


Fig. 14. Permanent-magnet spectrograph using photographic recording or electrical counting by means of an externally moveable array of semiconductor detectors (9) situated on a precision screw (10). For low energy spectra, a post-accelerating plate electrode (8) is inserted immediately behind the photoplate (6). The source-holder (1) is introduced through a lock device, passing an evaporation chamber (25). The spectrograph is designed for studies of radioactive sources as well as of photo-electrons expelled by an externally focused X-ray beam (17) or other possible external beams. The field is measured by a magnetometer (11) and can be changed by exciting coils (24). The magnetic field is produced by a large number of permanent magnets (22) situated in the upper and lower parts of the spectrograph. There are additional airgaps in the pole plates in order to homogenize the magnetic field. The sample to be evaporated (4) is introduced through the bottom of the evaporation vessel by means of a special arrangement (3). The evaporation is made through a slit (5) in contact with the backing of the source holder. The evaporated source can be immediately scanned by means of a semiconductor detector (26) before the source rod is put into the position for photographic registering.

It is known from the construction of cyclotrons and betatrons⁴⁰ that a magnetic field having rotational symmetry and a field gradient forces the electrons to describe oscillatory paths in the ρ - as well as the z -coordinates of the particles. If we define an electron-optical axis of the focusing device as a circle in the symmetry plane of the magnetic field, electrons starting from a point on this optical axis and making angles ϕ_0 and ψ_0 with this axis (see Fig. 15) will return to the axis after certain 'focusing angles' ϕ_ρ and ϕ_z . For small angles ϕ_0 and ψ_0 these focusing angles are given by

$$\phi_\rho = \pi \left[1 + \frac{\rho_0 B'(\rho_0)}{B(\rho_0)} \right]^{-\frac{1}{2}}, \quad \phi_z = \pi \left[-\frac{\rho_0 B'(\rho_0)}{B(\rho_0)} \right]^{-\frac{1}{2}}. \quad (31)$$

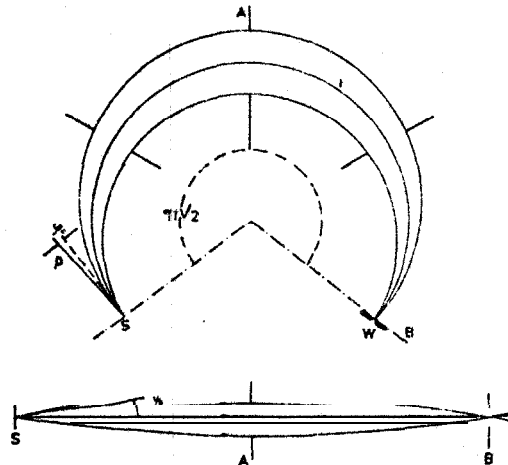


Fig. 15. $1/\sqrt{r}$ -double focusing.

The two focusing angles are related by

$$\frac{1}{\phi_\rho^2} + \frac{1}{\phi_z^2} = \frac{1}{\pi^2}. \quad (32)$$

The focusing system is obviously an-astigmatic if $\phi_\rho = \phi_z$, which gives as the condition for double focusing the following differential equation:

$$B'(\rho_0) = -\frac{1}{2\rho_0} B(\rho_0). \quad (33)$$

The solution of this equation imposes on the magnetic field the condition that the field should decrease as $1/\sqrt{\rho}$ in the vicinity of $\rho = \rho_0$ (the central path). According to (32) the double focusing takes place after an angle of $\pi\sqrt{2} = 254^\circ.56$, instead of 180° as in the homogeneous field case.

⁴⁰ D. W. Kerst and R. Serber, Phys. Rev. 60 (1941) 53.

These conclusions can also be drawn if one starts from the expressions valid for the frequencies of oscillations in the betatron field⁴⁰ $B(\rho) = B(\rho_0)(\rho_0/\rho)^n$. For an equal frequency of the vertical (z) and radial (ρ) oscillations one gets $n=1/2$ in agreement with the result above^{41, 42}.

So far we have only considered 'paraxial' rays (ϕ_0 and ψ_0 small). It is of interest to see if the focusing conditions still hold for non-central rays⁴³⁻⁴⁵. As one might expect, this is so. In fact it is found that the $1/\sqrt{\rho}$ condition from many points of view is still the best choice of fieldform, though extended analyses show that other

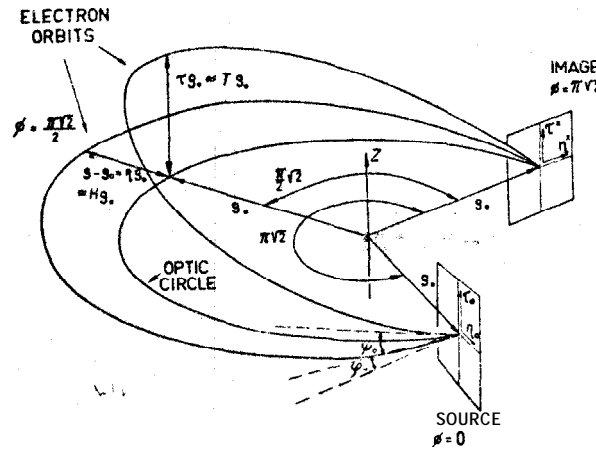


Fig. 16. Geometry and coordinates of a double focusing spectrometer.

slightly different fieldforms can also be used. The procedure is to consider the general fieldform

$$B_z(\rho, 0) = B_0 \left\{ 1 + \alpha \frac{\rho - \rho_0}{\rho_0} + \beta \left(\frac{\rho - \rho_0}{\rho_0} \right)^2 + \dots \right\} = B_0 \{ 1 + \alpha \eta + \beta \eta^2 + \dots \}, \quad (34)$$

where $\eta = (\rho - \rho_0)/\rho_0$ and α, β, \dots are constants to be determined to minimize aberration.

The equations of motion are solved for a particle leaving the source at a point $\eta_0 = \delta\rho/\rho_0$, $\phi_0 = \delta z/\rho_0$ and in a direction ϕ_0 and ψ_0 to the optical axis (ϕ_0 being in the symmetry plane perpendicular to the lines of force, see Fig. 16). It is then found, in agreement with the elementary theory given above, that an-astigmatic focusing occurs when $\alpha = -\frac{1}{2}$, i.e. after $\phi = \pi\sqrt{2}$. The particle will strike the plane $\phi = \pi\sqrt{2}$ at a point characterized by the coordinates:

⁴¹ F. N. D. Kurie, J. S. Osoba and L. Slack, Rev. Sci. Instr. 19 (1948) 771.

⁴² A. A. Bartlett and K. T. Bainbridge, Rev. Sci. Instr. 22 (1951) 517.

⁴³ E. McMillan, private communication (1946).

⁴⁴ N. Svartholm, Ark. Mat. Astr. Fys. 33A (1946) No. 24.

⁴⁵ F. B. Shull and D. M. Dennison, Phys. Rev. 71 (1947) 681; 72 (1947) 256.

$$\eta^* = -\eta_0 + \frac{1}{3}(2-4\beta)\eta_0^2 + \frac{1}{3}(4\beta-3)\tau_0^2 + \frac{1}{3}(2-16\beta)\varphi_0^2 + \frac{1}{3}(16\beta-6)\psi_0^2 \quad (35)$$

$$\tau^* = -\tau_0 + \frac{8}{3}\beta\eta_0\tau_0 + \frac{1}{3}(32\beta-12)\varphi_0\psi_0 \quad (36)$$

where η and τ are the particle's radial and axial coordinates measured from the optical circle in units of ρ_0 . η_0 and τ_0 are the coordinates at the source and η^* and τ^* at the image plane.

Equation (33) determines the line width and, since the dispersion is along the p-coordinate, eq. (33) gives the resolution.

It can be shown³⁸ that the dispersion in the double focusing case is $\gamma = 4/B$ as compared to $2/B$ for the homogeneous field. Introducing the source width s and height h , the detector width w , and the defining aperture angles φ_0 and ψ_0 we then get the base resolution from eq. (35), remembering the value of the dispersion:

$$R^0 = \frac{s}{4\rho} + \frac{w}{4\rho} + \frac{4\beta-3}{48\rho^2} h^2 + \frac{2-16\beta}{12} \varphi_0^2 + \frac{16\beta-6}{12} \psi_0^2. \quad (37)$$

The $l/l/p$ -field obviously corresponds to $\beta = \frac{3}{8}$. This value of β makes the last term in (37) zero, i.e. the resolution is independent of ψ_0 . If $\beta = \frac{1}{8}$, the resolution is instead independent of φ_0 . In the first case one can speak of a 'high aperture' instrument, in the second case of a 'wide aperture' one. Furthermore if $\varphi_0 = \psi_0$, i.e. if we use a square (or circular) entrance aperture, the resolution is independent of β (except for the term containing the source height, which in most cases is small).

The β -value at double focusing can evidently be chosen with a certain degree of freedom. Commonly used p-values are the above discussed $\beta = \frac{3}{8}$ and $\frac{1}{8}$. In the first case the resolution is set by the width of the radial shutters, whereas the axial width of the rays can be quite extended without influencing the resolution (higher order z-focusing). Usually there is a practical limit as to the maximum height or width of the beam. This may be set by the fixed distance between the pole pieces or perhaps by the difficulties in obtaining the correct fieldform for large variations of ρ . An ironfree double focusing spectrometer may be realized, as will be discussed later, by means of two concentric solenoids or a system of coils. In this case the natural choice of β is $\frac{3}{8}$, since there is no limit for the field in the z-direction. Also, the β -value of $\frac{2}{8}$ is commonly used because of the simple way one can obtain this fieldform by the use of iron pole pieces. In this case the fieldform is $B(\rho) = B_0 \cdot 2\rho_0/(\rho + \rho_0)$. Assuming infinite permeability of the iron, this fieldform is attained with conical pole pieces⁴⁶. The pole distance is $2z = z_0(\rho + \rho_0)/\rho_0$, where z_0 refers to $\rho = \rho_0$.

Other &values can be obtained with slightly curved pole faces. The first large double focusing spectrometer⁴⁷ ($\rho_0 = 50$ cm) further discussed in this chapter has a β -value of $\frac{3}{8}$ obtained by forming the air gap between the pole faces as a parabola $z = c\sqrt{\rho}$, i.e. with the vertex at the centre of the magnet.

The condition for an-astigmatic double focusing is that $a = \frac{1}{2}$ in eq. (34). As stated above, the value of β may not be so critical, since it will mainly influence the

⁴⁶ N. Svartholm, Ark. f. Fysik 2 (1949) 115.

⁴⁷ A. Hedgran, K. Siegbahn and N. Svartholm, Proc. Phys. Soc. A63 (1950) 960.

REFERENCE ONLY

PHYSICS-111-LAB.

DO NOT REMOVE

choice of shutter system. However, if ϵ is different from $-\frac{1}{2}$, say $= -\frac{1}{2}(1 + \epsilon)$, an astigmatic error will be introduced. In the image plane $\phi = \pi\sqrt{2}$ and for $\beta = \frac{3}{8}$ this will introduce an extra line broadening of the magnitude $\delta_{ast} = \rho_0 \varphi_0 \epsilon \pi\sqrt{2}$.

Quite generally, if the source and the detector slit are situated on a circle of radius ρ_1 , which differs by $\Delta\rho$ from the radius ρ_0 of the optical axis, there is an astigmatism expressed by $\epsilon = (3 - 8\beta)\Delta\rho/2\rho_0$. Evidently this vanishes for $\beta = \frac{3}{8}$, which means that there is only one fieldform that gives double focusing for every value of ρ , namely that varying as $1/\sqrt{\rho}$.

A small astigmatic error can be reduced by moving the detector slit along the optical axis out of the plane $\phi = \pi\sqrt{2}$ until a minimum in radial width is found. If $\epsilon = -\frac{1}{2}(1 + \epsilon)$ the dispersion will no longer be $4/B$ but $4(1 + \epsilon)/B$. The easiest way to measure ϵ accurately is either to determine the dispersion or to determine the true values of ϕ_s and ϕ_p .

For optimum conditions the different terms in the expression (37) for the resolving power should be made approximately equal, just as in the semicircular case. In practice, however, the height of the source is made smaller than this condition calls for.

The image form can be derived in exactly the same way as in § 4 for the semicircular case. It is found⁴⁷ that for rectangular shutters and for $\beta = \frac{3}{8}$ and $\frac{3}{8}$ the line shape is the same as for the semicircular focusing system (Fig. 4).

The above treatment is only carried out to the second order. It is of interest to study the higher order terms in order to minimize the spherical aberrations still further. The procedure is complex but straightforward@*⁴⁹.

Putting $\epsilon = -\frac{1}{2}$ and $\beta = \frac{3}{8}$ the coefficient γ in the third order calculation can be determined from :

$$\begin{aligned}\eta^* = & -\eta_0 + \frac{1}{6}\eta_0^2 - \frac{1}{3}\eta_0^3 - \frac{1}{2}\tau_0^2 + \frac{7}{12}\eta_0\tau_0^2 - \frac{4}{3}\varphi_0^2 - \frac{3}{2}\pi\sqrt{2}(\gamma + \frac{43}{144})\varphi_0^3 \\ & + \frac{9}{2}\pi\sqrt{2}(\gamma + \frac{43}{144})\varphi_0\psi_0^2 - \frac{3}{4}\pi\sqrt{2}(\gamma + \frac{43}{144})\eta_0^2\varphi_0 + \frac{3}{4}\pi\sqrt{2}(\gamma + \frac{25}{48})\tau_0^2\varphi_0 \\ & + \frac{3}{2}\pi\sqrt{2}(\gamma + \frac{3}{8})\eta_0\tau_0\psi_0 - \frac{2}{6}\eta_0\varphi_0^2 - \frac{4}{3}\tau_0\varphi_0\psi_0,\end{aligned}\quad (38)$$

$$\begin{aligned}\tau^* = & -\tau_0 + \eta_0\tau_0 + \frac{1}{4}\tau_0^3 - \frac{7}{12}\eta_0^2\tau_0 + \frac{9}{2}\pi\sqrt{2}(\gamma + \frac{43}{144})\varphi_0^2\psi_0 \\ & - \frac{3}{2}\pi\sqrt{2}(\gamma + \frac{17}{48})\psi_0^3 + \frac{3}{4}\pi\sqrt{2}(\gamma + \frac{25}{48})\eta_0^2\psi_0 + \frac{3}{2}\pi\sqrt{2}(\gamma + \frac{3}{16})\eta_0\tau_0\varphi_0 \\ & - \frac{3}{4}\pi\sqrt{2}(\gamma + \frac{17}{48})\tau_0^2\psi_0 + \frac{2}{3}\tau_0\varphi_0^2.\end{aligned}\quad (39)$$

Obviously, by choosing $\gamma = -\frac{43}{144}$ the radial aberration for rays with large axial orbit departures is minimized. Lee-Whiting and Taylor⁴⁹ have extended the calculations to the sixth order. It is interesting to note how close the coefficients in the expansion (34) calculated in this way come to the $1/\sqrt{\rho}$ field. See Table 2.

Since the higher order terms are essential for the radial spherical aberration of rays of large orbit departures it is difficult to give theoretical values for the transmission and luminosity without a very detailed knowledge of the actual magnetic field realized

⁴⁸ H. Wild and O. Huber, Helv. Phys. Acta 30 (1957) 3.

⁴⁹ G. E. Lee-Whiting and E. A. Taylor, Can. Phys. 35 (1957) 1.

TABLE 2
Values of magnetic field expansion coefficients according to eq. (34)

	<i>Optimum</i>	$1/\sqrt{\rho}$
0	1	1
1	$-\frac{1}{2}$	$-\frac{1}{2}$
2	$\frac{3}{8}$	$\frac{3}{8}$
3	$-\frac{43}{144} = -0.2986$	$-\frac{5}{16} = -0.3125$
4	$\frac{553}{2304} = 0.2400$	$\frac{35}{128} = 0.2734$
5	$-\frac{69709}{345600} = -0.2017$	$-\frac{63}{256} = -0.2461$
6	$\frac{60299}{345600} + \frac{35\pi^2}{147456} = 0.1768$	$\frac{231}{1024} = 0.2256$

in a special instrument. From second order theory it is seen that (neglecting the unimportant term containing the height of the source) the resolution is given by (37):

$$R^0 = R_s + R_w + R_{ab}, \quad (40)$$

where

$$R_s = s/4\rho, \quad R_w = w/4\rho \quad \text{and} \quad R_{ab} = \frac{1}{6}\{(1 - 8\beta)\varphi_0^2 + (8\beta - 3)\psi_0^2\}. \quad (41)$$

In this approximation R_{ab} is independent of the β -value for $\varphi_0 = \psi_0$, i.e. if square shutters are used: $R_{ab} = \frac{1}{3}\varphi_0^2$. If we put $R_s = R_w = R_{ab}$, we get $R^0 = \varphi_0^2$. If $R_{\square} = \frac{1}{2}R^0$ and $T = \frac{1}{2}\Omega$ the relation between R_{\square} and T is very approximately:

$$R_{\square} = \pi T. \quad (42)$$

Usually, this relation can be regarded as a lower limit for the actual figures. For the $\beta = \frac{1}{4}$ field both the φ and the ψ defining baffles have to be decreased in order to gain resolution under the optimum conditions. For the $\beta = \frac{1}{8}$ or $\beta = \frac{3}{8}$ field this is not so, since the radial or the axial defining angles do not contribute to the spherical aberration (in the above approximation). By a suitable choice of nearly rectangular shutters a substantial gain can be obtained in resolution at a given transmission using either the $\beta = \frac{1}{8}$ or the $\beta = \frac{3}{8}$ field, provided that a fairly good fit to the optimum field can be realized.

Since the $\beta = \frac{1}{4}$ field can be easily calculated regarding solid angle at a certain resolution (circular shutters are advantageous), we give some explicit figures for this case in an actual design ($\rho_0 = 18.5$ cm)⁵⁰ (see Table 3, p. 105).

⁵⁰ E. Arbman and N. Svartholm, Ark. f. Fysik 10 (1955) 1.

For high resolution work there are strong reasons for choosing $\beta = \frac{1}{2}$ or, with some preference, $\beta = \frac{3}{8}$ ('high aperture' double focusing). Since the trends are towards high resolution, it is of particular interest to study this case somewhat more closely.

The electron trajectory projections on the cylindrical surface defined by the optical circle and on the symmetry plane are sine functions of the angle ϕ with zero point at $\phi = \pi\sqrt{2}$. The maximum amplitude in the z-direction is denoted by T and in the ρ -direction by H (see Fig. 16). It can be shown that H and T , expressed in units of ρ_0 , are given with good accuracy by:

$$H = \sqrt{2} \operatorname{tg} \psi_0, \quad T = \sqrt{2} \operatorname{tg} \psi_0. \quad (43)$$

Using these parameters the sixth order optimum field (see Table 2) will cause spherical aberrations for a point emitting source situated at $\eta = 0$ and $\tau = 0$, given by the coordinates at $\phi = \pi\sqrt{2}$:

$$\eta^* = -\frac{2}{3} H^2 + \frac{8}{45} H^2 T^2 + \frac{8}{27} H^4 + \dots \quad (44a)$$

$$\tau^* = -\frac{\pi}{24} T^3 - \frac{14}{135} H^3 T + 0.019635 T^5 + \dots \quad (44b)$$

The high aperture case is consequently first order radial and axial focusing and second order radial focusing for axial angles ψ . The dispersion direction is along ρ , and η^* will be a measure of the resolution. With a fixed detector slit the dispersion relationship for double focusing gives:

$$\eta^* = \frac{4\Delta(B\rho)}{B\rho} = \frac{4\Delta I}{I}, \quad (45)$$

where $\Delta I/I$ is the relative change in spectrometer current due to the spherical aberration. The first term in the radial aberration gives:

$$\eta^* \approx -\frac{2}{3} H^2. \quad (46)$$

If $T < 1$ ($\psi < 35^\circ$) (46) should be a good approximation for the radial aberration. The lack of axial focusing is given by (44b). This is usually of little harm and can be taken care of by using a detector slit slightly longer than the source height. If we require a resolution in momentum of $\lesssim 0.1\%$ then $|H| \lesssim 0.08$ (corresponding to $\psi_0 \leq 3.2^\circ$ according to (45) and (46)). If T is made equal to 0.25 (corresponding to $\psi_0 = 10^\circ$) the resolution should not be affected at all according to (44a) (actually, a much larger T would be allowable for the ideal fieldform treated here). The axial aberration for this T -value would require a counter slit 2 mm longer than the source for $\rho_0 = 50$ cm according to (44b). The solid angle Ω would be

$$\Omega = \frac{2\psi_0 \cdot 2\psi_0}{4\pi} \approx \frac{HT}{2\pi} \approx 0.3\%. \quad (47)$$

If we make the assumption that $R_s = R_w = R_{ab}$, then $s = w = 2$ mm. The base resolution is now $\lesssim 0.3\%$ and the resolution $\lesssim 0.15\%$. The transmission is about half of the solid angle, i.e. $T \approx 0.15\%$. The luminosity is more difficult to calculate since the

height of the source (and detector) for optimum conditions would be impractically long and the question of a long and slightly curved detector slit enters into the calculations. These problems have been discussed by Graham *et al.*⁵¹ in their descriptions of the double focusing spectrometer at Chalk River ($\rho_0 = 100$ cm).

The focusing properties of a spectrometer are given by its 'iso-aberration' contours in the HT -plane. For the fieldform used at Chalk River these have been calculated for different resolutions using a point source. Experimentally it is very easy to measure these contours by placing a small-sized hole shutter in the spectrometer, variable in the HT -plane. Line peaks focused at the same current form one iso-aberration contour. Figure 17 shows the theoretical and experimental results of the Chalk River instrument⁵². The cross-hatched regions correspond to forbidden zones where the

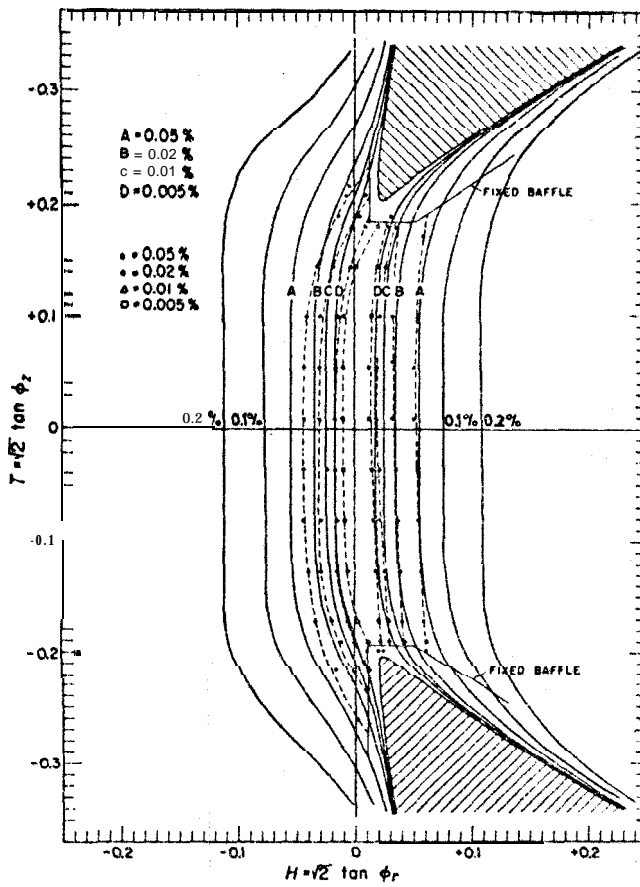


Fig. 17. Theoretical and experimental (dashed lines) iso-aberration contours of the Chalk River double focusing spectrometer.

⁵¹ R. L. Graham, G. T. Ewan and J. S. Geiger, Nucl. Instr. and Methods 9 (1960) 245.

⁵² J. S. Geiger and R. L. Graham, Nucl. Instr. and Methods 24 (1963)

spherical aberration quickly takes on positive values, i.e. electrons are arriving at the detector plane on the high energy side, with detrimental effects on the line shape. The contours are slightly curved, the curvature being almost zero for small T . The agreement between theory and experiment is very satisfactory. From such a curve the solid angle at a given resolution can be immediately determined.

The spectrometer magnetic field can be produced either by a coil system only, or by using iron for the field shaping. In the latter case the two possibilities shown in Fig. 18 occur. The alternative in the upper part of the figure has the advantage that the fringing fluxes are easy to handle and is better in some ways for smaller magnets. A spectrometer of this type is described in ref. 50, where ρ_0 is 18.5 cm, and the maximum transmission is around 4%. The β -value chosen is $\frac{2}{3}$ which has permitted the use of simple conical pole faces. In Table 3 some data for this spectrometer are given. In all cases the source height was 20 mm and a circular shutter was used. The maximum resolving power used so far is 0.3% with a source width of 1 mm and a GM slit of 2 mm. The transmission is then 0.35 %.

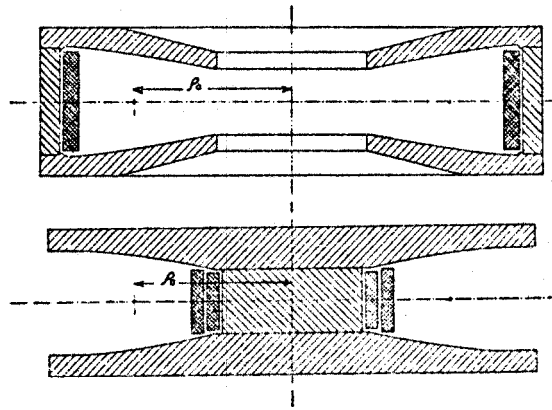


Fig. 18. Double focusing magnets.

TABLE 3

Source width (s) (mm)	Detector slit (w) (mm)	R in %							
		$\Omega = \frac{1}{2} \%$		$\Omega = 1 \%$		$\Omega = 2 \%$		$\Omega = 4 \%$	
		Calc.	Mea- sured	Calc.	Mea- sured	Calc.	Mea- sured	Calc.	Mea- sured
2	2	0.44	0.50	0.60	0.64	0.94	0.92	1.5	1.3
4	4	0.71	0.70	0.87	0.85			1.7	1.5
8	8			1.4	1.3	1.7	1.6	2.4	1.8
16	20	2.6	2.3					3.5	2.9

Bartlett et al.⁵³ have designed a flexible iron instrument provided with a set of 'inner' and 'outer' coils. By means of these it is possible to produce any fieldform required, with variable field coefficients. For instance, both the high aperture and the wide aperture case can be obtained and the various higher order calculations (see below) can be tested. A maximum transmission of 5% can be obtained at a resolution of 1.5%. The best resolution is 0.07% at a transmission of 0.5%. Figure 19 shows a cross section of this instrument ($\rho_0=30$ cm). A similar instrument was previously built by Wild and Huber^{49, 54}.

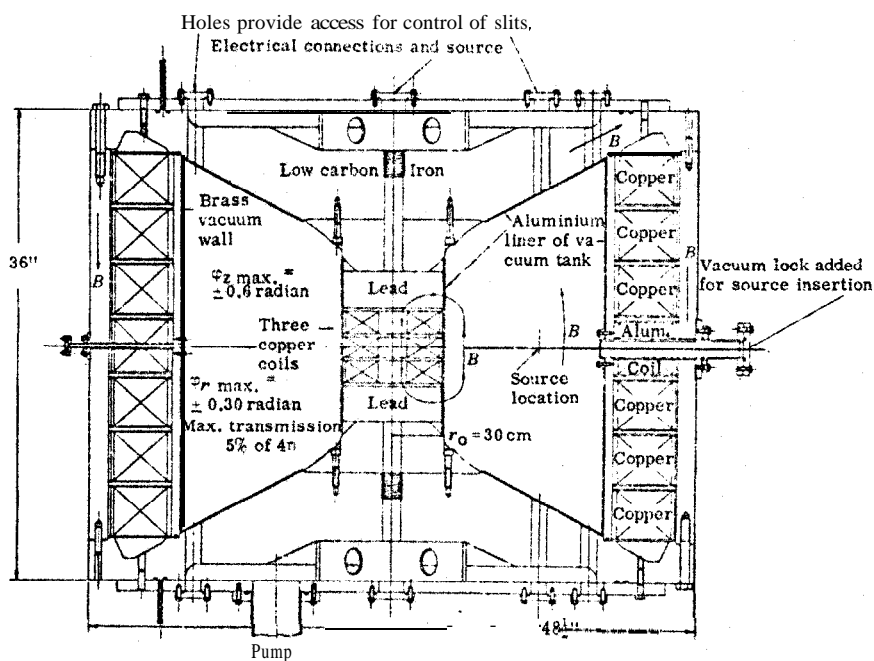


Fig. 19. Double focusing spectrometer due to Bartlett et al.

The first precision spectrometer of large radius of curvature ($\rho_0=50$ cm) was designed by Hedgran, Siegbahn, and Svartholm^{47, 55} soon after the double focusing principle was established. This instrument increased the dispersion previously obtainable in β -ray spectroscopy by an order of magnitude. The magnet was of the type shown in the lower part of Fig. 18, in order to facilitate measurements. A rotating coil system was developed for the continuous field measurements in this spectrometers". The definition of the minimum in the magnetic balancing system permitted an accuracy in the field setting of 2 to 3 parts in 10^5 , although it was not possible to measure the effective field with that accuracy because of the iron. With this spectro-

⁵³ A. A. Bartlett, R. A. Ristinen and R. P. Bird, Nucl. Instr. and Methods 17 (1962) 188.

⁵⁴ O. Huber, L. Schellenberg and H. Wild, Helv. Phys. Acta 33 (1960) 534; T. Y. Chen, J. Kern, O. Huber, L. Schellenberg, B. Walthard and H. Wild, Nucl. Instr. and Methods (1964).

⁵⁵ A. Hedgran, Ark. f. Fysik 5 (1952) 1.

meter a great number of spectra have been measured with an accuracy of 1 or 2 parts in 10^4 . Figure 80 on p. 179 shows part of the spectrum of Au 194, which contains some hundred lines⁵⁶.

The field measuring system has been further developed in order to permit automatic operation^{57,58}. For routine work in high resolution spectroscopy this feature can now be regarded as indispensable. In principle, the field of the spectrometer is set against a permanent magnet standard by comparison of signals generated by two rotating coils, one in the spectrometer and the other in the permanent magnet field, both coils being mounted on the same shaft. This comparison is made using a relay-operated precision voltage divider and detecting the difference in ac voltages with a frequency selective amplifier followed by a phase sensitive detector. operating on the output from the latter, the transistor power-supply regulates the spectrometer field with a precision of $\approx 1 : 10^5$. Figure 20 shows a photograph of the 50 cm iron yoke double focusing spectrometer. Figure 21 shows a block diagram of the automatic field regulating system and outputs. A new scheme is at present being worked out for the 'peaking-strip' method for field balancing. The latter scheme has the advantage that no moving parts are necessary. It also requires less space..

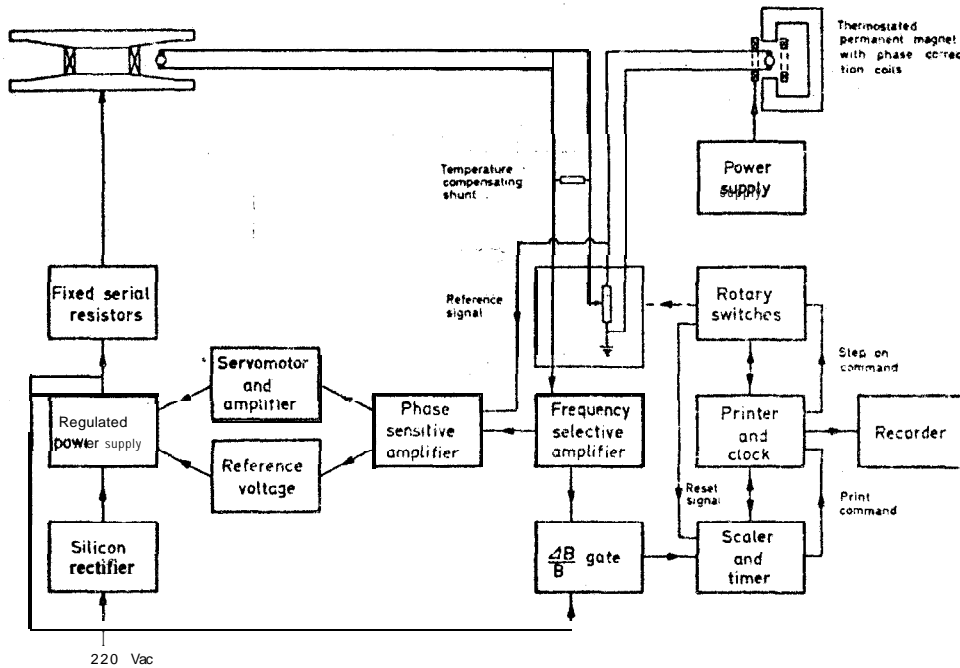


Fig. 21. Scheme of the automatic field regulation system and outputs. The field settings are accurate to within $\approx 1 : 10^5$.

⁵⁶ G. Backstrom, O. Bergman, J. Burde and J. Lindskog, Nucl. Phys. 15 (1960) 566.

⁵⁷ G. Backstrom, A. Backlin, N. E. Holmberg and K. E. Bergkvist, Nucl. Instr. and Methods It (1962) 199.

⁵⁸ O. Bergman, G. Backstrom, Y. Grunditz, H. Pettersson, E. Aasa and S. Antman, Ark. f. Fysik (1964).

By giving the pole faces a parabolic shape and adding some additional iron at the periphery to compensate for the stray Aux it is fairly easy to achieve the required $1/\sqrt{\rho}$ field. The fieldform will to a higher order of approximation be a function of the field strength due to the change of permeability of the iron with field strength. This also puts a natural limit on the ultimate accuracy even if the field-setting at the position of the rotating coil can be set with a precision of $\approx 1:10^5$. In practice, the obtainable accuracy, down to say 50 keV, is around one part in 10^4 , although much lower energies can be measured. The high dispersion instrument described is usually run at a resolution of between 1 and $2:10^3$ and a transmission of about the same magnitude. By a careful external magnetic shimming of such an instrument a resolution of $5:10^4$ at a solid angle of $2:10^3$ was recently obtained^{58a}.

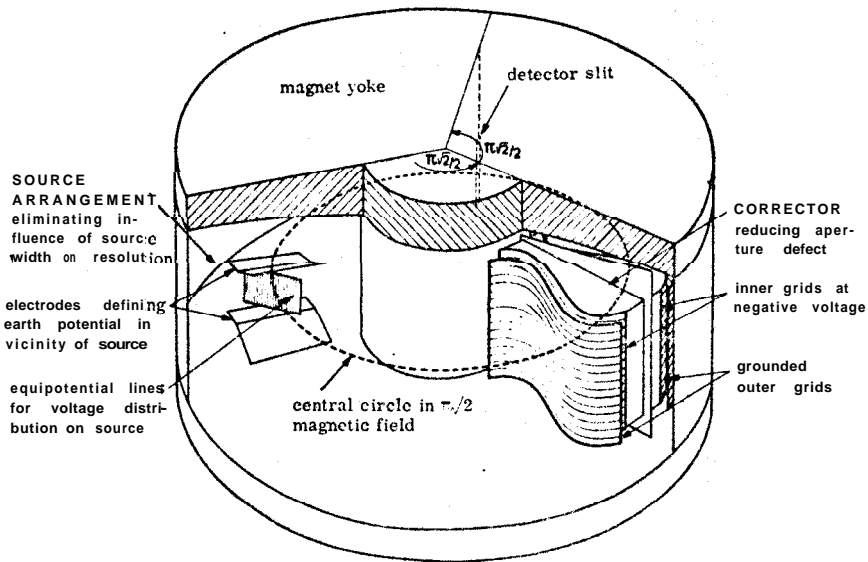


Fig. 22. Electrostatic correctors for a double focusing spectrometer due to Bergkvist.

The luminosity of the instrument has recently been substantially improved by Bergkvist⁵⁹ by adding two electrostatic correctors, one for the influence of the source width and one for the spherical aberration. The principle is shown in Fig. 22. The extended source, either a β -source or a converter for γ -radiation, should according to theory be placed with its plane at an angle of $\sim 43^\circ$ relative to the radius. By means of a number of vertical wires an electric field gradient along the source is introduced. It is possible to apply a total electric potential over the source which is sufficient to compensate for the difference in ρ coordinates of the source points. An earth defining grid can be placed at some distance from the source, but in practice this is not necessary. By this simple arrangement very extended sources can be used in such

^{58a} M. Perlman, Brookhaven, private communication (1963).

⁵⁹ K. E. Bergkvist, Ark. f. Fysik 13 (1958) 256; private communication (1963).

cases where the specific activity constitutes a major problem. Electromagnetically separated radioactive sources can normally be collected on the backing within narrow widths, but in other cases, for instance when converters are used, the counting rate at a certain resolution may be highly dependent on the source area which can be used. One obvious example is given by the (n, e) studies by means of the double focusing instruments'. In this case the number of conversion electrons produced by the neutron beam from the reactor at the source in the spectrometer is proportional to the source area. These experiments are further described in Chapter XIII. In a typical case (Cd^{114}) the source area was as large as $4 \times 6 \text{ cm}^2$ at a resolution of 0.15 %. Figure 23 shows the simple design of the potential gradient source holder used in these experiments. At an energy of 2 MeV the total potential applied to the source was 20 kV. For -sources more elaborate designs have been used. The electrostatic corrector for the spherical aberration is placed symmetrically in the spectrometer between the source and the detector according to Fig. 22. Theoretically, it is possible to achieve a very high cancellation of the spherical aberration by a conveniently shaped grid system. The final limitation is set by cross terms of the third order between the parameters η_1 , τ_1 , describing the aperture of the corrector, and η_0 , τ_0 , describing the dimensions of the source. According to theory a very high increase in luminosity of the system should be possible. This is also so in practice, the best results being obtained at resolutions around 0.1 % or somewhat more. Below this, imperfections of the corrector and also unavoidable imperfections in the fieldform (especially when iron is used for shaping the field) soon put a practical limit on the performance data. At a solid angle of 0.5 % and a source width of 4 cm a resolution of 0.11% could be achieved. The potentials applied on the spherical aberration corrector V_c and on the source V_s for the 412 keV K-line of Au^{198} were then $V_c = -3.2$ kV and $V_s = 10.0$ kV. The detector slit necessary to collect the radiation was 2 mm. A decrease in the aperture did not improve the resolution very much. in the quoted example the source area which could be used was 30 times larger than normal. In order to reach the same resolution, i.e. 0.11 %, the aperture would normally have been 3 or 4 times smaller, and consequently the gain in luminosity is of the order of 100 times. The greatest gain is evidently in the source dimension. Although full use of this effect can be made use of in several cases (such as that discussed above), an even more interesting possibility would perhaps be to try to increase the solid angle at better resolutions ($\gtrsim 0.05\%$). This might possibly be done with ironfree double focusing instruments built for ultra-high resolution. Only electric correctors for spherical aberration have been tried so far. Magnetic correctors, similar to those described in § 8, for reducing the spherical aberration in magnetic lenses would undoubtedly be most interesting to study and might have several practical advantages.

In order to try to increase the attainable precision from $\approx 1 : 10^4$, as obtained with the iron instrument, by one order of magnitude, i.e. $\approx 1 : 10^5$, Siegbahn^{60, 61} designed, in 1952, an *ironfree* double focusing instrument. It consists of two concentric coils

⁶⁰ K. Siegbahn, Physica 18 (1952) 1043.

⁶¹ K. Siegbahn and K. Edvarson, Nucl. Phys. 1 (1956) 137.

with radii $\rho_1=24$ and $\rho_2=36$ cm and height $h = 48.7$ cm (see Fig. 24). The space between ρ_1 and ρ_2 contains the tank ($\rho_0=30$ cm). It turns out that the ratio between the ampere turns of the two coils essentially determines the value of α , whereas the height of the coils h determines β . By means of a simple semi-empirical procedure the $1/\sqrt{\rho}$ field could be produced over the region from ρ_2 to ρ_1 .

Since there are no limiting pole shoes in this case an axially extended spectrometer tank could be conveniently used, according to the requirements of the β -value of $\frac{3}{2}$. Since the external magnetic fields (including the earth's magnetic field) were eliminated by means of a large Helmholtz coil arrangement, the magnetic field was strictly proportional to the current through the spectrometer coils. Field-settings better than 1 part in 10^5 were therefore achieved. With a temperature constancy of better than 0.1° for the different parts in the spectrometer and measuring equipment, and a careful adjustment of the spectrometer, it was possible to obtain a resolving power of better than 2 parts in 10^4 and a precision in the $B\rho$ -measurements of 1 or 2 parts in 10^5 . The electron-optical properties of the focusing system closely followed that expected according to the theory presented above.

The experience from working with this instrument indicated that the resolution region $52: 10^4$ was profitable. Precise $B\rho$ -measurements could be performed and detailed line studies were feasible. The instrument has, apart from radioactivity studies, been used extensively in combination with an X-ray tube to explore the photo-electron method of determining the electron binding energies of the various atomic levels in the elements (see Appendix 2).

The coils of the above simple scheme have to be constructed with great care. The instrument has, however, the virtue of simplicity and precision in alignment. This is perhaps best illustrated by the fact that the recent careful measurements performed by de Vries and Wapstra⁶² in Amsterdam and by the group at Chalk River⁵¹, also using ironfree double focusing instruments, have all yielded results which are in quite satisfactory agreement with those obtained using this early instrument, although somewhat greater weight has to be given to those most recently performed at Chalk River (see § 11 of this chapter and Chapter XVIIIB). De Vries' instrument⁶² is the same as the 30 cm Uppsala instrument concerning coil geometry and ampere turn ratio. The coil pair is, however, provided with an efficient cooling system which permits the focusing of higher energy electrons. Mladjenović⁹ has made a scaled up version of the same instrument with $\rho_0=50$ cm.

Quite recently two ironfree instruments with $\rho_0=50$ cm have been built according to the two-coil system based on computer results concerning the coil geometry, one at Berkeley⁶³ and the other at Uppsala⁶⁴. The resolution obtained is $\lesssim 1: 10^4$.

⁶² C. de Vries and A. If. Wapstra, Nucl. Instr. and Methods 8 (1960) 121;
C. de Vries, Thesis, Amsterdam (1960)

⁶³ K. Siegbahn, C. Nordling and J. M. Hollander (1962) UCRL-10023.

⁶⁴ K. Siegbahn and C. Nordling, Ark. f. Fysik 22 (1962) 436;

K. Siegbahn, C. Nordling, S.-E. Karlsson, S. Hagstrom, A. Fahlman and I. Andersson, Nucl. Instr. and Methods 27 (1964) 173.

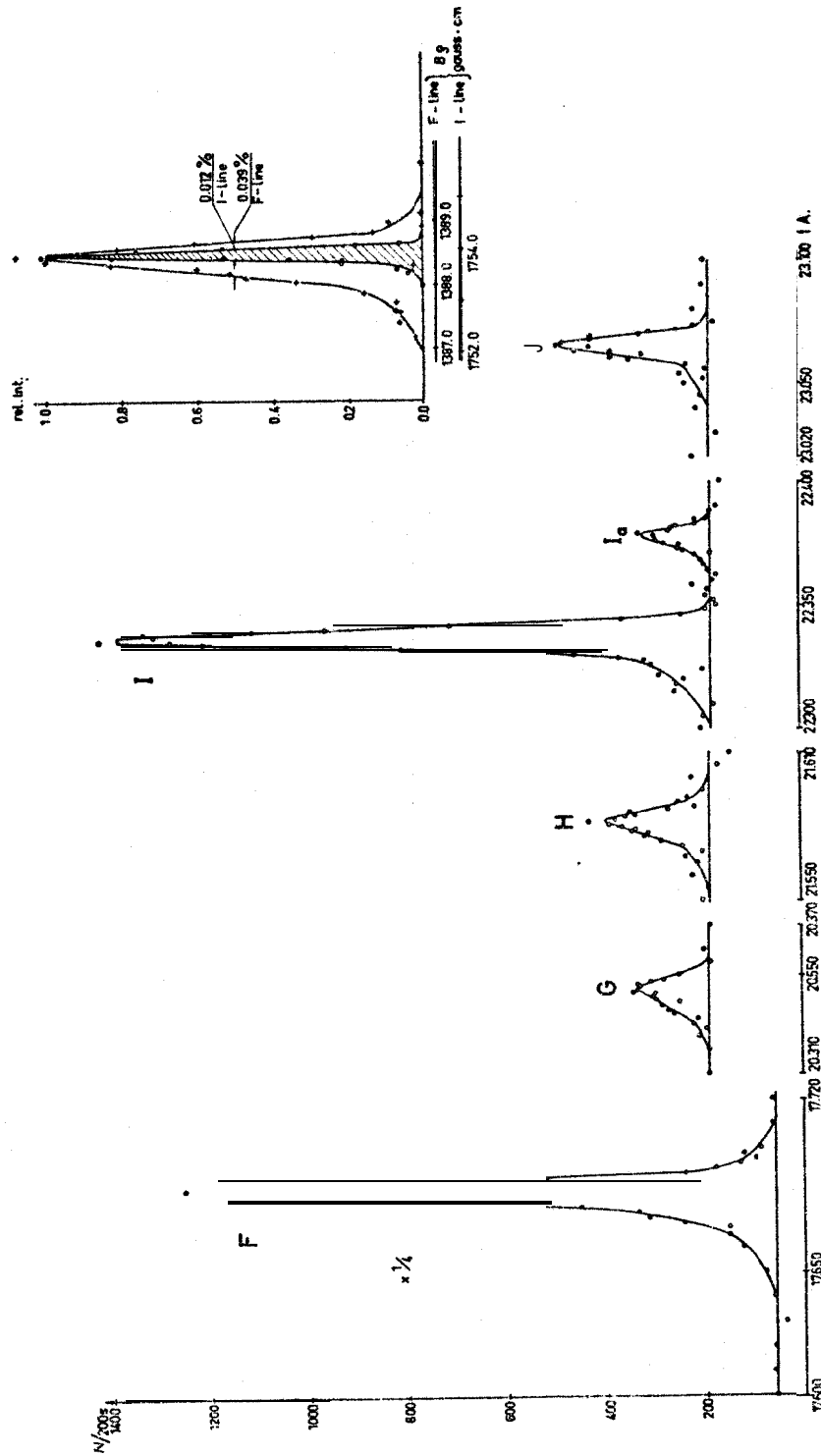


Fig. 25. The F, G, H, I, I_a, and J lines in the spectrum of Th(B+C+C'') taken at high resolution (0.04%) with the $\varrho_0 = 50$ cm ironfree double focusing instrument at Uppsala. In the inset, a comparison of F and I lines taken at a resolution of 0.01 %. The difference in 'inherent' line widths between the two lines is due to the different atomic level widths in the K and L₁ shells, respectively (see Chapter XVIIIB).

Figure 25 shows part of the ThB spectrum taken with the latter instrument. The iso-aberration curves in the HT-plane of this instrument are similar to those of the Chalk River instrument (see Fig. 17). They are slightly more curved and give about the same M-acceptance but somewhat less T-acceptance. This is because of the closer magnetic field fitting (up to the fourth order) of the more elaborate Chalk River coil arrangement. Figure 26 shows the coil arrangement of the Chalk River instrument with $p_0 = 100$ cm. In order to obtain this good field fitting the largest coil radius has been made 200 cm. The radial and axial tolerances are around 0.5 mm for the external coils and around 0.25 mm for the other. The relative tolerances for the two-coil arrangement are about the same. Figure 27 shows how the magnetic field is composed

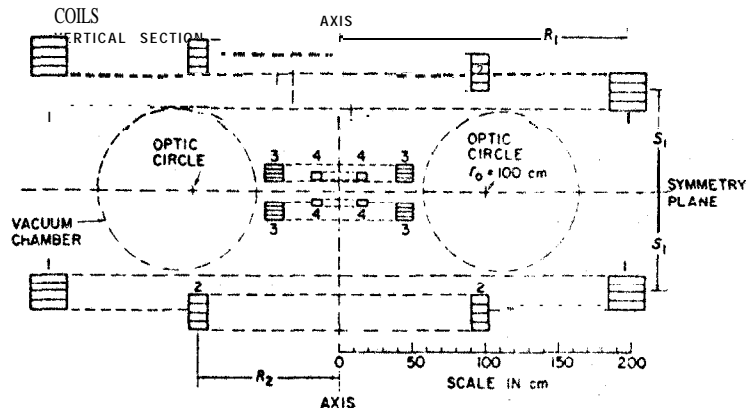


Fig. 26. Coil arrangement of the $q_0 = 100$ cm Chalk River instrument,

of the contributions from the different coils for the Uppsala and the Chalk River systems. Both spectrometer designs allow focusing of 4 MeV electrons. They are provided with automatically operated cooling systems keeping the temperature constant.

As mentioned in connection with the 50 cm high resolution iron instrument, it is quite essential to have such high resolution instruments working under completely automatic conditions. The Chalk River and the Berkeley-Uppsala instruments are provided with such systems that are basically the same (see Fig. 28). The problem for an iron instrument is naturally simpler than for an iron instrument, since in the latter case the *magnetic field* itself, rather than the *current*, has to be measured and stepwise regulated. High precision instruments like these have to be housed in iron-free surroundings, preferably located at some distance from other magnetic-field producing equipment since, unlike the iron instruments, there is no magnetic shielding of the spectrometer field. External fields, including the earth field, have to be accurately compensated for ($< 10^{-4}$ gauss). An improvement over the ordinary Helmholtz two-coil arrangement, which is sufficient for smaller radius instruments like the original

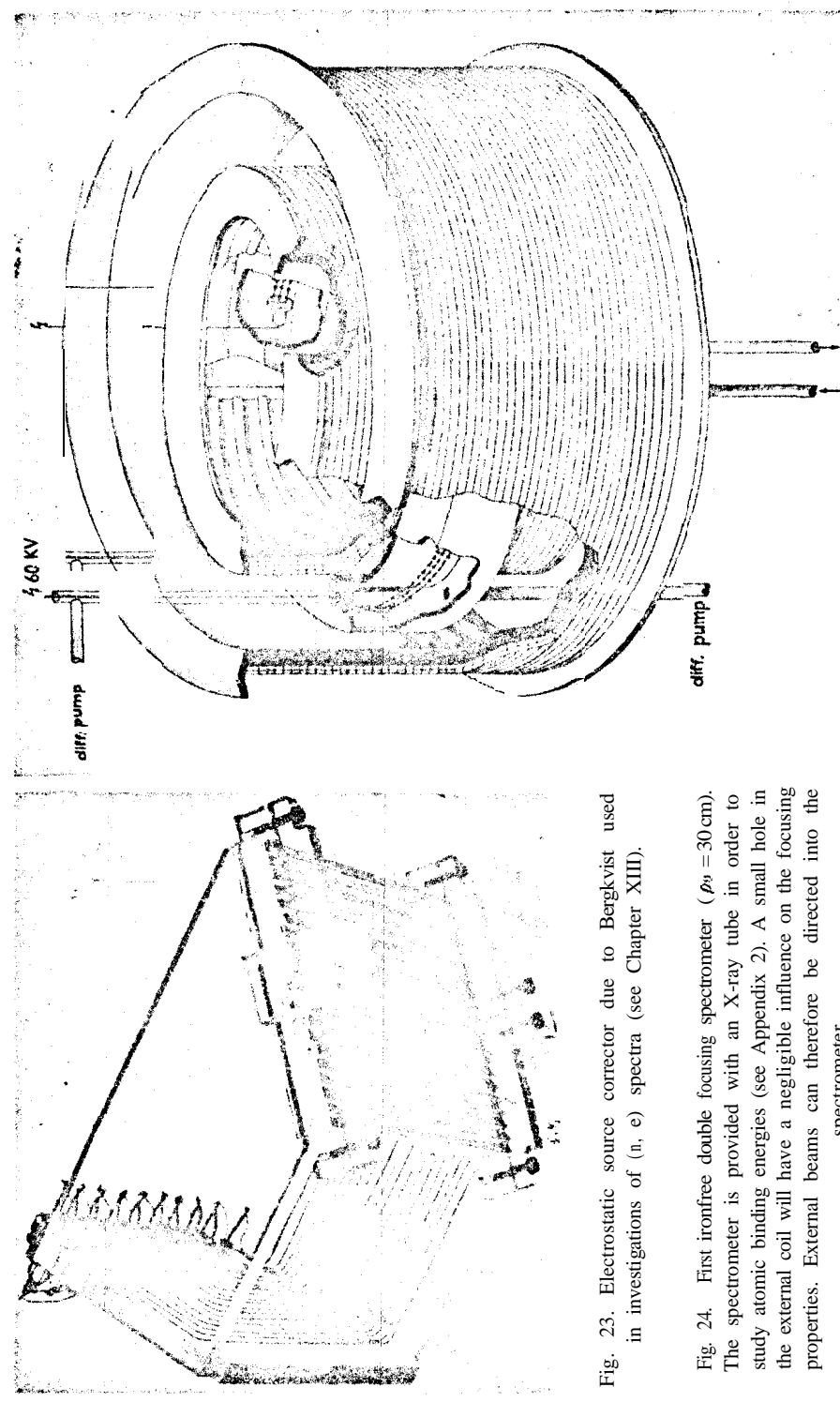


Fig. 23. Electrostatic source corrector due to Bergkvist used in investigations of (n, e) spectra (see Chapter XIII).

Fig. 24. First iron-free double focusing spectrometer ($\rho_9 = 30$ cm). The spectrometer is provided with an X-ray tube in order to study atomic binding energies (see Appendix 2). A small hole in the external coil will have a negligible influence on the focusing properties. External beams can therefore be directed into the spectrometer.

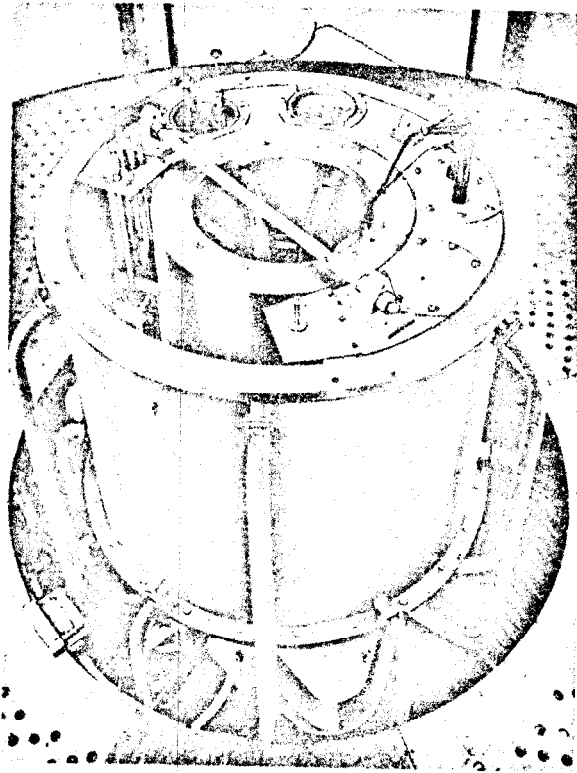


Fig. 29. $q_0 = 50$ cm ironfree double focusing instrument with the two-coil system.

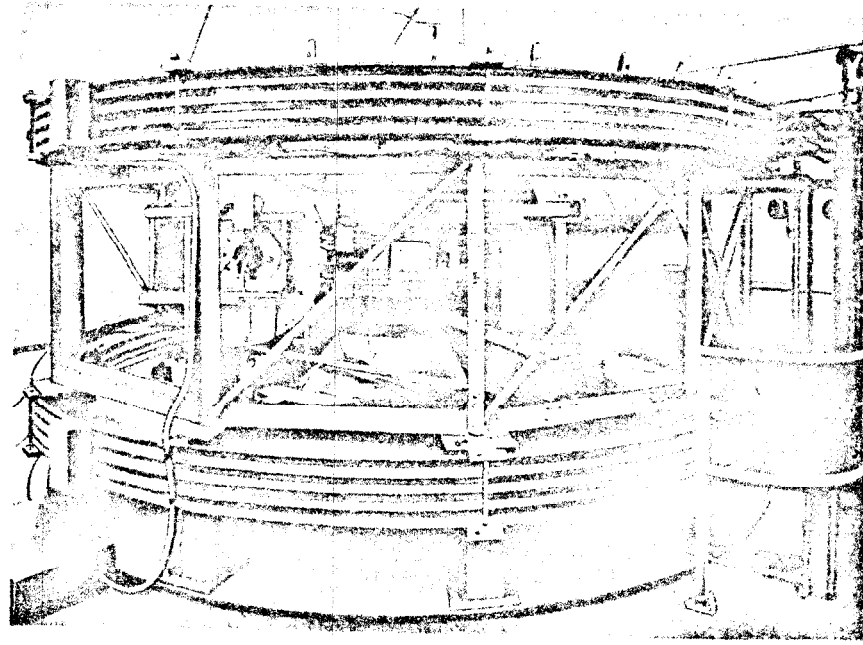


Fig. 30. $q_0 = 100$ cm ironfree double focusing instrument at Chalk River.

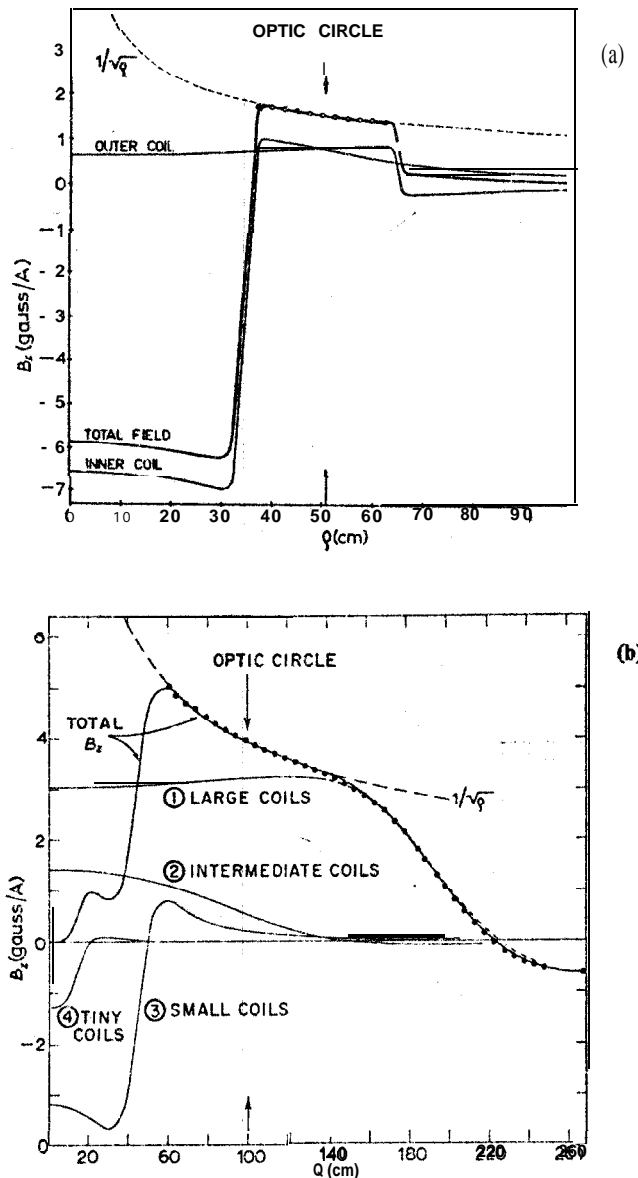


Fig. 27. Contributions to the magnetic field from the different coils of the $Q_0 = 50$ cm Uppsala instrument (a) and the $Q_0 = 100$ cm Chalk River instrument (b).

30 cm one, was worked out by Lee-Whiting⁶⁵ using a four-coil system giving a better homogeneity over a larger volume. The diameter of these coils in the Chalk River instrument is ≈ 9 m and for the Berkeley and Uppsala instruments 6 m. Any residual magnetic field due to imperfections in the compensating coil arrangement, etc., can be corrected for by measuring the field along the optical circle $\rho = \rho_0$

and then using the formula of Hartree⁶⁶ applied to a $\pi\sqrt{2}$ -spectrometer⁶⁷:

$$B_{\text{eff}} = B_0 + \frac{\frac{\pi\sqrt{2}}{0} \int \Delta B(\phi) \sin(\phi/\sqrt{2}) d\phi}{\int_0^{\pi\sqrt{2}} \sin(\phi/\sqrt{2}) d\phi} \quad (48)$$

In practice, this correction is necessary only at very low energies and when the highest precision is required.

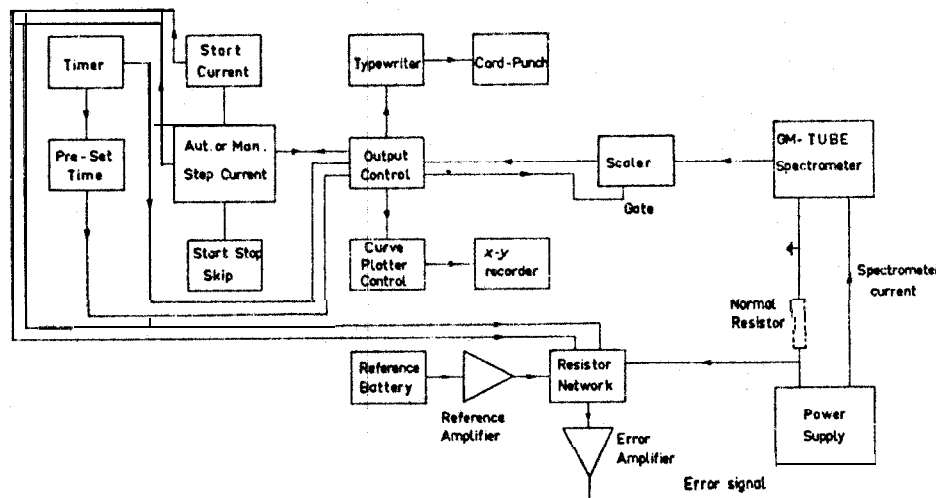


Fig. 28. Automatic current regulating system with outputs for ironfree double focusing instruments. The accuracy and the stability of the current are better than $1 : 10^5$.

Figures 29 and 30 show photos of the 50 cm ironfree instrument at Uppsala and the 100 cm instrument at Chalk River.

The coil system producing a double focusing field can, of course, be varied in an infinite number of ways. The two systems discussed here, namely the compact two-coil system, as originally used and later on improved, and the Chalk River multi-coil system, are only special cases. One multi-coil system was, for instance, built by Moussa and Bellicard⁶⁸ and later on also used by Baird et al.⁶⁹. Baranov⁷⁰

⁶⁶ D. R. Hartree, Proc. Cambridge Phil. Soc. 21 (1923) 746.

⁶⁷ E. Sokolowski, Ark. f. Fysik 15 (1959) 1.

⁶⁸ A. Moussa and J.-B. Bellicard, J. Phys. Radium 15 (1954) 85A; 17 (1956) 532; J.-B. Bellicard, Ann. Phys. (Paris) 13, 2 (1957) 419.

⁶⁹ Q. L. Baird, J. C. Nall, S. K. Haynes and J. H. Hamilton, Nucl. Instr. and Methods 16 (1962) 275; Q. L. Baird, Thesis, Vanderbilt University (1958)

⁷⁰ V. F. Baranov, PTE 1958, No. 3, 15. (Engl. transl. Instr. Exp. Techn. 1958, 334).

has made a small four-coil arrangement for $\rho_0=10$ cm. A comparison between the calculations of the higher order focusing properties of the double focusing field and the actual iso-aberration curves obtained by the coil arrangements discussed above, clearly shows that better coil arrangements no doubt exist. Such would in particular show up in a much better \$-focusing ('observe the abrupt limitation in the T-direction in Fig. 17) resulting in a substantial gain in solid angle at a given resolution. The relevant figures obtained so far, taking the Chalk River values, are: at resolution settings of 1×10^{-4} , 10×10^{-4} and 100×10^{-4} , the corresponding transmissions are 8×10^{-4} , 26×10^{-4} and 110×10^{-4} . Almost identical figures have been obtained by a recently scaled down version ($\rho_0=35$ cm) by Wolfson *et al.*⁷¹.

There are a few interesting possibilities that have been suggested for improving the resolution and the luminosity. In the analysis of the double focusing method given above it is obvious that extremely high resolution can be, and has been, achieved. The limitation is the fact that the radial focusing cannot be made independent of both φ^2 and ψ^2 simultaneously. Daniel⁷² performed a second-order perturbation calculation on the general fieldform expressed by (34) not specifying the value of a . The momentum dispersion is defined as $\gamma=d\rho/d(B\rho)$ (§ 3). The dispersion as described by the *relative* displacement $d\rho/\rho$ for a given *relative* momentum change $d(B\rho)/B\rho$ is also commonly used and is consequently defined as

$$D = \frac{d\rho/\rho}{d(B\rho)/B\rho}. \quad (49a)$$

With the fieldform (34) the so defined dispersion is:

$$D = \frac{2}{1 + \alpha}. \quad (49b)$$

The homogeneous field ($\alpha=0$) yields $D=2$, and the $1/\sqrt{\rho}$ field ($\alpha=-\frac{1}{2}$) yields $D=4$ in agreement with our previous findings. The second order perturbation calculations give:

$$\begin{aligned} \eta^* &= -\eta_0 - \frac{3 + 7\alpha + 4\beta}{3(1 + \alpha)^2} \varphi_0^2 - \frac{1 + 5\alpha + 4\beta}{(1 + \alpha)(1 + 5\alpha)} \psi_0^2 - \\ &\quad - \frac{2\alpha + \beta}{3(1 + \alpha)} \eta_0^2 + \frac{a(1 + 5\alpha) + 2\beta(1 + 3\alpha)}{(1 + \alpha)(1 + 5\alpha)} \tau_0^2, \end{aligned} \quad (50)$$

$$\tau^* = -\tau_0 - \frac{2(1 + 4\beta + 5\alpha)}{(1 + a)(1 + 5\alpha)} \varphi_0 \psi_0 - \frac{4\beta}{1 + 5\alpha} \eta_0 \tau_0. \quad (51)$$

⁷¹ J. L. Wolfson, W. J. King and J. J. H. Park, Cm. J. Phys. 41 (1963) 1489.

⁷² H. Daniel, Rev. Sci. Instr. 31 (1960) 249.

According to (31), the radial and axial focusing angles are:

$$\phi_\rho = \pi \left[1 + \frac{\rho_0 B'(\rho_0)}{B(\rho_0)} \right]^{-\frac{1}{2}} = \frac{\pi}{(1+\alpha)^{\frac{1}{2}}} \quad (52a)$$

$$\phi_z = \pi \left[- \frac{\rho_0 B'(\rho_0)}{B(\rho_0)} \right]^{-\frac{1}{2}} = \frac{\pi}{(-\alpha)^{\frac{1}{2}}} \quad (52b)$$

Radial and axial focusing occur more generally for

$$\phi_\rho^* = m\phi_\rho \quad (53a)$$

$$\phi_z^* = n\phi_z \quad (53b)$$

where m and n are integers. The case $n = 1$ and $m = 1$ corresponds to the 'normal' case.

It was first pointed out by Lee-Whiting⁷³ that the dispersion in the double focusing method increases rapidly by using $n > 1$. It can easily be seen that for double focusing:

$$\phi = \pi(m^2 + n^2)^{\frac{1}{2}} \quad (54)$$

$$\alpha = -n^2(m^2 + n^2)^{-1}, \quad (55)$$

$$D = [1 - (-1)^m] [1 + n^2/m^2]. \quad (56)$$

Obviously, when m is even the dispersion is zero. The maximum dispersion is obtained for $m = 1$. Then

$$D = 2(1 + n^2) \quad (57)$$

$$\phi = \pi(1 + n^2)^{\frac{1}{2}}. \quad (58)$$

Thus, going from $n = 1$ to 2 or 3 the dispersion is increased from 4 to 10 or 20. The drawback with this scheme is, of course, the fact that focusing angles $> 2\pi$ have to be chosen; for $n=2$ or 3, $\phi = 360^\circ + 42^\circ$ and $360^\circ + 209^\circ$. The electrons have to pass the source and the detector before they are focused on its slit. If the electron bundle is wide enough at these passages this drawback may not be too serious. The 'background' caused by this effect can be calculated and it turns out that odd values of n are preferable from this point of view. The 'wide'-aperture case is the more advantageous one in this case.

Optimum values of the coefficients α, β, \dots have been calculated for the wide aperture case by Saulit⁷⁴ and by Huster et al.⁷⁵. Wide aperture focusing of any order for any angle ϕ can in principle be achieved. At $\phi = \pi\sqrt{2}$ one gets additional axial focusing. If these 'wide' aperture calculations are brought to the fifth order⁷⁵ one gets (denoting $C = (\pi/\phi)^2$):

⁷³ G. E. Lee-Whiting, Can. J. Phys. 35 (1957) 570.

⁷⁴ V. R. Saulit, Izv. Akad. Nauk, SSSR Ser. Fiz. 18 (1954) 227.

⁷⁵ E. I-luster, G. Lehr and W. Walcher, Z. Naturforsch. 10a (1955) 83;

G. Lehr Marburger Stizungsberichte 78

47.

$$\begin{aligned}
 &= C - 1 \\
 \beta &= -\frac{7}{4}C + 1 \\
 \gamma &= \frac{19}{8}C - \frac{1}{2}C^2 - 1 \\
 \delta &= -\frac{187}{64}C + \frac{87}{64}C^2 + 1 \\
 \varepsilon &= \frac{437}{128}C - \frac{1587}{640}C^2 + \frac{9}{40}C^3 - 1.
 \end{aligned} \tag{59}$$

It is interesting to note that the case where $\phi = \pi$, i.e. $C = 1$, gives

$$B_z(\rho, 0) = B_0 \left\{ 1 - \frac{3}{4}\eta^2 + \frac{7}{8}\eta^3 - \frac{9}{16}\eta^4 + \frac{51}{320}\eta^5 + \dots \right\}. \tag{60}$$

This is the Beiduk-Konopinski field which is briefly discussed in § 6. This field does not give axial focusing. For $\phi = \pi\sqrt{2}$ ($C = \frac{1}{2}$) one gets the optimum field for wide aperture double focusing:

$$B_z(\rho, 0) = B_0 \left\{ 1 - \frac{1}{2}\eta + \frac{1}{8}\eta^2 + \frac{1}{16}\eta^3 - \frac{31}{256}\eta^4 + \frac{59}{512}\eta^5 + \dots \right\}. \tag{61}$$

Angles of $2\varphi_0 \approx 46^\circ$ and $2\psi_0 \approx 12^\circ$ can be used at a resolution of $\lesssim 1\%$, provided, of course, that the fieldform can be realized accurately over this large solid angle. Calculations show that aberrations do not increase very much with n in the $\pi(1+n^2)^{\frac{1}{2}}$ focusing. Going from $n = 1$ to $n = 3$ the gain in luminosity would be ≈ 23 .

Returning now to eqs. (50) and (51) one notices that, in agreement with the $\pi\sqrt{2}$ case, the aperture aberration is either independent of φ or ψ if:

$$\beta = -\frac{1}{4}(3 + 7\alpha) \quad \text{wide aperture case} \tag{62}$$

or

$$\beta = -\frac{1}{4}(1 + 5\alpha) \quad \text{high aperture case.} \tag{63}$$

Both equations cannot be satisfied simultaneously for any value of $0 > \alpha > -1$. For $m > 1$, however, for instance $m = 3$, solutions exist (see Daniel⁷²), but the α -values are small and consequently the dispersion relatively low. Focusing angles would furthermore have to be more than 2π . Daniel has pointed out that in fact it is not necessary to have radial focusing independent of ψ^2 for a spectrometer with a resolving power independent of both φ^2 and ψ^2 . It is only necessary that the radial aberration is independent of φ^2 . Without first order double focusing, the exit slit can be made curved in order to accept electrons starting with different emission angles. Each emission angle has a corresponding height, τ , at the exit slit. The equation of the exit slit can then be calculated for a convenient choice of parameters. Choosing $m = 1$ and $n = 2$, one gains the advantage of having a strong dependence of ψ on η^2 , a minimum in source height aberration (i.e. high sources can be used), and further, a focusing angle of less than 360° (higher n -values could be used if source and detector are displaced somewhat from $\rho = \rho_0$, in opposite directions). More precisely, α turns out to be $-\frac{9}{13}$, $\beta = \frac{6}{13}$, $\phi = 324.5^\circ$, and $D = 6.5$. Using the higher order calculations

⁷² H. Daniel and L. Jackson Laslett, Rev. Sci. Instr. 31 (1960) 1225; Nucl. Instr. and Methods 10 (1961) 48.

according to reference 76 to shape the most convenient field, it seems possible to achieve extremely good focusing conditions by this procedure. A spectrometer with $p_0=30\text{ cm}$ is now being constructed according to this choice of parameters by Daniel et al.⁷⁷.

The possibility of having a *combination* of different α -values giving a focusing angle less than 2π with improved dispersion has been suggested by Mladjenović⁷⁸. Recently Sessler⁷⁹ has made an interesting analysis of the case where the restriction of axial symmetry on the field is removed. This corresponds to the introduction of azimuthally varying fields as in accelerator techniques (FFAG). In fact, one can show that such a field can make both the radial and the vertical contributions to the spherical aberration vanish in the second order. The higher order calculations are still in progress, as well as the design study of an ironfree configuration of coils to produce this somewhat complex fieldform.

As mentioned earlier, an improved ironfree coil system would make the 'normal' double focusing system, in particular the 'high aperture' case, much more favourable than at present, since full use of the higher order #-focusing has not been realized so far. Probably a compromise between the Uppsala and the Chalk River systems would be a good solution together with a more or less smooth variation in ampere turn density along the z-direction. Such a system provided with electrostatic or, even better, magnetic correctors as discussed earlier would constitute a very powerful high resolution - high luminosity instrument.

With or without correctors, the *information number* $I = n L$, where n is the number of detector slits in the focal plane, can be very high for a double focusing device. This property has to be considered more seriously now after the advent of semiconductors and the development of convenient multichannel storage units.

Third order π focusing, as mentioned on p. 117, deserves some brief comments. The semicircular focusing spectrometer described in § 4 is a first focusing instrument, since the resolving power contains only terms of higher order than the first with respect to the opening-angle φ . It is obviously possible to shape the magnetic field in such a way that the resulting resolving power only contains terms of higher orders in φ . Looking at Fig. 3, this means that the field is shaped so that the internal as well as the external rays B and C are slightly moved to the right until they intersect the central ray A. Naturally this would result in an improvement in resolution at a given opening angle φ . The transmission, however, will, of course, also depend on the type of focusing (or defocusing) taking place in the z-direction. Reiduk and Konopinski⁷⁹ in collaboration with Langer⁸⁰ investigated the fieldform giving a third focusing in φ after 180° . It was found that the appropriate fieldform was given by eq. (60).

⁷⁷ H. Daniel and P. Jahn, Nucl. Instr. and Methods 14 (1961) 353.

⁷⁸ A. M. Sessler, Nucl. Instr. and Methods 23 (1963) 165.

⁷⁹ F. M. Beiduk and E. J. Konopinski, Rev. Sci. Instr. 19 (1948) 594.

⁸⁰ L. M. Langer and C. S. Cook, Rev. Sci. Instr. 19 (1948) 257.

With this fieldform one finds for the base resolution:

$$R^0 = \frac{s}{2\rho_0} + \frac{w}{2\rho_0} + 11.86\psi_0^2 + 2\psi_0^2 \frac{s}{w} + 18.8\varphi_0\psi_0^2 + 2.5\varphi_0^4. \quad (64)$$

The dispersion is the same as in the semicircular case, i.e. half of the double focusing case. Apart from the lower dispersion, the transmission at a given resolution is not as favourable as in the double focusing case, if one considers the axial focusing. It is easy to see that rays *outside* the central ray will experience a slight z-focusing, whereas rays *inside* the central ray will be correspondingly defocused.

In Langer and Cook's spectrometer $\rho_0=40$ cm and $\varphi=32^\circ$. At an estimated transmission of about 0.1 % the resolving power obtained with a 0.4 mm wide source was 0.5 %. The magnetic field in this spectrometer is measured by means of a rotating coil, the induced e.m.f. of which is balanced against a Helmholtz field. The accuracy is around 0.1%. Another of smaller design is due to Bruner and Scott⁸¹, having $\rho_0=15$ cm. In this instrument only rays outside the central ray $\rho_0=15$ cm are used. With $\varphi=33^\circ$ the calculated transmission is 0.2%. The resolving power obtained with a 1 mm wide source was 0.4 %.

Before the theory of one-dimensional, third order focusing was worked out by Beiduk and Konopinski similar focusing had been tried by Korsunsky *et al.*⁸², Dzhelepopov *et al.*⁸³ and also by Voges and Rutheman⁸⁴. These approaches were semi-empirical. The improvement in radial focusing was observed though not perfected. An investigation was also made by Bock⁸⁵ in connection with mass spectroscopy. This improvement of semicircular focusing has been applied in the electromagnetic separation of isotopes in large quantities.

S6. Sector field spectrometers

When good access to the area around the source (and the detector) is required, e.g. in coincidence spectroscopy and in experiments on beams from accelerators, *sector* focusing devices are advantageous. The first to use the double focusing $1/\sqrt{\rho}$ field in this form were Lauritsen *et al.*⁸⁶ who utilized the pole profile of ref. 38 and then arbitrarily cut the field to bend the particles (in this case heavy particles like α and p) through 180° . The source and detector could then be placed outside the field. Since this successful attempt, several heavy particle, double focusing sector spectro-

⁸¹ J. A. Bruner and F. R. Scott, Rev. Sci. Instr. 21 (1950) 545.

⁸² M. Karsunsky, V. Kelman and B. Petrov, J. of Physics 9 (1945) 7.

⁸³ B. S. Dzhelepopov and A. A. Bashilov, Izv. Akad. Nauk SSSR Ser. Fiz. 14 (1950) 263; A. A. Bashilov and V. I. Rernotas, Izv. Akad. Nauk SSSR Ser. Fiz. 18 (1954) 192.

⁸⁴ H. Voges and G. Rutheman, Z. f. Physik 114 (1939) 709.

⁸⁵ C. D. Bock, Rev. Sci. Instr. 4 (1933) 575,

⁸⁶ C. W. Snyder, S. Rubin, W. A. Fowler and C. C. Lauritsen, Rev. Sci. Instr. 21 (1950) 852; Phys. Rev. 74 (1948) 1564;

S. Rubin and D. Sachs, Rev. Sci. Instr. (1955) 1029.

meters have been constructed, e.g. by Mileikowsky⁸⁷, Judd⁸⁸ and most recently by Whaling⁸⁹. One of the most well-known double focusing sector spectrometers with a radius of 1 m was used by Hofstadter⁹⁰ in the studies of the charge distribution in nuclei by electron scattering at high energies. Because of the high magnetic rigidity of these particles it was not possible to use big pole distances and the solid angles were consequently low. On the other hand, the demands on the resolution were high and the maximum solid angles had in any case to be fairly small.

Sector-shaped, *uniform* magnetic fields have been investigated by several workers⁹¹⁻⁹⁵ and in particular the fringing fields have been utilized to obtain double focusing. The second order focusing in the medium plane of such fields has been studied by others^{96, 97}. There exist a number of possibilities of arranging a focusing magnetic prism field, which have been considered in mass spectroscopy⁹⁸.

In β -ray spectroscopy the demands for large solid angles are usually more pronounced, particularly in coincidence spectroscopy. The focusing conditions for a double focusing sector field have been studied by several authors⁹⁹⁻¹⁰¹, and most recently by Sakai and Ikegami¹⁰². They have studied the optimum conditions without explicitly considering the fringing fluxes in the calculations. Judd⁸⁸ has studied the influence of the latter by introducing the factorization approximation (see p. 99). Ikegami¹⁰³ has also given the conditions for second order focusing with curved magnetic boundaries. Sakai *et al.*¹⁰⁴ and Bergström¹⁰⁵ have designed sector double focusing instruments for coincidence purposes.

Barber's law in magneto-optics implies that the source, image and 'bending edge'

⁸⁷ C. Miicikowsky, Ark. f. Fysik 4 (1952) 337; 7 (1953) 33; 7 (1953) 57.

⁸⁸ D. L. Judd and S. A. Bludman, Nucl. Instr. and Methods 1 (1957) 46.

⁸⁹ W. Whaling, personal communication (1962).

⁹⁰ E. E. Chambers and R. Hofstadter, Phys. Rev. 103 (1956) 1454.

⁹¹ W. G. Cross, Rev. Sci. Instr. 22 (1951) 717.

⁹² M. Camac, Rev. Sci. Instr. 22 (1951) 197.

⁹³ M. Cotte, Ann. phys. 10 (1938) 333.

⁹⁴ L. Lavatelli, P. B.-52433 U.S. Dep. of Corn., O. Techn. Serv. (1946) MDDC Report 350.

⁹⁵ C. Reutersward, Ark. f. Fysik 3 (1951) 53.

⁹⁶ H. Hintenberger, Z. Naturforsch. 3a \$1948) 125,669; 6a (1951) 275; Rev. Sci. fnstr. 20 (1949) 748.

⁹⁷ L. Kerwin, Rev. Sci. Instr. 20 (1949) 36; 21 (1950) Q6.

L. Kerwin and C. Geoffrion, Rev. Sci. Instr. 20 (1949) 381.

⁹⁸ See for instance:

K. T. Bainbridge, Experimental Nuclear Physics I (ed. E. Segre; J. Wiley & Sons, New York, 1953) p. 559.
Advances in Mass Spectrometry (ed. J. D. Waldron; Pergamon Press, New York, 1959).

⁹⁹ D. L. Judd, Rev. Sci. Instr. 21 (1950) 213.

¹⁰⁰ N. Svartholm, Ark. f. Fysik 2 (1950) 115.

¹⁰¹ E. S. Rosenblum, Rev. Sci. Instr. 21 (1950) 586.

¹⁰² M. Sakai, Nucl. Instr. and Methods 8 (1960) 61;

M. Sakai and H. Ikegami, J. Phys. Soc. Japan 13 (19%) 1076.

¹⁰³ H. Ikegami, Rev. Sci. Instr. 29 (1958) 943.

¹⁰⁴ M. Sakai, H. Ikegami and T. Yamazaki, Nucl. Instr. and Methods 9 (1960) 154; 25 (1964) 328.

¹⁰⁵ I. Bergstrom and coworkers, personal communication (1963).

REFERENCE ONLY

PHYSICS -111- LAB.

DO NOT REMOVE

of the homogeneous magnetic prism are situated on a straight line. For an inhomogeneous field characterized by the general expression (34) with field constants α, β, \dots one can find a generalization of Barber's law if one introduces the new variables:

$$\phi' \equiv (1 + \alpha)^{\frac{1}{2}}\phi \quad (65)$$

$$l'_{1,2} \equiv (1 + \alpha)^{\frac{1}{2}}l_{1,2} \quad (66)$$

where the subscripts 1 and 2 refer to object and image space. All lengths are given in units of ρ_0 . The lateral 'magnification' M is defined as the ratio of image width to object width.

$$M = \cos \phi' - l'_2 \sin \phi' = -l'_2/l'_1. \quad (67)$$

Figures 31a and 31b show the generalization of Barber's law according to this notation. In the case of $\alpha = -\frac{1}{2}$ one gets:

$$\equiv \phi'_{\alpha=-\frac{1}{2}} = \phi/\sqrt{2} \quad (68)$$

$$\operatorname{tg} \theta_{1,2} = (l'_{1,2})_{\alpha=-\frac{1}{2}} = l_{1,2}/\sqrt{2} \quad (69)$$

$$\theta_1 + \theta + \theta_2 = \pi \quad (70)$$

$$M = \cos \theta - \operatorname{tg} \theta_2 \sin \theta. \quad (71)$$

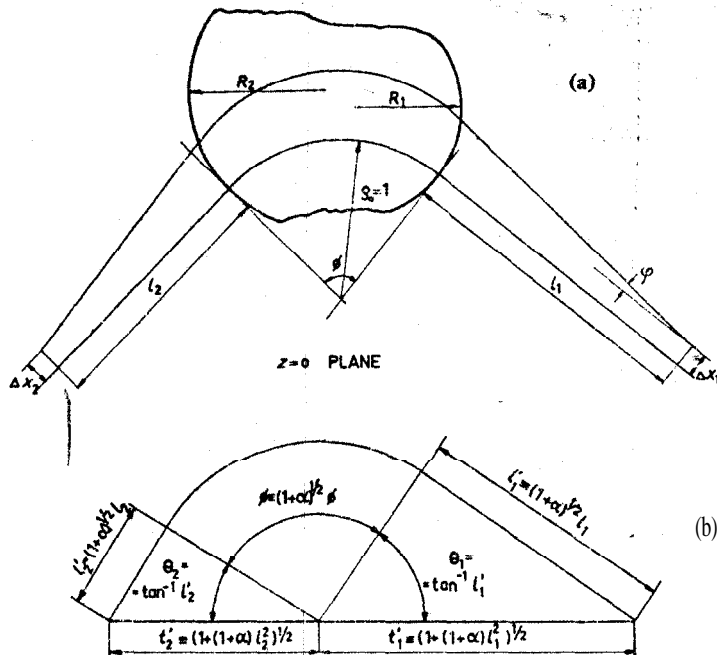


Fig. 31. Radial focusing in a sector shaped magnetic double focusing field.
 (a) Particle trajectories. (b) Generalized Barber's rule.

Particularly favourable is $\beta = \frac{2}{3}$. Rosenblum¹⁰¹ has given the second order aberration for this case as quoted by Sakai:

$$\begin{aligned} \eta^* = M \eta_0 + \frac{1}{6} (\cos \theta - 1) (1 + \cos \theta - 2M) \tau_0^2 + \frac{1}{3} \frac{(2 \cos \theta + 1)}{\sin^2 \theta} \times \\ \times \frac{M - 1}{M^2} [3M - (2 \cos \theta - 1)(M^2 + M + 1)] \psi_0^2 - \frac{1}{3} \frac{(1 - M^3)}{M^2} \psi_0^2 \\ - \frac{\sqrt{2} (\cos \theta - 1)}{\sin \theta} [1 + \cos \theta - M - M^2] \tau_0 \psi_0. \end{aligned} \quad (72)$$

The third term in eq. (72) will vanish independent of θ_2 (i.e. independent of object and image distances) if

$$2 \cos \theta + 1 = 0. \quad (73)$$

In this case $\theta = \frac{3}{4}\pi$, i.e. $\phi = \frac{3}{4}\pi\sqrt{2} \approx 170^\circ$. If this value of θ is set into the last term the condition for making this coefficient vanish is:

$$M^2 + M - \frac{1}{2} = 0, \quad (74)$$

$M = -\frac{1}{2}(1 + \sqrt{3})$ and $\tan \theta_2 = 1$, consequently $\theta_2 = \frac{1}{4}\pi$.

Then, according to Barber's generalized scheme $\theta_1 = \frac{1}{12}\pi$. The aberration is now given by:

$$\eta^* = -\frac{1 + \sqrt{3}}{2} \eta_0 - \frac{2\sqrt{3} + 3}{8} \tau_0^2 - \frac{3 + \sqrt{3}}{2(2 + \sqrt{3})} \psi_0^2 \quad (75)$$

and the line width w

$$w = (1 + \sqrt{3}) \eta_0 + \frac{2\sqrt{3} + 3}{8} \tau_0^2 + \frac{3 + \sqrt{3}}{2(2 + \sqrt{3})} \psi_0^2. \quad (76)$$

According to Judd the dispersion D is given by:

$$D = 2(1 - M). \quad (77)$$

The resolution is then

$$R^0 = \frac{1}{\sqrt{3}} \eta_0 + \frac{2 + \sqrt{3}}{8(\sqrt{3} + 1)} \tau_0^2 + \frac{1}{2(2 + \sqrt{3})} \psi_0^2. \quad (78)$$

Sakai et al. have chosen a slightly different case in their actual design, namely $\phi = 180^\circ$, i.e. $\theta = \pi/\sqrt{2}$ and $l_2 = 0$, i.e. $\theta_2 = 0$. Following the above procedure one then gets $l_1 = 1.86$ and $M = -0.607$. Numerically the resolution with this choice of parameters is:

$$R^0 = 0.38\eta_0 + 0.133\tau_0^2 + 0.021\psi_0^2 + 0.35\psi_0^2 + 1.12\tau_0\psi_0$$

which is also nearly independent of the aberration.

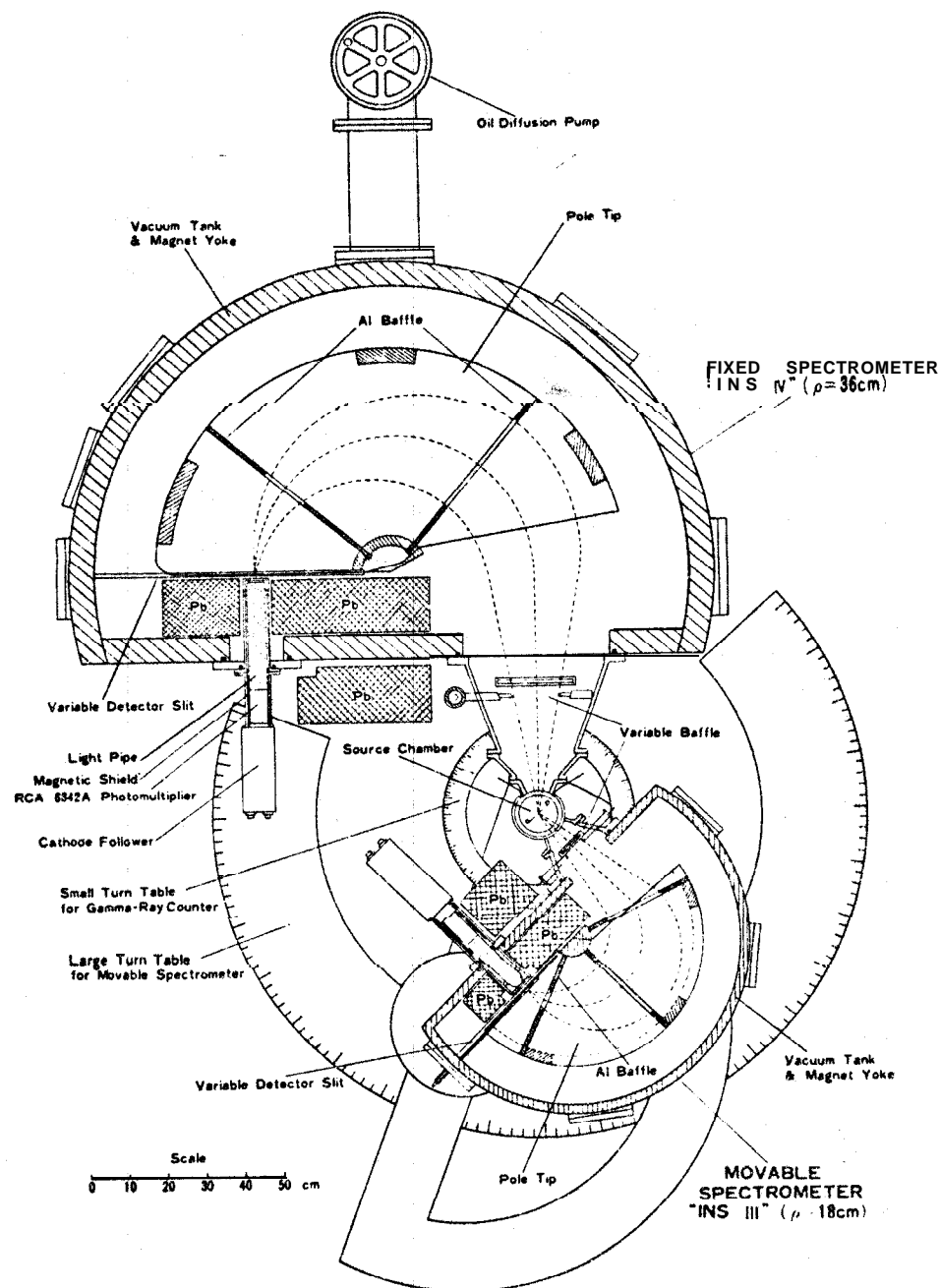


Fig. 32. Electron-electron coincidence spectrometer using two double focusing sector spectrometers.

In practice the fringing flux has to be considered and the simple procedure outlined above has to be modified. According to Coggeshall¹⁰⁶ the effective pole boundary lies 0.6 pole gap outside the actual pole edge. In Sakai's spectrometer the boundaries are made somewhat less than 180° corresponding to this estimate. The magnetic return flux passes through the vacuum tank itself and forms an efficient magnetic shield for the detector. ρ_0 is 18 cm. Maximum transmission is 1% and best obtainable resolution is 0.3%. When the source was 2 cm long and 2.5 mm wide and the detector slit 3 mm wide, the resolution was found to be 0.6% (at half maximum) and the effective solid angle 0.3 %.

Figure 32 shows an arrangement of two such sector spectrometers adapted for e-e coincidences¹⁰⁴. A similar spectrometer with $\rho_0 = 10$ cm has been built by Tendow and Hashizume¹⁰⁷.

Bergstrom's spectrometer is similar, having $\rho_0 = 15$ cm. ϕ is chosen to be 135° and $l_1 \approx l_2$. Due to some remaining aberrations the maximum solid angle that can be used in practice is 1%. The resolution is then as good as 0.27%. The best resolution obtained is 0.14%, but then the transmission had to be reduced to 0.02%.

It is very likely that the sector double focusing instrument can be greatly improved in the future. In particular two problems should be further investigated: the influence of the fringing flux on the focusing and the introduction of curved pole boundaries. Judd's⁸⁸ theoretical treatment of the first problem should form the starting point. He points out that the effects of a fringing field with the extension defined by the parameter a (in units of ρ_0) are primarily the following: (1) The optic axes outside the magnet are bent through angles of the order of a , bringing image and object closer to each other. (2) The symmetrical paraxial conjugate foci (source and image points) are moved a distance of the order of a along the optic axis. (3) The optimum values of β, γ, \dots (i.e. those that eliminate aberrations) are altered from their values in the absence of fringing by amounts of the order of a . Each of these effects may be expanded in a power series in a , the coefficients involving the integrals of the field shape in the fringing region. The field expansion would then be:

$$B(\rho, 0) = B_0 \{1 + \alpha\eta + (\beta_0 + \beta_1 a + \beta_2 a^2)\eta^2 + (\gamma_0 + \gamma_1 a + \dots)\eta^3 \dots\}, \quad (80)$$

For the double focusing a-spectrograph at Berkeley with $\rho_0 = 35$ cm and a pole gap of 2.54 cm, Judd found that $\beta_0 = 0.236$ and $\beta_1 a = 0.032$. At a solid angle of 0.009 steradians the resolution was 0.1%. For a spectrometer with larger solid angle the corrections of the field coefficient may be much greater.

The second problem, namely that of using curved pole boundaries, has been treated theoretically by Ikegami¹⁰³. According to these calculations it is possible to achieve simultaneous double and second order focusing (aberration coefficients of ϕ_0^2 and ψ_0^2 vanish simultaneously). This is because of the new parameter available, namely the

¹⁰⁶ N. D. Coggeshall, J. Appl. Phys. 18 (1947) 855.

¹⁰⁷ Y. Tendow and A. Hashizume, Sci. Papers Inst. Phys. Chem. Res. 57 (1963) 1.

field boundary radius R . If one restricts oneself to the case of a symmetrical spectrometer with $l_1 = l_2 = l$, one obtains:

$$R = \frac{3(1 + \alpha)^2 l^3}{[3(1 + \alpha) + 2(\alpha + \beta) \{2 + 3(1 + \alpha)l^2\}]} \quad (81)$$

The β -value can be chosen so as to minimize the coefficient before ψ^2 . In Fig. 33 the curvature of the field boundary calculated from eq. (81) with $\alpha = -\frac{1}{2}$ is plotted as a function of l or ϕ for several values of β . The dotted curve in the figure indicates Bainbridge's radius in the special case $\alpha = \beta = 0$ (homogeneous sector field).

A further possibility is to extend the second-order focusing calculations for the cylinder symmetrical crossed electric and magnetic field¹⁰⁸ to sector shaped fields.

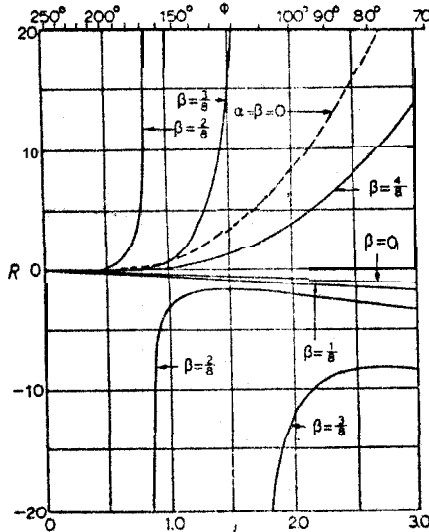


Fig. 33. Relation between the curvature of field boundary R , and object and image distance l , taking the value of β as a parameter for simultaneous double and second-order focusing in the case of symmetrical arrangement. The dotted curve indicates Bainbridge's radius for comparison.

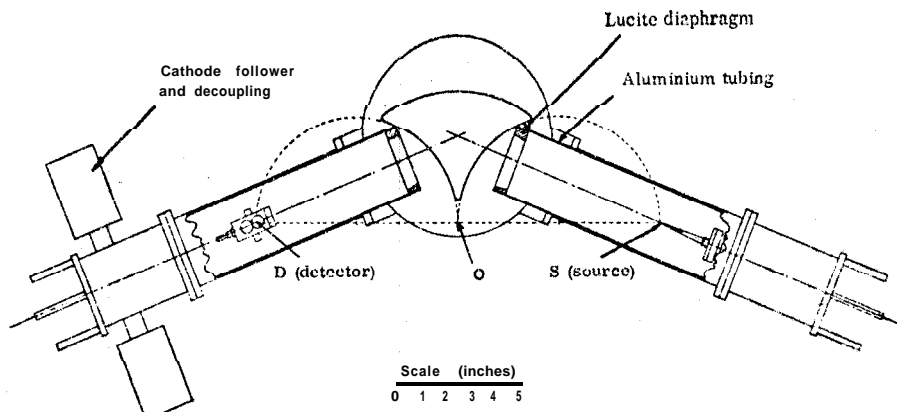


Fig. 34. Prismatic spectrometer due to Bainbridge, Benner and Lavatelli

Bainbridge and Bender¹⁰⁹ first designed a & spectrometer of the prismatic type (see Fig. 34) with an inhomogeneous sector field varying as $1/\rho$, where ρ is the distance to a given point at the centre of the field. The pole piece boundaries were shaped so that a large fraction of the radiation was accepted by the spectrometer. The best resolution obtained was about 0.5 %.

A similar fieldform was first discussed by Richardson¹¹⁰, in which the field varies as $1/\rho$, where ρ is the distance to a symmetry axis through the source and detector. This is the field that is obtained, for example, outside a linear wire, where the lines of force form circular loops around the wire. The same field may be obtained between inclined plane pole faces as investigated by Richardson. A spectrometer of this type has recently been built by Kato *et al.*¹¹¹.

The corresponding sector field was first studied by Kofoed-Hansen, Lindhard and Nielsen¹¹². They showed how the magnetic boundaries should be shaped in order to accept a large angle in the plane containing the source, detector (situated on the z-axis) and the r-direction. Since the field has no components other than $B_\phi = A_0/r$ (B_z and B_r being zero), all the electron trajectories for each ϕ_0 lie in the plane defined by $\phi = \phi_0$. For obvious reasons a simple iron gap instrument can then be designed having, in the first approximation, space focusing properties. The particular virtue of this system is that several such gaps can be added together in an 'orange' array as has been done by Kofoed-Hansen et al. (see Figs. 35a and 35b), who designed a six-gap system. By doing this the transmission at a given resolution is increased in the same proportion to the number of gaps, provided that the individual gaps can be made equal and without interference. Probably the best way of doing this is to produce the $1/\rho$ field in an ironfree way. This has recently been done by a number of workers¹¹³⁻¹¹⁶. A toroid coil with a correctly calculated profile shape has several advantages besides the fact that the usual non-linearities and remanences of the iron are avoided. By making the number of turns large the influence of the

¹⁰⁹ K. T. Bainbridge and R. S. Bender, private communication to M. Deutsch et al., Rev. Sci. Instr. 15 (1944) 178;

R. S. Bender, Thesis, Harvard (1947);

L. Lavatelli, Thesis, Harvard (1950).

¹¹⁰ H. O. W. Richardson, Proc. Phys. Soc. 59 (1947) 791.

¹¹¹ S. Kato, J. Phys. Soc. Japan 13 (1958) 544;

G. Shinoda, T. Suzuki, S. Kato and T. Shikata, Technical Reports Osaka Univ. 10 (1960) 347.

¹¹² O. Kofoed-Hansen, J. Lindhard and O. B. Nielsen, Mat. Fys. Medd., Dan. Vid. Selsk. 25 (1950) No. 16;

O. B. Nielsen and O. Kofoed-Hansen, Mat. Fys. Medd., Dan. Vid. Selsk. 29 (1955) No. 6.

¹¹³ V. V. Vladimirska, Eu. K. Tarasov and Yu. V. Trebukhovsky, PTE 1 (1956) 13.

¹¹⁴ Eu. F. Tretyakov, L. L. Goldin and G. I. Grishuk, PTE 6 (1957) 22;

Eu. F. Tretyakov, L. N. Kondratjev, G. I. Grishuk, G. I. Novikova and L. L. Goldin, Izv. Akad. Nauk SSSR Ser. Fiz. 26 (1962) 1470. (Engl. transl. Bull. Acad. Sci. USSR phys. ser. 26, 1498.)

¹¹⁵ N. A. Burgov, A. V. Davydov and G. R. Kartashov, Nucl. Instr. and Methods 12 (1961) 316.

¹¹⁶ M. S. Freedman, F. Wagner Jr., F. T. Porter, J. Terandy and P. P. Day, Nucl. Instr. and Methods 8 (1960) 255.

M. S. Freedman, private communication (1962).

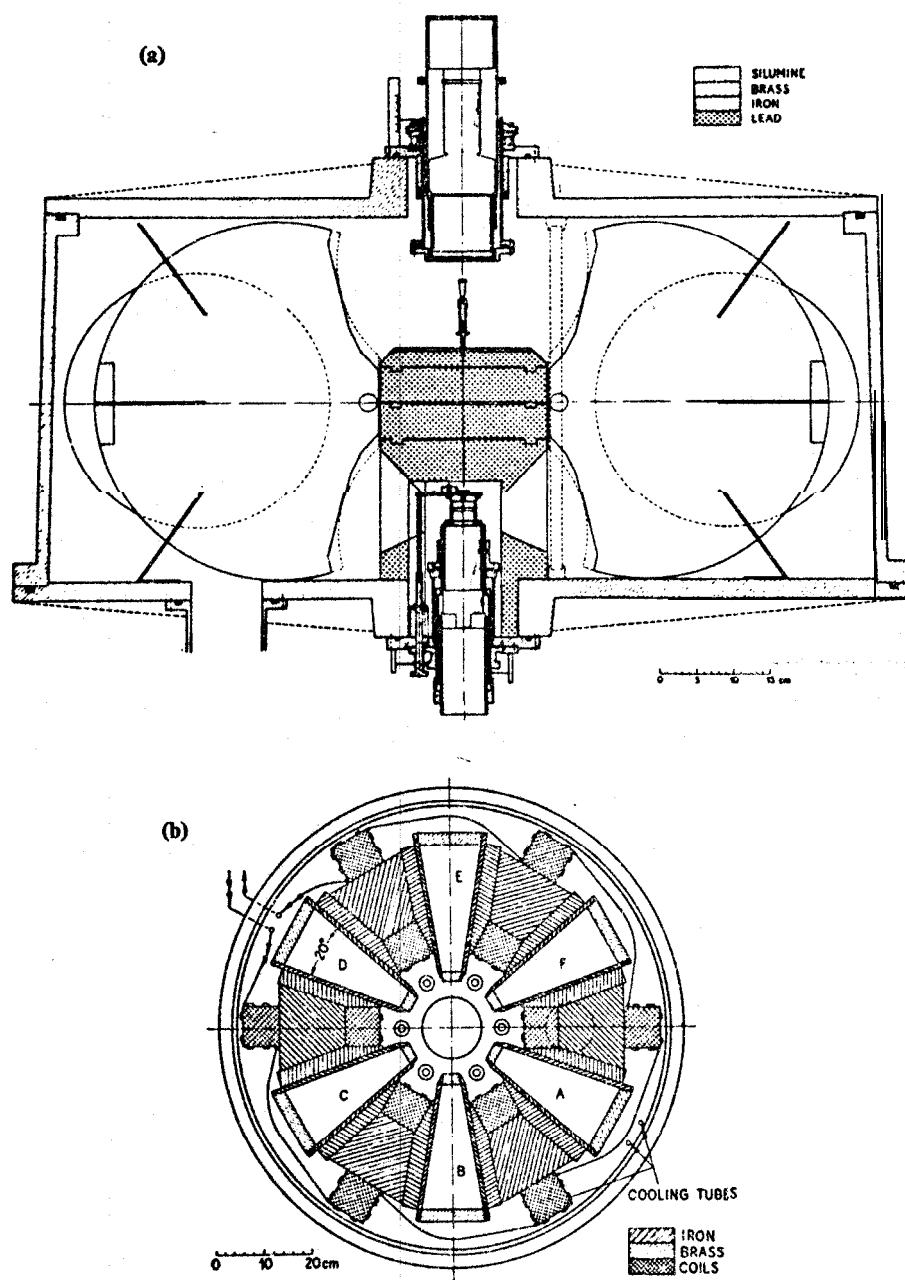


Fig. 35. Six-gap 'orange' spectrometer, (a) vertical section, (b) horizontal section.

fringing flux can be made much smaller, which is particularly important since this is the main cause of aberrations in the focusing system. Since the iron plates will become limiting factors in accepting a large solid angle and the shape of the coil geometry can also be attained more accurately by employing theoretical calculations, this 'ironfree toroid' spectrometer seems particularly useful for high transmission work. Transmissions as high as 20% can be obtained at a resolution of the order of 1%.

A brief summary of the relevant theory will be outlined here. For a more detailed account the reader is referred to the above quoted papers and in particular the more recent ones by Jaffey *et al.*¹¹⁷ (giving a very complete treatment of particle trajectories, boundary shapes, dispersion, resolution, and transmission, taking into consideration the effects of the fringing fields upon the image formation), and Burgov *et al.*¹¹⁵ who have given a survey of some of the most important formulas.

The K-value of a particle trajectory is defined by:

$$K = -\frac{mv}{A_0 e} = -\frac{p}{A_0 e} = \frac{B\rho_c}{A_0} = \frac{\rho_c}{r} \quad (82)$$

where ρ_c is the radius of curvature of the trajectory and r the distance to the z-axis. The K-value is dependent on the shape of the boundary and should be chosen to minimize aberrations. The general expression for the motion of the electrons in the field under consideration was derived by Richardson and was put into the following convenient form by Kofoed-Hansen *et al.*:

$$z = a K U(K, \psi) + z_m \quad (83)$$

$$r = a e^{-K \cos \psi} \quad (84)$$

where $z=z_m$ for $\psi = \pi$, and $r=a$ when $z=0$. $U(K, \psi)$ is the following function:

$$U(K, \psi) = \int_{-\pi}^{\pi} \cos \psi e^{-K \cos \psi} d\psi. \quad (85)$$

U can be expanded in a series of Bessel functions and is tabulated in the paper by Jaffey *et al.* The particle trajectory and notations used in these equations can be seen from Fig. 36. The particles describe a series of loops, each loop displaced relative to the other by an amount

$$z(\psi + 2\pi) - z(\psi) = 2\pi a K i J_1(iK). \quad (86)$$

Passing to the sector case, one requires that the straight electron paths from a point source on the z-axis when passing the magnetic boundary from $B=0$ to $B \approx 1/r$ join the curved trajectories inside the toroid in a continuous way (see Fig. 37). In order to eliminate 'ghost' peaks it is preferable to use paths without any loops, although in principle some advantage might be obtained concerning resolution (at the cost of

¹¹⁷ A. H. Jaffey, C. A. Mailman, J. Suarez-Etchepare and T. Suter, Argonne National Laboratory Report ANL-6222 (1960).

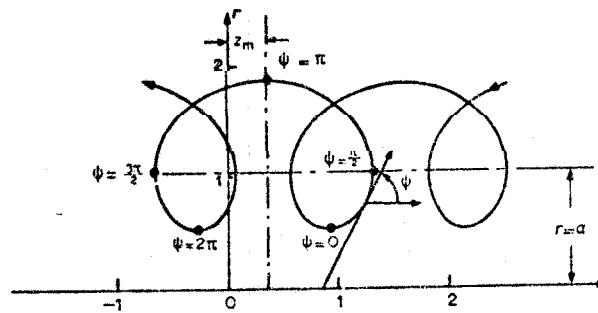


Fig. 36. Particle trajectories and notations used in treating the properties of the toroidal field $B = A_0/r$.

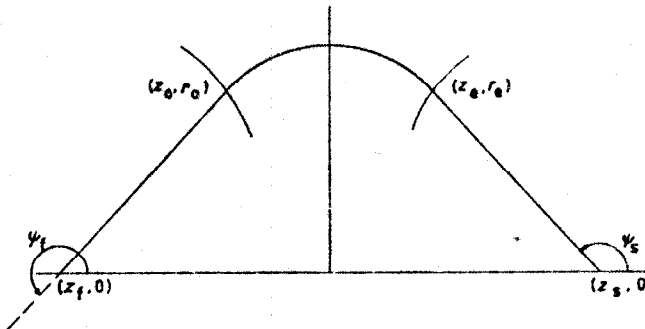


Fig. 37. Scheme for calculating equation of boundaries of toroidal sector coil.

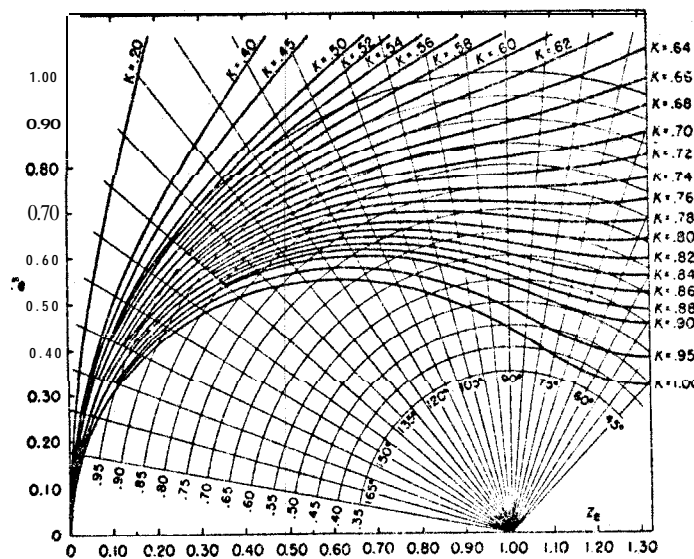


Fig. 38. Shapes of symmetric entrance and exit boundaries in toroidal focusing for different K -values.

transmission) by using loop trajectories. In the same way one requires that the boundary at the exit side of the toroid is given a form such that the trajectories passing into the fieldfree region join smoothly to the straight paths and furthermore that these straight paths converge towards one common point, the image, on the z-axis. These calculations are straightforward and yield the equations of the boundaries.

There are some practical advantages in making the entrance and exit boundaries equal, which results in a symmetric spectrometer. Fig. 38 shows the boundary in this case using the K-value as a parameter. Taking the aberrations due to the influence of the fringing field into consideration, it is advisable to choose boundaries that coincide as nearly as possible with circles so that all electrons approach the boundary nearly perpendicularly. A K-value somewhere between 0.5 and 0.6 is then convenient. The loss in transmission due to the lens action of the fringing fields at the boundaries actually slightly favours a K-value near 0.6.

Since the aberrations in the toroidal focusing are determined by the action of the fringing flux, a careful analysis of the different factors is essential. To a certain extent this can be done analytically when an ironfree system is used. In such cases one can even arrive at closed expressions for the aberrations. As an example, Burgov¹¹⁵ treats the somewhat simplified problem of the fringing flux between n infinite wires of a given shape. One can also use computer techniques. Jaffey et al. have given an extensive treatment of the different aberrations. For iron instruments empirical procedures are convenient and have been discussed in detail by Bisgard¹¹⁸.

The fringing field at a certain point on the boundary somewhere between two adjacent wires or pole shoes can be separated into different field components and to the first order it is possible to treat the entire perturbation as a linear superposition of the different effects. If we disregard the bowing of the lines of force toward larger r owing to 'mutual repulsion', one can distinguish the following three main causes of aberrations :

- (a) The ϕ -deflection due to the B_ϕ -component of the fringing field. This component is in the same direction as the interior toroidal field and consequently causes an additional change in the ϕ -coordinate of the trajectory in the same direction as the focusing field. The added ϕ -deflection is equivalent to having a larger field region, i.e. the *effective* boundaries are *outside* the real ones. Furthermore, since the fringing field has different effects for different ψ_s -values, the profiles computed from the simple theory outlined above will no longer be quite correct. This can be compensated for by reducing the region enclosed by the profile and changing the profile somewhat.
- (b) Variation of the ψ -deflection with ϕ_s . In the *median* plane in the gap we have $\mathbf{B} = \mathbf{B}_\phi$. On all other non-median planes the value of the B_ϕ -component is different. The trajectories passing the median plane have therefore different ϕ -deflections in the fringing field to the non-median trajectories. Although the profile, as discussed under (a), may be corrected for the change in ϕ -deflection on the median plane, this correction does not remove the variation of ϕ -deflection with ϕ_s .

¹¹⁸ K. M. Bisgard, Nucl. Instr. and Methods 22 (1963) 221; Nucl. Instr. and Methods (1964)

(c) Lateral deflections due to \mathbf{B}_\perp . The fringing field at a given point at the entrance can be decomposed into \mathbf{B}_ϕ and \mathbf{B}_{rz} , the latter being in the rz-plane (see Fig. 39). This component can be further separated into B_t and \mathbf{B}_\perp , B_t being directed along the trajectory and \mathbf{B}_\perp normal to it. This component of the fringing field acts as a *cylindrical lens* and transforms a point source into a line image. The lens action is zero at the median plane ϕ_M and increases with $\phi - \phi_M$. It is not constant along the boundary but varies with ψ_s . Actually, with an appropriate field shape the lens action can gradually change with ψ_s from a converging to a diverging cylindrical lens.

The lens action causes a point, source to become a line image with the extension perpendicular to the rz-plane. Thus the optimum slit for a single sector instrument

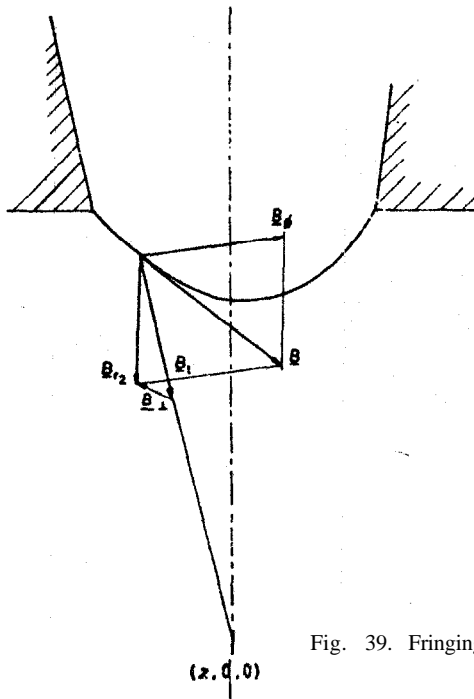


Fig. 39. Fringing field components in toroidal sector focusing.

should have the shape of a distorted line which is narrowest at the z-axis and symmetrically fans out at the ends to an extent determined by the ψ_s range covered. This curvature is marked only when the gap angle is large. If a toroidal geometry or a multigap arrangement is used, then the lack of focusing in the one dimension would cause a loss in resolution, since two sectors at 90° to each other would require a detector slit which had to be much broader than for a single sector in order to collect the radiation. For an iron instrument this difficulty can be overcome by tilting the z-axis of each sector somewhat from each other so that each sector may have its own slit (a common detector may still be used). toroidal instruments however must be built with a coincident z-axis. For this case it is feasible to use a

ring focus arrangement (see Fig. 40) similar to that used for lens spectrometers (see S8). In order to do this one has to shape the boundary so as to give a non-axial focus for finite sources. This has recently been done¹¹⁹.

The dispersion can be calculated by an ordinary variation procedure (see e.g. Jaffey *et al.*¹¹⁷). If we use the definition of the dispersion factor

$$G = \frac{\delta z_t / (z_s - z_t)}{\delta p/p} . \quad (87)$$

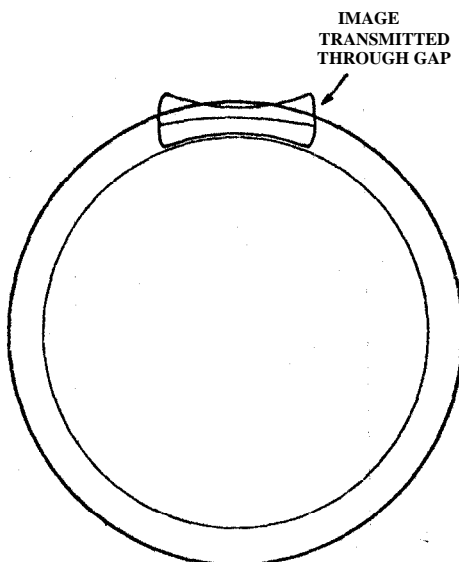


Fig. 40. Ring focus arrangement for accepting image, distorted due to lens action of fringing field in toroidal sector focusing.

This quantity is independent of the size of the instrument. Another way to define the dispersion is

$$\sigma_t = \frac{\delta z_t}{\delta p/p} . \quad (88)$$

In the symmetrical case

$$\sigma_t = 2z_s G . \quad (89)$$

G is plotted in Fig. 41 as a function of ψ_s with K as a parameter. In the same units the dispersion factor for the semicircular spectrograph is G = 1.

The resolution depends on the details of the perturbations due to the fringing fields. Although these can be approximately calculated, at least for the toroid ironfree case, it is better to give here some representative figures for recent spectrometers.

In the six-gap iron instrument by Bisgård¹¹⁸, which is an enlarged and improved

¹¹⁹ P. Moll, Labor. f. techn. Phys. T. H. Miinchen, private communication (1963).

version of the original spectrometer due to Kofoed-Hansen et al.¹¹², the diameter of the magnets $2R=100$ cm, the distance between source and focus $2z_s=340$ mm, and there is a mean dispersion of ≈ 600 mm. Some figures of merit are (source $2 \times 6 \text{ mm}^2$):

$$\begin{array}{ccc} T = 1 & 5 & 10\% \\ R = 0.4 & 0.8 & 1.4\% \end{array}$$

The resolution versus the transmission when source dimensions can be neglected fits the relationship $T^2=1.25R-0.0075$, as shown in Fig. 42. For comparison the corre-

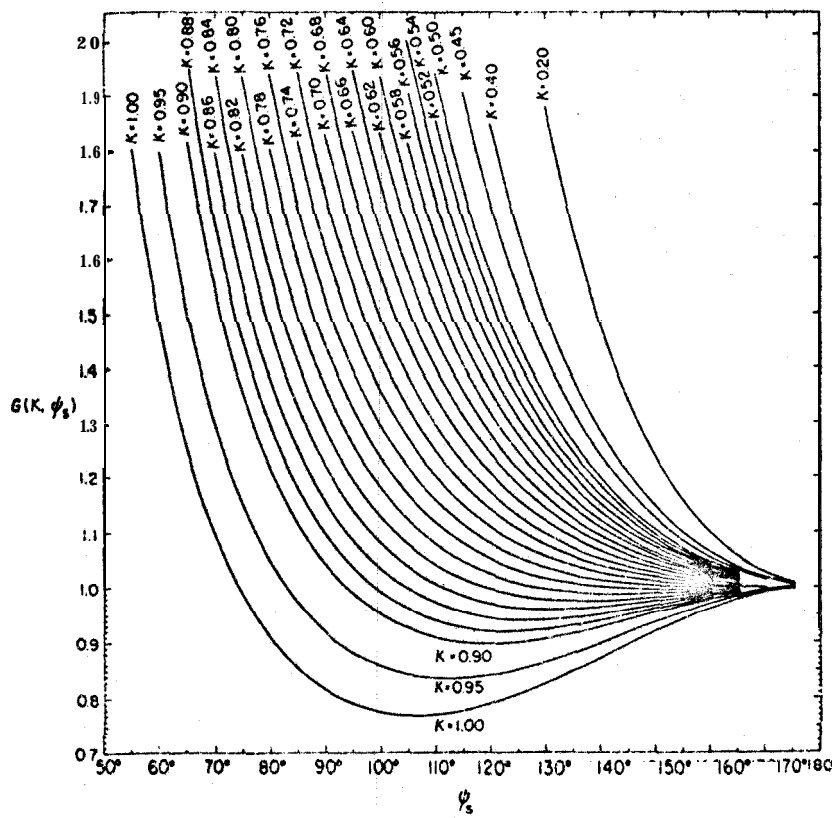


Fig. 41. The dispersion factor G versus ψ_s (defined in Fig. 37) for various K -values. For the semi-circular case $G = 1$.

sponding theoretical curve valid for a homogeneous field ring focus spectrometer with an axial emission angle $\alpha=45^\circ$ is inserted. The corresponding relation (see § 8) is $T^2=0.16R$. The transmission is at least a factor of 2 better at optimum transmission for the six-gap spectrometer. According to Bisgard the luminosity $L=AT$ for the six-gap instrument is 10 times greater than the solenoidal one but $\frac{1}{6}$ to $\frac{1}{20}$ of the double focusing type. The luminosity improvement by using aberration correctors for the lattice type discussed in the previous section (see p. 108) is not included in this comparison. In one sense, such correctors may be regarded as equivalent to using

the degree of freedom of shaping the boundaries of sectors. Toroidal spectrometers have also been constructed at Brookhaven¹²⁰ and Buenos Aires¹²¹. Another type of toroidal spectrometer has been developed in Hungary by Horvath, Szalay and Berényi¹²².

Ironfree toroidal spectrometers can be designed to have improved figures of merit. Such instruments were first built by Vladimirs^{ky}¹¹³ and Tretyakov¹¹⁴. The instrument by Burgov *et al.*¹¹⁵, which is designed with the particular purpose of allowing work with gaseous sources, has a maximum solid angle of 20%. At a transmission of 13%

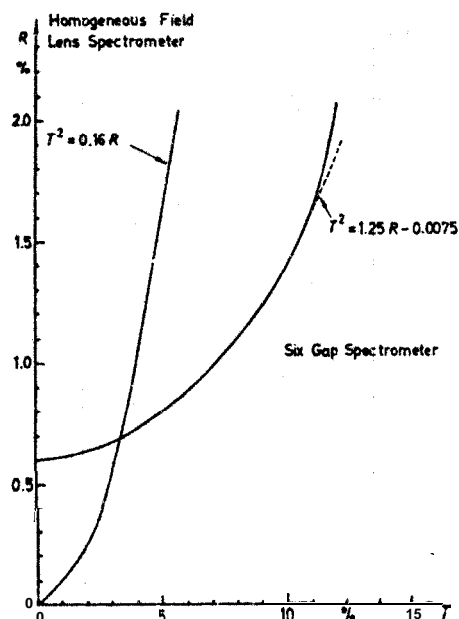


Fig. 42. Resolution versus transmission for a six-gap spectrometer according to Bisgard. The corresponding relation for a homogeneous ring focus lens spectrometer is inserted for comparison.

the resolution for a gaseous source (diameter 10 mm, height 12 mm) is 2.3%. Freedman *et al.*¹¹⁶ have made an extensive design study of the optimum conditions of the toroidal spectrometer. They have built an instrument consisting of two identical independent toroidal coils of 1 meter over-all diameter mounted 15 cm apart in a 1.15 meter diameter, 1.6 meter long vacuum chamber (see Fig. 43 and 44*). Each coil consists of 100 turns with gaps between through which the electrons can pass. The K-value has been chosen to be 0.59 and in this choice the cylindrical lens defocusing effects discussed above have been decisive. Electrons emitted between 30° and 70°

* Facing p. 152.

¹²⁰ E. L. Church, Bull. Am. Phys. Soc. 8 (1963) 390, XA9.

¹²¹ C. A. Mailman, Physica 18 (1952) 1139; Publ. CNEA (Argentina) 1 (1953) No. 1.
L. Lagatta, C. A. Mailman, C. Molina y Vedia, 3. Peyre and J. Suarez-Etchepare, Second U.N. Inter. Conf. on Peaceful Uses of Atomic Energy, Reports 1973, 1974.

¹²² I. Horvath, Experientia 5 (1949) 112;
A. Szalay and D. Berenyi Acta Physica, Acad. Sci. Hung. 10 (1959) 57.

to the axis can be focused, $2z_s = 67$ cm. With a 3 mm diameter source the transmission is 19% and the resolution 0.93 %. At a transmission of 2.8 % the resolution is 0.21 %. A practical problem in the coil design is the difficulty of space for the necessary ampere turns. In the present case focusing of 4 MeV electrons requires 1300 A at 140 kW. The instrument can be used for electron-electron coincidences giving exceptionally high coincidence efficiency. By inserting γ - and r-detectors coincidences between electrons and γ - or -particles can also be taken. The double toroidal spectrometer can also be run in 'tandem' fashion, allowing a slight increase in resolution at essentially unchanged transmission.

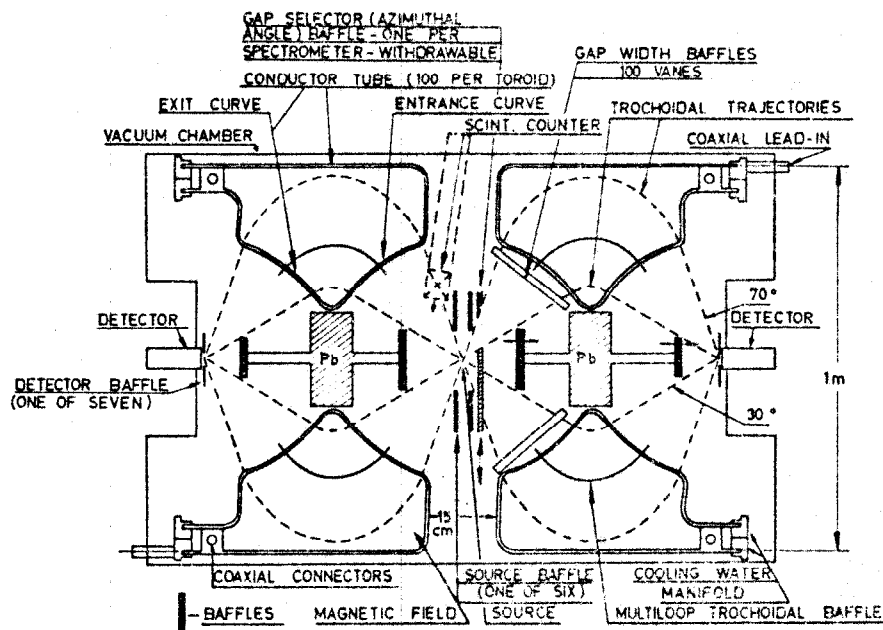


Fig. 43. Scheme of the Argonne double toroidal spectrometer. Maximum transmission 19% at a resolution of 0.93 %.

A precision prism \$-spectrometer has been built by Kelman and coworkers¹²³. It is interesting to note that a scheme for a similar type was suggested by Klemperer in 1935 when he made the first design of a short lens (see § 8). It is a close analogue to the optical spectroscope consisting of one collimator lens, one dispersive prism and one focusing lens. Figure 45 shows Kelman's arrangement. The collimator lens forms a parallel beam which enters the rectangular prism. It is important that this deflecting field is 'two-dimensional' in the sense that it is constant in the direction parallel to the x-axis. As discussed above the fringing field has the action of a cylindrical lens

¹²³ V. M. Kelman, B. P. Peregud and V. I. Skopina, Zhur. Tekhn. Fiz. 32 (1962) 1446; 1465. (Engl. transl. Soviet Physics - Techn. Phys. 7, 1068, 1082.) Further references are given in this paper.

and the strength of the field (i.e. the angle α) is chosen so that the line focus is situated on the x -axis, thus providing a symmetrical passage of the beam through the prism. It consequently emerges from the prism and forms a parallel beam with $\alpha_f = \alpha_c$. This beam is then brought to a focus by the focusing lens. Contrary to other devices, one has separated the dispersive and focusing actions. It can be shown that the linear dispersion of this electron-optical system is

$$D = 2f_t \operatorname{tg} \alpha \quad (90)$$

Evidently the dispersion can be simply increased by increasing f_t , which is the focal distance of the focusing lens. If a line source is used, one has to compensate for the

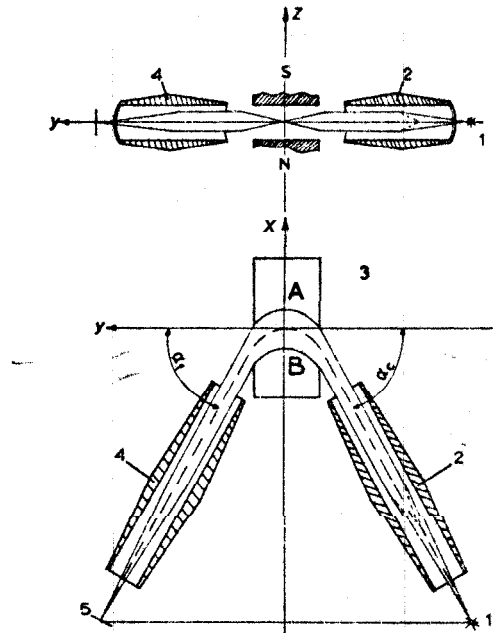


Fig. 45. Electron-optical scheme of Kelman's spectrometer. (1) Radioactive source; (2) collimator lens; (3) deflecting magnet; (4) focusing lens; (5) detector slit.

rotation of the image of the magnetic lenses (see § 8). For this purpose one rotates the source in the spectrometer through an angle which is equal in magnitude and opposite in direction to the angle of rotation of the image in the collimator lens and turns the detector slit in the direction of the rotation of the image in the focusing lens and sets it parallel to the image.

The spherical aberration of a magnetic lens is of the third order in aperture angle and leads, for a point source, to a confusion disk with diameters d_c and d_t . The broadening of the image in the detector plane, due to the spherical aberration of the lenses, is then

$$\Delta_{\text{sph}} = d_c M + d_t \quad (91)$$

where $M = f_t/f_c$ the magnification.

The spherical aberration of the lens action of the prism will cause a broadening of the line focus which in turn causes a spread of angles in the vertical direction in the beam which has passed through the prism. A point source will therefore form a line image but the direction of this is parallel to the direction of the detector slit, and consequently the aberration of the prism will not contribute to the resolving power of the spectrometer. It is furthermore easy to show that a finite length of a line source will not cause a line broadening but a slightly curved line image. The slit should be shaped according to this curvature. The resolving power can then be written

$$R = \frac{\Delta_{\text{image}} + \Delta_{\text{slit}}}{2D}, \quad (92)$$

$$\Delta_{\text{image}} = sM + \Delta_{\text{sp.a}} + \Delta_{\text{ts}}. \quad (93)$$

The image broadening, Δ_{ts} , appears because of the difficulty in matching the lens and prism fields exactly. If a misadjustment in one of the lenses corresponds to a change in current of ΔI and d is the width of the parallel beam, an approximate value of Δ_{ts} is:

$$\Delta_{\text{ts}} \approx 2d \Delta I/I. \quad (94)$$

If d is 5 cm, $\Delta_{\text{ts}} \approx 10 \Delta I/I$. Consequently this adjustment is rather critical. The other difficulty is the requirement of having the two-dimensional property of the prism. Actually this condition can be somewhat modified, namely:

$$\phi = \int_{-\infty}^{\infty} B(I) \cos \alpha(I) dl = \text{constant} \quad (95)$$

where I is the distance measured along any trajectory.

The magnetic lenses have to be well shielded from the prism field (and vice versa) and have therefore been made in a slightly unusual way. Magnetic lenses are treated in S8. It can be shown that an ordinary lens is fairly well described by the field along the axis:

$$B(z) = \frac{B_0}{1 + (z/a)^2}. \quad (96)$$

One can avoid disturbing tails in the field distribution at large r by means of a magnetic shielding screen of iron and distributing the coil turns along the tube as shown in Fig. 46. It is then found that the field has practically dropped to zero at 20 cm from the edge of the lens tube.

The adjustments of this spectrometer are more elaborate than for most other types. Some of these have been briefly discussed above. Figure 47 shows the adjustment of the angle of deflection $\alpha (\approx 57^\circ - 58^\circ)$. A change in transmission is performed by lengthening or shortening the source-to-center distance of the collimator lens. This in turn requires new sets of values for currents, changes in the compensation for

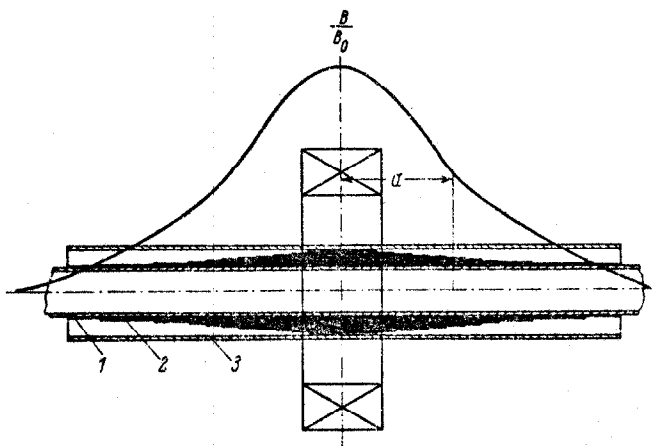


Fig. 46. Construction of the magnetic lens. (1) Spectrometer tube; (2) distributed winding; (3) shielding screen.

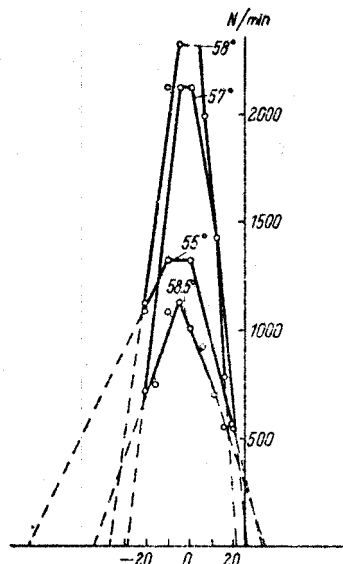


Fig. 47. Dependence of the counting intensity at the peak on the position of the detector slit for various values of the angle α . The abscissas give the displacement of the detector slit in mm along a vertical line from its original position (0). The value of the angle α is indicated for each curve.

rotation of the image, etc. The large value of the dispersion is noteworthy, however, which is due to the fact pointed out before, that D can be increased without loss in transmission simply by changing f_1 . For $\alpha=57^\circ$ and $f_1=127$ cm D is 3.9 m according to (90). For a source slit of 1 mm the 'geometrical' term for the resolution gives $R=0.027\%$. The experimentally obtained value is 0.036%, which shows that if care is taken the instrument can be very well adjusted. The resolving power is found to vary from 0.014% at a solid angle of 0.005% to 0.20% at 0.8%. The instrument is more or less inherently an iron one, since an ironfree design, if possible, would probably cause difficulties due to stray fields etc. The accuracy in energy

ments are therefore not primarily set by the resolving power but by non-linearities. Within small energy regions it is found, however, that the reproducibilities in energy and intensity measurements are 0.02 % and 2-3 %, respectively. Figure 48 shows a conversion Spectrum of the L and M-subshell groups from the 316 keV γ -line of Pt^{192} . For convenience, instead of changing the spectrometer current over this small energy interval, a voltage over the source has been varied stepwise. A β -spectrometer of the same design has also been built by Mazets and Sergeenkov¹²⁴.

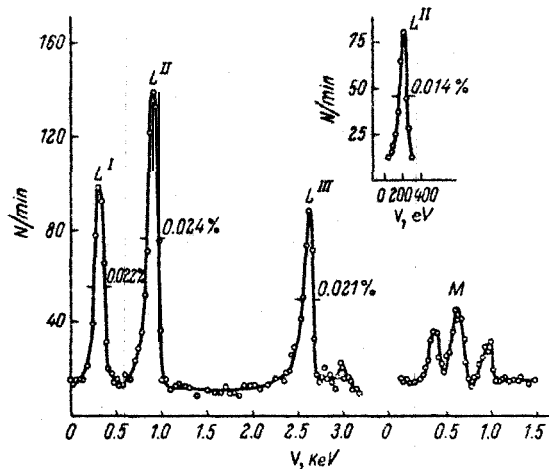


Fig. 48. L and M conversion lines of the 316 keV transition of Pt^{192} . The L_{II} conversion line was measured with the highest resolution (0.014%).

§ 7. Some proposed high transmission instruments

As seen from the discussion of the toroid focusing spectrometer, exceptionally high transmissions can be obtained if one can find a focusing system where the source is located so that electrons leaving within a solid angle of about 2π around it will be accepted by the focusing field. In principle this is feasible for many systems but usually geometrical limitations on the detector side or loss in resolving power limit the possibilities. High transmission instruments of this type having very low resolutions and practical detector difficulties have been used for particular purposes by Libby and Lee¹²⁵, Siegbahn and Slatis¹²⁶ and Rae¹²⁷.

Miyamoto¹²⁸, Sakai¹²⁹ and Shpinel¹³⁰ have designed so called ‘spiral-orbit’

¹²⁴ E. P. Mazets and Yu. V. Sergeenkov, Izv. Akad. Nauk SSSR Ser. Fiz. 26 (1962) 248. (Engl. transl. Bull. Acad. Sci. USSR ser. phys. 26, 246).

¹²⁵ W. F. Libby and D. D. Lee, Phys. Rev. 55 (1939) 245.

¹²⁶ K. Siegbahn and H. Slatis, Ark. Mat. Astr. Fys. 36A (1949) No. 22.

¹²⁷ E. Rae, Phil. Mag. 41 (1950) 525.

¹²⁸ G. Miyamoto, Proc. Phys.-Math. Soc. Japan (in Japanese) 17 (1943) 587; R. Sagana, G. Miyamoto, K. Nakamura and Takechi, Proc. Phys.-Math. Soc. Japan 25 (1943) 273.

¹²⁹ M. Snkai, J. Phys. Soc. Japan 5 (1950) 178, 184; 6 (1951) 409, 529.

¹³⁰ V. S. Shpinel, Doklady Akad. Nauk SSSR 53 (1946) 801; Zhur. Eksp. Teor. Fiz. 20 (1950) 834; V. S. Shpinel and O. Sh. Grois, Zhur. Tekhn. Fiz. 26 (1956) 2259. (Engl. transl. Soviet Physics - Techn. Phys. 1, 2191).

instruments, and although the theoretical figures of merit look interesting, too little spectroscopic work has been done with them to be able to judge the practical advantages. Particles leave the source at the center of the field which decreases symmetrically outwards. The fieldform can be adjusted so that the particles spiral outwards, eventually converging to a definite circle, the radius of which depends upon the $B\rho$ of the particles (see Fig. 49). The fieldform is essentially bell-shaped with the maximum at the centre of the magnet. There is a strong z-focusing also which gives the particles an oscillatory movement around the symmetry plane $z=0$. Theoretically, the combined p - and z-focusing should give a transmission of $\approx 75\%$ at a resolution of 1.3%, which would no doubt be extremely useful, e.g. in coincidence work. It has, unfortunately, been quite difficult to apply this focusing principle in practice, probably because of the rather critical adjustments of the parameters involved.

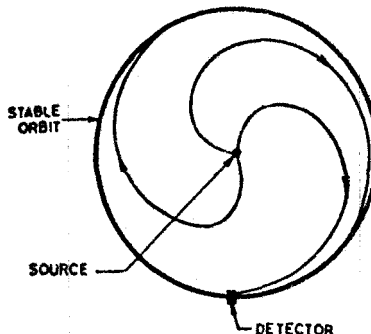


Fig. 49. Electron paths in spiral orbit spectrometer.

Another class of proposed high transmission instruments is based on 'trochoidal' orbits. These were first used by Thibaud ¹³¹ in his well-known studies of magnetically separated positrons and electrons and have been used for similar purposes by others since then. The general scheme is to allow the electrons to pass through a strong and inhomogeneous magnetic field, so that the electrons will cycle with a certain drift velocity directed perpendicular to the field and the field gradient. Positrons and electrons drift in opposite directions. The transmission is obviously very high but the magnetic resolution is at first sight nonexistent since all energies take part in the cyclic movement. Malmfors ¹³² pointed out, however, that such a device could be used as an energy measuring device if the drift velocity was determined by means of *time of flight* techniques. Malmfors studied the case of a magnetic field with rotational symmetry and the radial dependence $1/r^n$. The motion consists of a superposition of a trochoidal motion and an oscillation through the symmetry plane.

¹³¹ J. Thibaud, Phys. Rev. 45 (1934) 781; Nuovo Cimento 15 (1938) 313.

¹³² K. G. Malmfors, Nucl. Instr. and Methods 1 (1957) 251; Ark. f. Fysik 13 (1958) 237.

K. G. Malmfors and A. Ark. f. Fysik 13 (1958) 247.

The time T for a complete oscillation is found to be

$$T = \frac{2\pi r_0}{v} \sqrt{2} \left(1 + \frac{3n^2 - 4}{16} \cdot \frac{z_1^2}{r_0^2} + \dots \right) \quad (97)$$

and the azimuthal angle A corresponding to one complete oscillation:

$$A = \pi \sqrt{2} \frac{\rho_0}{r_0} \left(1 - \frac{n^2 - 8n + 4}{16} \cdot \frac{z_1^2}{r_0^2} + \dots \right). \quad (98)$$

The drift velocity is then

$$v_{\text{drift}} = \frac{r_0 A}{T} = \frac{n \rho_0}{2 r_0} v \left(1 + \frac{n(2 - n)}{4} \cdot \frac{z_1^2}{r_0^2} + \dots \right) \quad (99)$$

where ρ_0 = radius of curvature of an electron cycle,

r_0 = mean radius of motion in the magnet,

v = electron velocity,

z_1 = maximum oscillation amplitude.

If one inserts the particle energy in units of $m_0 c^2$ and writes down the time taken for a particle to proceed one half turn round the magnet one gets:

$$\tau = \frac{\pi r_0}{v_{\text{drift}}} = \frac{\pi e}{m_0 c^2} \frac{B_0 r_0^2}{n} \frac{E + 1}{E(1 + \frac{1}{2}E)} \left(1 + \frac{n(n - 2)}{4} \cdot \frac{z_1^2}{r_0^2} + \dots \right). \quad (100)$$

The drift velocity is evidently essentially proportional to the particle energy and by a time of flight measurement one can use (100) to get the particle energy.

From (100) it is obvious that $n=2$ represents an especially favourable case since, for this value, the flight time is independent of both the mean radius r_0 (since $B_0 \approx 1/r_0^2$) and to a first approximation of the oscillation amplitude z_1 (since the correction term vanishes). With a reasonable magnet ($r_0 = 50$ cm and $B_0 = 12000$ gauss) and a particle energy of 1 MeV the time of flight is of the order of 1 μ sec. With a fast scintillation detector one can usually measure flight times with a time resolution $\Delta\tau$ of a few nanoseconds. The starting point may be either the pulse from an accelerator or a γ -ray emitted in cascade with the electron. The energy resolution due to $\Delta\tau$ can be obtained from (100):

$$\left(\frac{\Delta E}{E} \right)_1 = \frac{\Delta\tau}{\pi r_0} v \frac{n\rho}{2r_0} \quad (101)$$

with $n=2$, $r_0=50$ cm, $\Delta\tau=2$ nsec and $v \approx 3 \times 10^{10}$ cm/sec,

$$\left(\frac{\Delta E}{E} \right)_1 = \frac{8\rho}{1000}. \quad (102)$$

If different starting directions from a point source are taken into consideration the spread in flight path will be of the order of ρ . This gives a contribution $(\Delta E/E)_2$ to the resolution which is $\approx \rho/\pi r_0$

$$\left(\frac{\Delta E}{E} \right)_2 = \frac{6\rho}{1000}. \quad (103)$$

The source may consequently have an extension in the azimuthal direction of $\approx \rho$ without appreciably affecting the resolution. As mentioned before, the extension in the radial direction has no influence on the resolution for $n=2$.

The transmission can easily be calculated in the simple case of a point source at the symmetry plane emitting particles isotropically. The transmission is then set by the height h of the magnetic pole gap which can accept particles with the maximum starting angle ψ_0 with the symmetry plane. One obtains:

$$\sin \psi_0 = \frac{n}{2\sqrt{2}} \frac{h}{r_0}. \quad (104)$$

With $n=2$ and $r_0 = 50$ cm and a pole gap of 10 cm one gets $T = 14\%$.

It is likely that this trochoid spectrometer is particularly suited as a pair spectrometer since the positive and negative electrons are directly separated in opposite directions due to the drift motion. With a pulsed source the energies of electrons and

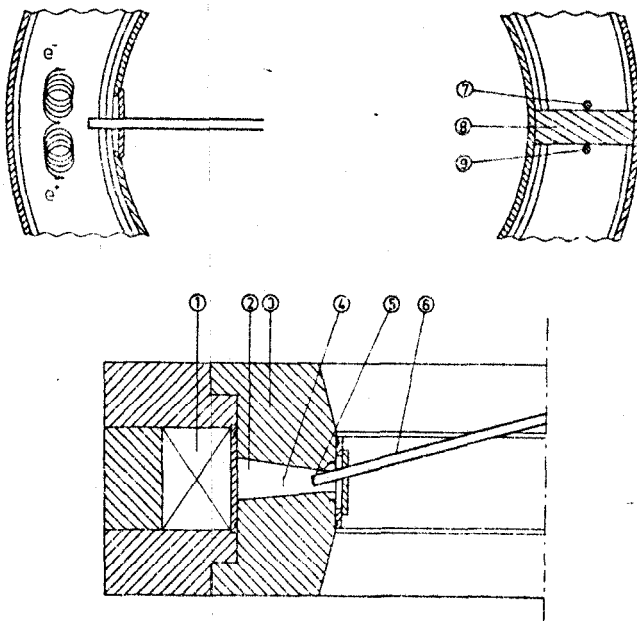


Fig. 50. Trochoid spectrometer, applied as pair spectrometer. (1) Magnet coil, (2) vacuum chamber, (3) magnet poles, (4) pair converter, (5) target, (6) vacuum tube for cyclotron beam, (7) scintillation detector for electrons, (8) lead shielding, (9) scintillation detector for positrons.

positrons in pairs can be individually measured over a wide range. Pairs are furthermore strongly peaked in the direction of the β -ray and therefore both the resolution and the transmission will be improved, the former because of the reduced spread in flight path and the latter because of a better confinement in the β -direction. For β -energies of a few MeV one can expect that almost all pairs are accepted in the spectrometer,

One of the main advantages with Malmfors' trochoid device is that the time of flight technique allows simultaneous broad energy range electronical registering over the entire spectrum by means of a multichannel analyzer. This is a feature that has to be included in discussions of the figures of merit just like luminosity, transmission or the focal plane property.

So far the time of flight trochoid spectrometer has only been used to a small extent. **Malmfors**¹³³ has designed an instrument according to the above quoted parameters (see Fig. 50) and has applied it in a few cases, e.g. the γ -radiation from $F^{19}(p, \alpha)O^{16}$ with the γ -energies 6.14, 6.92 and 7.12 MeV. The resolution obtained was 1.8 %.

A field with rotational symmetry and the radial dependence characterized by $n=1$, i.e. $B_z(r, 0) \approx 1/r$, possesses remarkable focusing properties as was first found by Lafoucriere¹³⁴.

A trochoid orbit starting at the source S at r_0 making an angle ψ with the tangent of the **source circle** $r=r_0$ will return to this circle, $r=r_0$, after a complete trochoid turn at F (see Fig. 51). The angle θ subtended at the origin by the arc SF can be shown to be

$$\theta = 2\pi [k(k^2 - 1)^{-\frac{1}{2}} - 1] \quad (105)$$

where k is assumed to be > 1 and is defined by r_0/ρ_0 (ρ_0 = radius of curvature at $r=r_0$). Lafoucriere noticed that θ is independent of ψ . Thus all the particles emitted in the plane of symmetry by a point source at S are focused at F, regardless of the value of ψ . The focusing exists for all values of r_0 and obviously the planar orbits

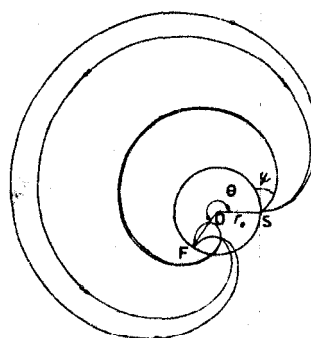


Fig. 51. Focusing in $1/r$ field.

¹³³ K. G. Malmfors personal communication (1963).

¹³⁴ J. Lafoucriere, C.R. Acad. Sci. 229 11949) 523, 1005; 231 (1950) 137; Ann. Phys. 6 (1951) 610. C. Bastard and J. Lacouriere, J. Phys. Radium 19 (1958) 674; 20 (1959) 736; 21 (1960)

in the r^{-1} field will form a perfect image of a line source lying in the plane of symmetry; the different source points will all have the same k -value and consequently the same θ value.

Lee-Whiting¹³⁵ has recently made a closer theoretical examination of this focusing field. The dispersion D is defined as

$$D = \frac{\Delta S/r_0}{\Delta p/p} = 2\pi k(k^2 - 1)^{-\frac{1}{2}}. \quad (106)$$

With this definition, $D=4$ for the double focusing instrument. Figure 52 shows θ , D and the ratio of extreme values p_+/p_- , as functions of k . The planar focusing and the high dispersion suggest that the r^{-1} -field might be the basis of a very efficient spectrometer. Lee-Whiting has therefore studied also the motion of particles at an angle to the plane of symmetry and the effects of finite source heights. It is found that $k \approx 1.25$ should preferably be chosen. Then, both the axial aberration and the

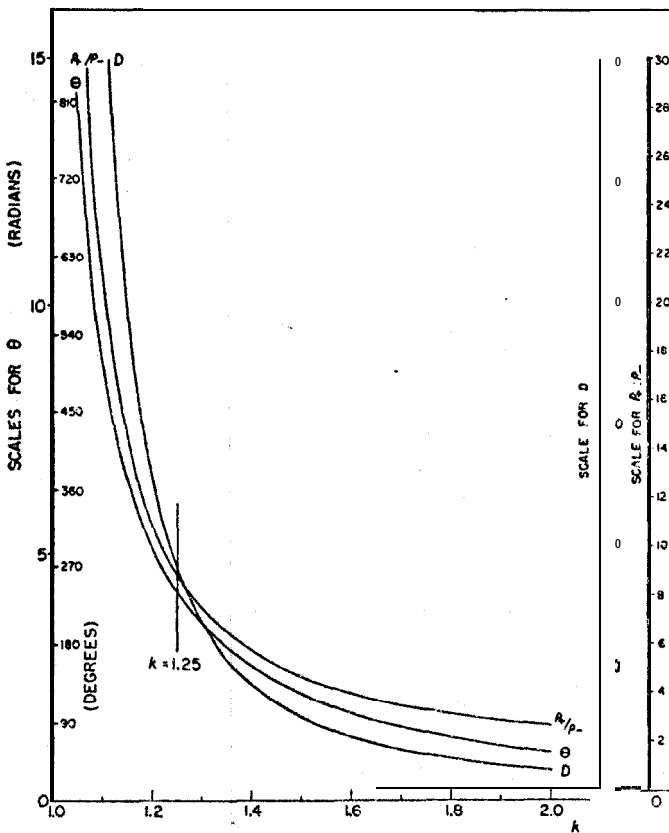


Fig. 52. Variation of focusing angle θ , dispersion D and the ratio of extreme values p_+/p_- versus k for $1/r$ focusing.

¹³⁵ G. E. Lee-Whiting, Can. J. Phys. 41 (1963) 496.

aberration along the direction of dispersion in the midplane are small over a wide range of emission angles roughly centered on the outward radial direction. For a point source such a spectrometer would have exceedingly favourable figures of merit concerning resolving power and transmission. At a transmission of $T=2.3\%$ the resolution would be $R=0.01\%$ and at $T=6\%$, $R=0.1\%$. Due to the occurrence of cross terms in the aberration between the emission angle relative to the symmetry plane and the η_0 coordinate of the source, which do not occur in the $1/\sqrt{r}$ case, the luminosity will be very much reduced, however. A comparison with the Chalk River instrument with $\rho_0 = 100$ cm shows that, although the $1/r$ instrument would have superior figures concerning transmission at a given resolution, the optimum source height would have to be 50 times smaller and because of this the luminosity would be 5 times smaller than for the $1/\sqrt{r}$ instrument. For small sources the $1/r$ instrument would still be promising. Lee-Whiting has also discussed the realization of this and similar magnetic field forms. Pole pieces of nearly conical form will approximate an $1/r$ field. Ironfree coils are also possible.

Similar results have been obtained by Richardson¹³⁶ in the study of the focusing properties of a 'prolate spheroidal' magnetic field. Values of $T = 15\%$ and $R = 1\%$ are theoretically attainable but the luminosity is less favourable.

§ 8. Lens spectrometers

The focusing action of short and long coils has been known for a long time. Busch¹³⁷ was the first, however, to point out the close analogy between ordinary light and electron optics when dealing with these 'magnetic lenses'. He showed that the ordinary lens formula $1/u + 1/v = 1/f$ could also be applied to such lenses and was able to calculate the focal length f for a short lens. He found ($B_z(z, 0)$ being the field component along the axis of the lens):

$$\frac{1}{f} = \frac{1}{4(B\rho)^2} \int_{-\infty}^{+\infty} B_z^2(z, 0) dz. \quad (107)$$

In the special case of a long lens of uniform magnetic field $B_z(z) = B_0$. It is well known that the electrons then describe helical paths. The distance between the source and the image is given by

$$z_{u \rightarrow v} \approx 2\pi B\rho / B_0. \quad (108)$$

For ordinary optical lenses one gets a reversed image. This is also true for the double focusing spectrometer. For a short lens θ is given by the expression:

$$\theta = \frac{1}{2B\rho} \int_{-\infty}^{+\infty} B_z(z, 0) dz. \quad (109)$$

¹³⁶ D. Michelson and H. O. W. Richardson, Proc. Phys. Soc. 81 (1963) 553.

¹³⁷ H. Busch, Ann. Phys. 81 (1926) 974; Arch. Elektrot. 18 (1927) 583.

The first attempt to use the magnetic lens field for -spectroscopy as suggested by Kapitza¹³⁸ was made by Tricker¹³⁹, who used a long uniform field, and later on by Klemperer¹⁴⁰, who tried the short field. These early attempts were, however, not followed for some time by any serious efforts to perfect the instruments to such an extent that they could compete in any respect with the performance of the semi-circular spectrometer, the only type of spectrometer in use at that time. The subsequent work by Deutsch et al.^{141, 142} and of Siegbahn^{143, 18} showed, however, the potentialities of the short lens method. A resolving power as good as 1% was achieved in these early experiments. Witcher¹⁴⁴ simultaneously developed the uniform lens method. In particular the short lens method, extensively used by Deutsch and his coworkers in a long series of important publications and by several others, played a dominant role in the rapid accumulation of spectroscopic data which followed shortly after the introduction of the lens method. The source geometry could be made quite favourable, which was of particular importance when working with low specific activities and secondary electron converters of the g-radiation. It was furthermore easy to shield the counter against direct radiation from the source when secondary y-spectra were investigated. The short lens spectrometer is very flexible in performance and easy to construct.

Though most of the spectroscopic work was performed by means of the short lens method it became apparent that much better performance data could be obtained by using other forms of lens fields. The long lens field, in particular when properly adjusted with a ring focus slit as originally used by Witcher and later on further developed by others¹⁴⁵⁻¹⁴⁷, gives better figures of merit. Still better performance can be attained by giving the field a form reversed with respect to that of a short lens, i.e. having a minimum midway between the source and detector¹⁴⁸, which is used in the so-called 'intermediate image' focusing.

In order to obtain an estimate of the resolving power of a short lens one can neglect the spherical aberration. One can show that the geometry alone will yield a resolving power (at the base)

$$R^0 = \frac{ms + w}{(m + 1)d} \quad (110)$$

where m is the magnification, which is I for $u=v$; s and w are the radii of the source and detector slit respectively. w is made equal to ms in order to match the image size.

¹³⁸ P. Kapitza, Proc. Cambridge Phil. Soc. 22 (1924) Part 3.

¹³⁹ R. Tricker, Proc. Cambridge Phil. Soc. 22 (1924) 454.

¹⁴⁰ O. Klemperer Phil. Mag. 20 (1935) 545.

¹⁴¹ M. Deutsch, Phys. Rev. 59 (1941) 684.

¹⁴² M. Deutsch, L. G. Elliott and R. D. Evans, Rev. Sci. Instr. 15 (1944) 178.

¹⁴³ K. Siegbahn, Ark. Mat. Astr. Fys. 28A (1942) No. 17.

¹⁴⁴ C. M. Witcher, Phys. Rev. 60 (1941) 32.

¹⁴⁵ S. Frankel, Phys. Rev. 73 (1948) 804.

¹⁴⁶ E. Persico, Rev. Sci. Instr. 20 (1949) 191.

¹⁴⁷ J. W. M. DuMond, Rev. Sci. Instr. 20 (1949) 160, 616.

¹⁴⁸ K. Siegbahn Phil. Mag. 37 (1946) 162.

d is approximately the radius of the internal circular slit placed at the center of the coil. Remembering that R^0 in eq. (110) is the base spread, the relative half width is, if $m=1$:

$$R = \frac{s + w}{4d}. \quad (111)$$

If Δd is the width of the defining slit the transmission is

$$T = \frac{d \Delta d}{2u^2}. \quad (112)$$

The spherical aberration will of course make the actual resolving power less favourable than that given by eq. (111). On the other hand, a properly arranged ring focus slit will improve the performance ¹⁴⁹.

So far we have only considered a 'short' lens. The focal distance given in eq. (107) could then be found by solving the well-known differential equation in electron optics valid for paraxial rays, namely

$$\frac{d^2r}{dz^2} = \frac{e}{8mV} R^2(z) r \quad (113)$$

assuming that r does not change very much for the passage of different rays through the lens. In this case the form of the field will not be so significant but only the total integral of the field.

In order to investigate the more general case of an extended field it is convenient to remember that the field in space is completely determined by the field along the symmetry axis (optical axis) of the system. One can show that:

$$B_z(r,z) = B(z) - \frac{1}{4} B''(z) r^2 + \dots, \quad (114a)$$

$$B_r(r,z) = -\frac{1}{2} R'(z) r + \frac{1}{16} B'''(z) r^3 - \dots. \quad (114b)$$

The equation of motion of the electrons is given by:

$$\frac{d}{dt}(mv) = -e \cdot v \times R. \quad (115)$$

In a magnetic field v is a constant and therefore also m . One can then give the equations of motion in the following suitable form:

$$\dot{r} = -(e/m)^2 \left\{ \frac{1}{4} B(z)^2 r - \frac{1}{8} B(z) B''(z) r^3 + \left[\frac{3}{2} \frac{5}{8} B''(z)^2 + \dots \right] r^5 - \dots \right\} \quad (116a)$$

$$\dot{z} = -(e/m)^2 \left\{ \frac{1}{4} B(z) B'(z) r^2 - \left[\frac{1}{3} \frac{2}{2} B'(z) B''(z) + \frac{1}{3} B(z) B'''(z) \right] r^4 + \dots \right\} \quad (116b)$$

$$\dot{\phi} = -(e/m) \left\{ \frac{1}{2} B(z) - \frac{1}{16} B''(z) r^2 + \dots \right\}. \quad (116c)$$

Solution of these differential equations presents in general great mathematical difficulties. For some special fieldforms, such as a homogeneous field, the solution of

¹⁴⁹ W. W. Pratt, F. I. Boley and R. T. Nichols, Rev. Sci. Instr. 22 (1951) 92.

the equations and the elimination of t may be easily done. In this case one simply has:

$$\ddot{r} = - \left(\frac{eB}{2m} \right)^2 r, \quad z = 0, \quad \dot{\phi} = - \frac{eB}{2m}. \quad (117)$$

The solution will then be:

$$r = D \sin \alpha \sin \varphi \quad (118)$$

where

$$\varphi = \frac{z}{D \cos \alpha} \quad \text{and} \quad D = \frac{2mv}{eB} = \frac{2(B\rho)}{B}, \quad (119)$$

α being the angle of emission of the electron. Evidently D corresponds to the diameter of a circle described by an electron emitted with $\alpha=90^\circ$. In the rz -plane following

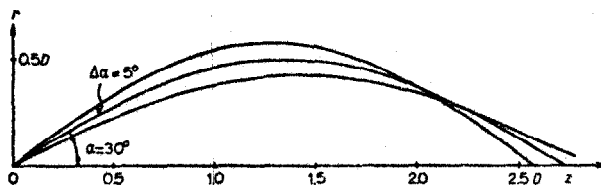


Fig. 53. Electron paths in a homogeneous field for $\alpha = 25^\circ, 30^\circ$ and 35° .

the electron in its helical motion, the path is a sine curve of amplitude $r_m = D \sin \alpha$ and half period $\pi D \cos \alpha$, when the electron crosses the axis, in accordance with (108), if $\cos \alpha \approx 1$.

Fig. 53 shows the electron paths for $\alpha=25^\circ, 30^\circ$ and 35° . The fact that the intersection of the electron with the axis is dependent on α causes a spherical aberration, always with a positive sign. According to Fig. 53 the different paths intersect each other rather closely within a certain region. The condition for such a ring focus can be expressed by $dr/d\alpha=0$. From (118) we then get:

$$\frac{\operatorname{tg} \varphi}{\varphi} = - \operatorname{tg}^2 \alpha. \quad (120)$$

In order to calculate the resolving power of the system one observes that in the ring focus the width of the 'image' is (neglecting higher order terms):

$$\Delta r = \frac{\partial^2 r}{\partial \alpha^2} \frac{1}{2} (\Delta \alpha)^2 \quad (121)$$

where $\Delta \alpha$ is half the opening angle. Differentiating (118) once more we get using (120):

$$\Delta r = D \frac{(\Delta \alpha)^2 \sin \varphi}{2 \sin \alpha} (3 + \cos^2 \alpha \operatorname{tg}^2 \varphi) \quad (122)$$

The resolving power R^0 is defined as $A(B\rho)/B\rho$. From (119) we have:

$$\Delta r = \frac{\partial r}{\partial D} \frac{D}{(B\rho)} A(B\rho) \quad (123)$$

or

$$r = \frac{\partial r}{\partial D} DR^0. \quad (124)$$

$\partial r/\partial D$ is obtained from (118) and (119):

$$\frac{\partial r}{\partial D} = \frac{\sin \varphi}{\sin \alpha}. \quad (125)$$

By means of (122), (124) and (125) we finally obtain for a point source:

$$R^0 = \frac{1}{2}(A\alpha)^2 (3 + \cos^2 \alpha \operatorname{tg}^2 \varphi). \quad (126)$$

The transmission is given by

$$T = \sin \alpha. \quad (127)$$

The relation between R^0 and T is then:

$$R^0 = \frac{1}{2} T^2 \left(\frac{3}{\sin^2 \alpha} + \cot^2 \alpha \operatorname{tg}^2 \varphi \right). \quad (128)$$

It is found (see Fig. 54) that the factor enclosed in the parentheses has a minimum value at $\alpha \approx 45^\circ$. If the width of the source is taken into account it is found that the optimum value of α is decreased to $< 40^\circ$. Since the coil has to be inconveniently large in order to accept electrons of 40° one often prefers an emission angle of 30° or less, in particular for angular correlation work where the angle of emission has to be well defined.

In a design due to Schmidt¹⁵⁰ it has been possible to attain $R = 8.9T^2$ which is very near the theoretical limit. Fig. 55 shows a drawing of this instrument. The maximum transmission is set to be 5 %. With a source diameter of ≈ 1.5 mm the resolution was 0.4 % and the transmission 2 %. It was furthermore verified that the resolution at constant transmission varied linearly with the source diameter, as expected.

Another design is due to DuMond *et al.*¹⁵¹. Particular care was taken to form as uniform a field as possible in order to be able to use the proton resonance method for field measurements and to adjust the spectrometer for high resolution. A very complete arrangement for adjustments was made. At a resolution of 0.1 % the source diameter is < 0.5 mm and at 0.65%, 3 mm.

¹⁵⁰ F. H. Schmidt., Rev. Sci. Instr. 23 (1952) 361.

¹⁵¹ J. W. M. DuMond, L. Bogart, J. Kohl, D. Muller and J. Wilts, Calif. Techn. Rep. (1952) No. 16; J. W. M. DuMond, Ann. Phys. (N.Y.) 2 (1947) 283.

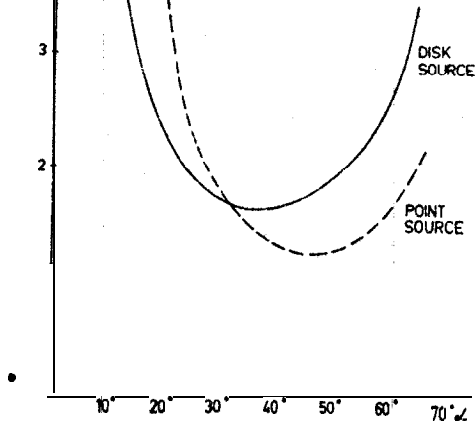


Fig. 54. Resolving power versus emission angle for a homogeneous field. Broken line: point source. Full line: disk source of optimum diameter.

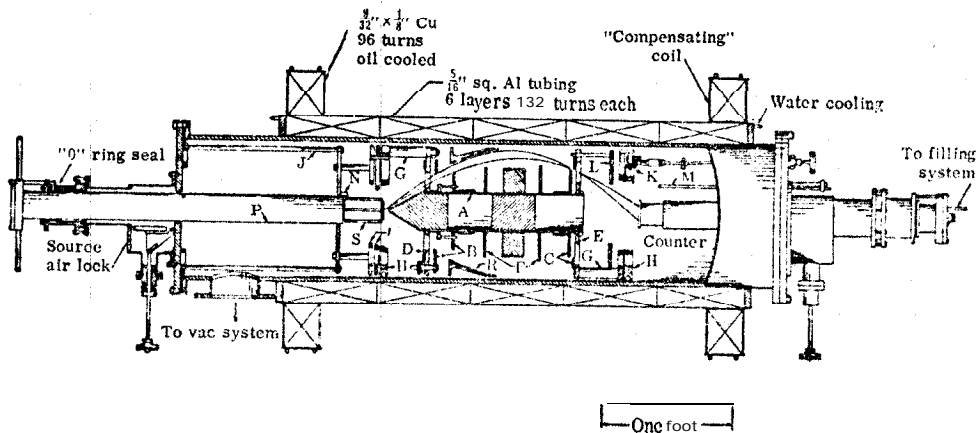


Fig. 55. Homogeneous field spectrometer with ring focus due to Schmidt.

A new precision solenoidal spectrometer has been built by Jungerman et al.¹⁵² It is a large instrument with the 'scale factor' $D = 2p/eB = 2(B\rho)/B = 78.8$ cm. The field is made uniform to 1 : 10⁴ within a volume of 2 m x 60 cm. By careful adjustment and using ThB sources with a diameter of <0.5 mm Jungerman et al. have reached resolutions of 0.05 % down to 0.018 % at transmissions of 0.36% and 0.04%, respectively. Using the proton resonance method for the field determination and pre-

¹⁵² J. A. Jungerman, M. E. Gardner, C. G. Patten and N. F. Peek, Nucl. Instr. and Methods I5 (1962) 1.

cision measurements of the lengths defining the geometry (giving D), 'absolute' B_p -values of several lines in the ThB spectrum could be measured.

Hofstadter¹⁵³ has suggested that a very much enlarged version of a solenoidal spectrometer due to DuMond could be used as a spectrometer for high energy particles of momenta up to 500 MeV/c. The dimensions of the ellipsoidal coil would have to be 4.5 m x 3 m. The required field is 19400 gauss and the power consumption 10 megawatts.

Obviously the homogeneous field spectrometer with properly adjusted ring focus shutters has good figures of merit. When judging its potentialities one also has to discuss some of its limitations. When the ring focus is set to accept a large fraction of the radiation, say several percent, the beam due to the spherical aberration broadens again considerably after passing the shutters and, in order to register the electrons, an uncomfortably large counter has to be used with a corresponding increase in background. If a GM counter is used, the window must be thin, which calls for a grid support. This support will reduce the actual transmission by as much as 30-50%. It is also not easy to get such a large thin window to be completely vacuum tight. The high background of such a large counter may be reduced by using a shield of anticoincidence counters. The detector problem limits the maximum useful transmission to about 5% or less.

At very good resolution, say less than a few tenths of a percent, other complications occur instead. Contrary to the double focusing method where narrow line sources are used, the fens method with a ring focus requires point sources, i.e. *one dimension of the source is wasted in order to get space focusing*. This seriously affects the luminosity. Furthermore the adjustments at high resolution are critical, since any small departure from the rotational symmetry of the field or of the general alignment of the system is detrimental. Again, the double focusing method is different in this respect since the adjustment for high resolution is a fairly straightforward procedure.

Obviously the choice of a uniform lens field is a fairly arbitrary one, apart from the fact that it is easy to handle mathematically, and is the only case in which accurate magnetic field measurements are possible by the proton resonance method. Examining eq. (114a), one would rather prefer a field that is concave upwards. If $B''(z)$ is positive then $\partial B_z(r,z)/\partial r \approx -\frac{1}{2}rB''(z)$ is negative, which means that B_z decreases outwards from the optical axis. This tends to counterbalance the positive spherical aberration. A long lens spectrometer with concave fieldform was built by Siegbahn¹⁴⁸ and the spherical aberration was thus reduced. Slatis and Siegbahn¹⁵⁴ later studied the focusing of strongly concave fields and found that at a certain strong field gradient a pronounced increase in the transmission of the instrument occurred. By photographic ray tracing using the strong F-line in ThB as a monokinetic electron source it was found that the rays crossed each other in the middle of the spectrometer, forming an intermediate ring-formed image there. The rays are then all concentrated and collected

¹⁵³ R. Hofstadter, Prop. to Nat. Sci. Found. (1960).

¹⁵⁴ H. Slatis and K. Siegbahn, Ark. f. Fysik 1 (1943) 339.

in the small slit of the counter. The focusing action is illustrated in Fig. 56. In the upper part of the figure the rays appearing in a homogeneous field are shown. The strong spherical aberration, requiring a correspondingly large counter for collecting a given solid angle of the radiation, is clearly seen. In the lower part of the figure is shown the focusing of the same solid angle of the radiation with the appropriate field gradient for intermediate image focusing. As can be seen, all rays are gathered again in a point on the axis. Thus, an ordinary small-sized counter can be used, in spite of the fact that around 8 % of the total solid angle is transmitted.

The fieldform for intermediate image focusing is given in Fig. 57. Similar fieldforms can also be realized without the use of iron¹⁵⁵.

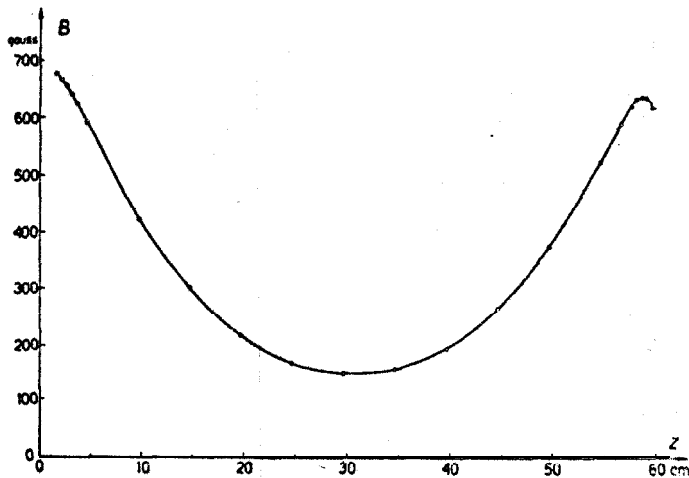


Fig. 57. Fieldform for intermediate image focusing.

The analytic treatment of the focusing action of lens fields defined by eq.(116) is limited to very special cases like the uniform field treated above. Using the paraxial approximation, it is certainly possible to find a number of useful expressions^{143, 156, 157}, but these, are mostly applicable to short lenses, e.g. those used in electron microscopy, and it is difficult to assess the validity of such solutions when they are applied to more realistic cases in β -ray spectroscopy. The introduction of the ring focus shutter and even more refined versions of such arrangements as suggested by Hubert¹⁵⁸ makes it in fact necessary to know the exact form of each separate trajectory in order to find the correct design parameters of each instrument. These can most easily be found by photographic ray tracing.

Although in many cases the demands for high transmission (or luminosity) and

¹⁵⁵ D. E. Alburger, Rev. Sci. Instr. 27 (1956) 991.

¹⁵⁶ W. Glaser, Z. f. Physik 117 (1941) 285.

¹⁵⁷ P. Grivet, C. R. Acad. Sci. 230 (1950) 936.

¹⁵⁸ P. Hubert, C.R. Acad. Sci. 230 (1950) 1464; Physica (1952) 1129.

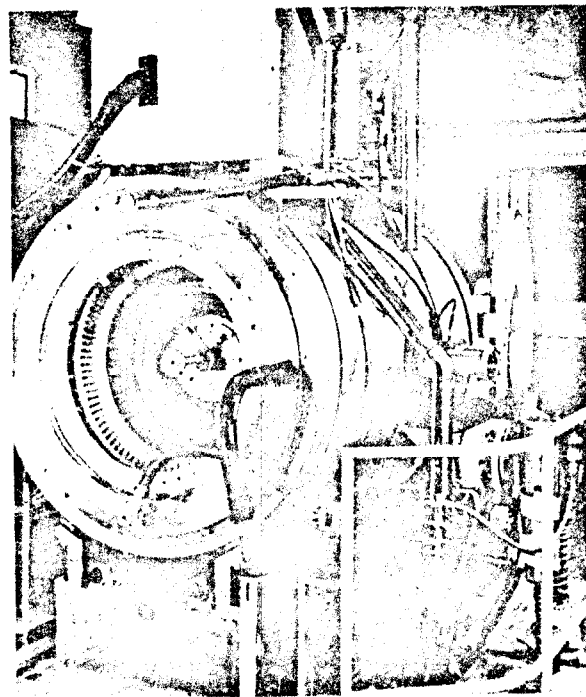


Fig. 44. The Argonne double toroidal spectrometer (see page 135).

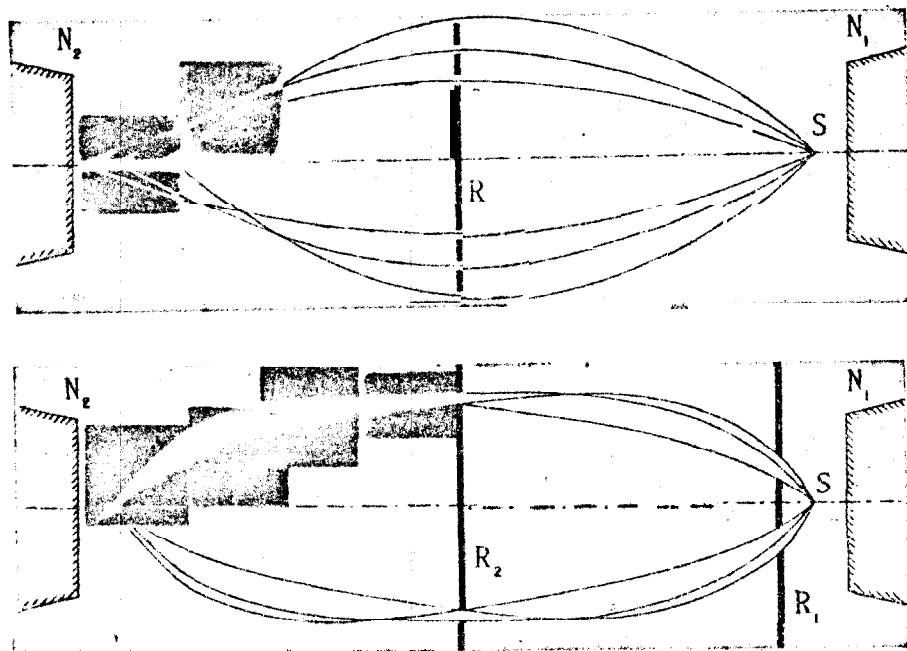


Fig. 56. Upper part: Electron paths in a homogeneous field showing the strong spherical aberration.
Lower part: Intermediate image focusing.

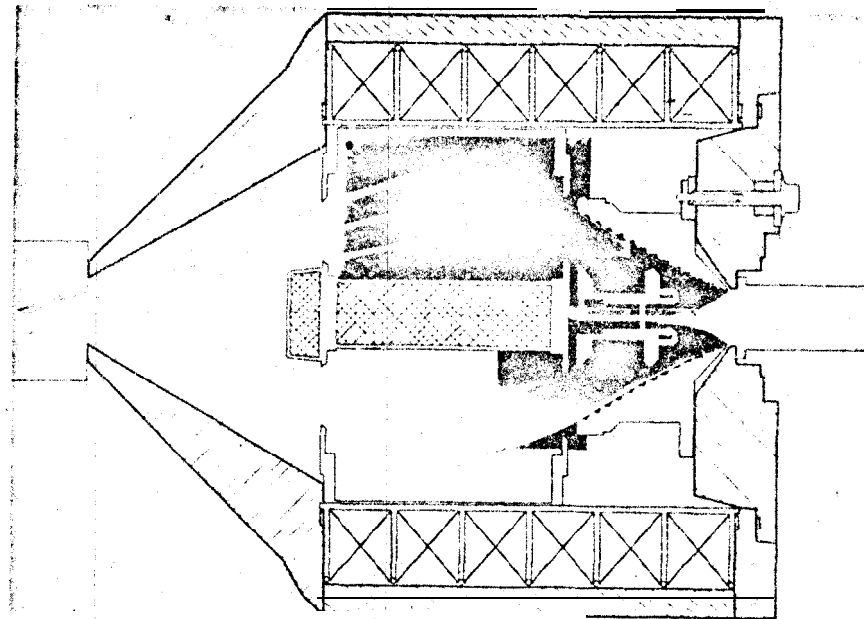


Fig. 58. Magnetic lens for angular correlation purposes with envelope baffle. Photographic ray tracing inserted.

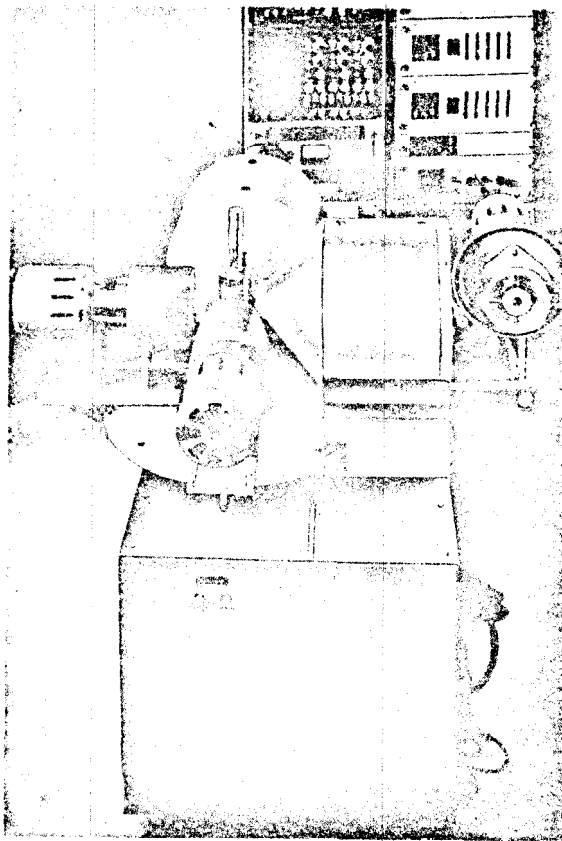


Fig. 64. Photograph of the electron angular correlation instrument shown in Fig. 61, arranged for e- angular correlation measurements according to Fig. 63d. The back 'door' of the right lens is opened, showing the baffle system mounted on its inside. It can be adjusted from outside under running conditions in two perpendicular co-ordinates and also with respect to resolution and transmission. One further lens can be added or one lens removed to meet different experimental requirements. The detectors are movable around the source in programmed steps.

good resolution are decisive for the choice of spectrometer and fieldform many experiments can invoke rather special problems like geometrical limitations, magnetic shielding, source accessibility, general flexibility, costs, etc. In such cases magnetic lenses of various designs may sometimes have special advantages compared to other types of instruments having much better figures of merit. As an example, Fig. 58 shows a magnetic lens recently designed for an electron angular correlation spectrometer¹⁵⁹. The following conditions were to be satisfied: (a) the source should be in a field free region, (b) it should be possible to add another identical lens in both the 90° and 180° positions (looking at the same source) without magnetic or mechanical interference, (c) it should also be possible to add one or two scintillation detectors to the set-up and to move them around the source, (d) the opening angle α should be limited to around 20° in order to get the solid angle correction for angular correlation measurements sufficiently small and accurately known. With these conditions a lens design of the type given in Fig. 58 was found to be suitable. The magnetic field-form of this lens does not represent any optimum case from a spherical aberration point of view, like the intermediate image one, but it allows one to carry out many experiments that cannot be so easily performed with other arrangements. By using the photographic ray tracing technique discussed above one can map very accurately the electron trajectories belonging to this field (see Fig. 58). As a result, a precision envelope shutter was designed, the final adjustments of which in all three coordinates could be made from outside the spectrometer during running conditions.

The behaviour of the envelope baffle or 'Hubert' baffle is well demonstrated in Fig. 59 where the K- and L-lines of Cs¹³⁷ are recorded in the spectrometer. For narrow beams (small line widths) the particular features of the envelope arrangement cannot be seen. As the central shutter is moved inwards, the detector accepts more and more of the electrons coming either from large or small take-off angles and the line profiles take on the typical asymmetric shape shown in Fig. 59. The reason for this is as follows (cf. Fig. 68): for a sufficiently low current all electrons belonging to a line hit the external envelope baffle. At a certain current, however, *all* electrons will just be able to miss the envelope baffle and pass to the detector. This corresponds to the sharp edge on the low energy side. On the high energy side, the shape will not be as steep but will depend in the usual way on the *slit width* determined by the position of the internal circular shutter. The resolution on the *low* energy side is virtually *independent* of the transmission up to the full transmission of the instrument, which in this case is set by the condition $\alpha \lesssim 20^\circ$. As an example, Fig. 60 shows that one can obtain complete separation without any interference at all between the L- and M-lines of the In^{114m} 192 keV transition, although these are separated from each other by less than 1%. In order to get the same momentum resolution ($\approx 0.4\%$) without an effective envelope baffle, one would have to reduce the transmission by a factor of about 10.

The Hubert baffle arrangement is interesting in principle since it shows that it is

¹⁵⁹ K. Siegbahn, Ark. f. Fysik 22 (1963) 435;

P. Kleinheinz, L. Samuelsson and K. Siegbahn, Nucl. Instr. and Methods (1964).

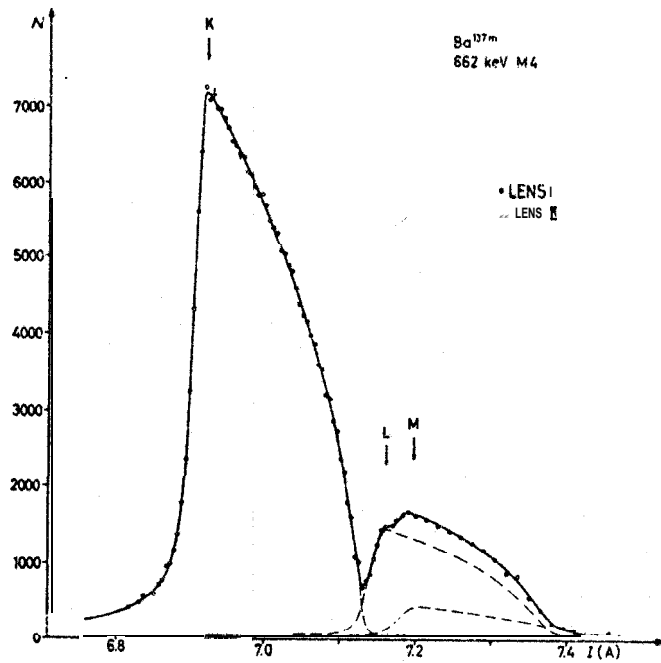


Fig. 59. Typical line profile at high transmission using envelope baffle. Even the L- and M-lines of the 662 keV -transition of Ba^{137m} are completely resolved by setting the current at the L-arrow.

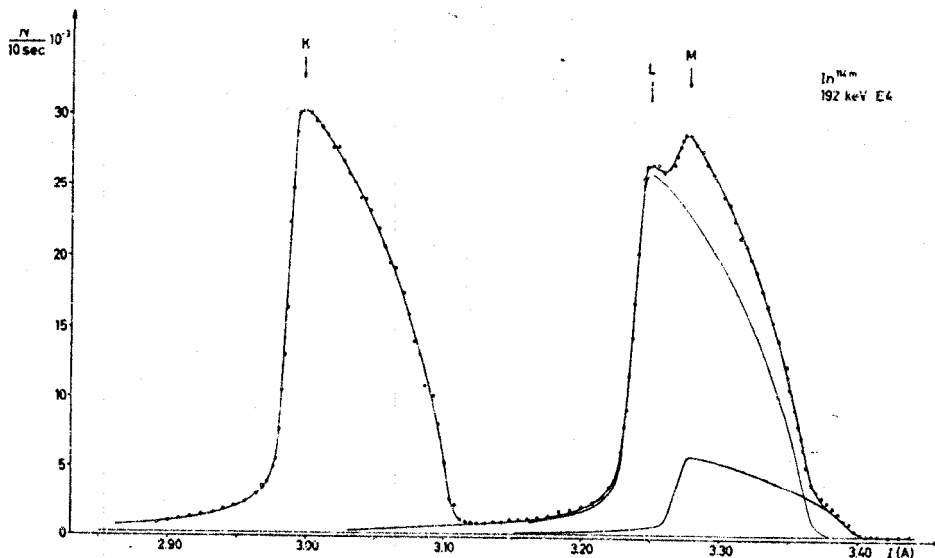


Fig. 60. Separation of lines belonging to the 192 keV transition in In^{114m} using an envelope baffle at high transmission. The Be-values of the L- and M-lines differ by less than 1%. The resolution on the low energy side would allow a line separation in momentum of $\approx 0.4\%$.

possible under certain conditions to eliminate the consequences of spherical aberration by a strategic positioning of the baffle system. An interesting possibility would be to use such baffle systems on other instruments such as the intermediate image type, etc.

The e-e coincidence arrangement (see Fig. 61) has the advantage over the corresponding e- and - set-up that high energy resolution can be arranged in both channels (without interfering with Compton distribution) and, furthermore, that a shorter time resolution of the coincidence system can be obtained since the NaI crystal is inferior in both respects to a magnetic lens combined with an organic scintillation detector. For angular correlation studies the e-e anisotropy gives the same information regarding spins and parity as the e- studies and more information than the - studies [see Chapter XIXA]. There are some additional possibilities offered by the combined e-e, e- and - angular correlations.

For ordinary e-e coincidence measurements in the 90° position it is often an advantage that no electrons have to pass through the backing material of the source. This is of importance as Moller scattering can give rise¹⁶⁰ to ghost lines in the coinci-

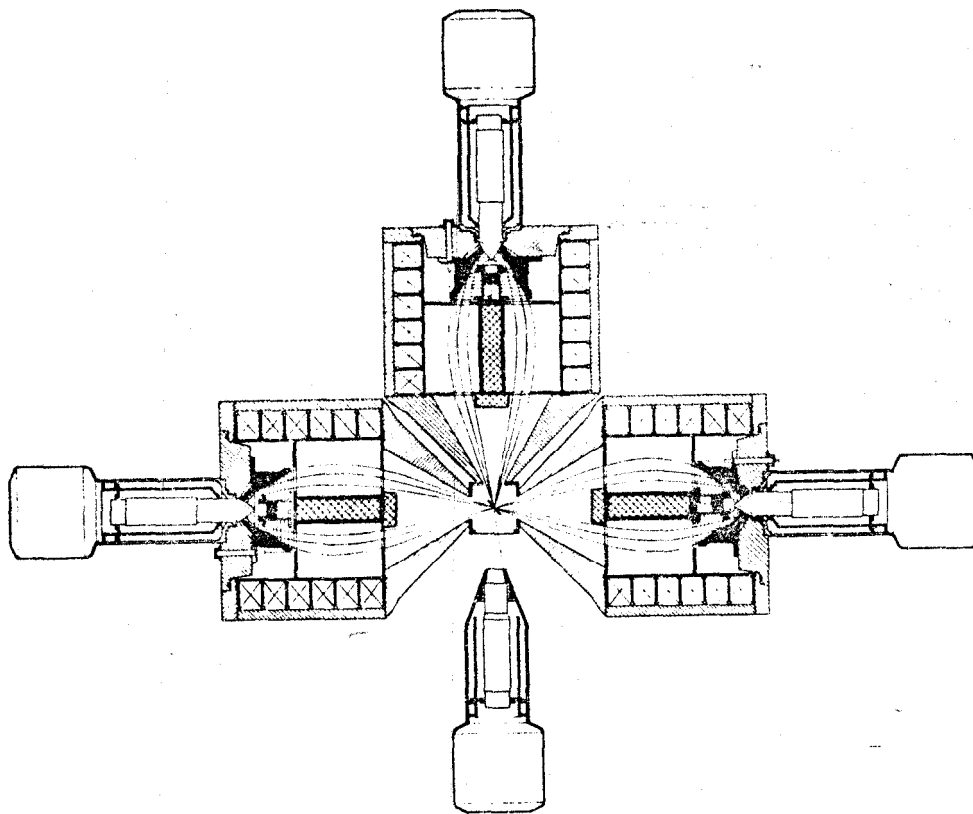


Fig. 61. The electron angular correlation spectrometer described in ref. 159 when set up for e-e and e- angular correlation studies.

¹⁶⁰ P. Kleinheinz, L. Samuelsson, R. Vukanovic and K. Siegbahn, Nucl. Phys. 55 (1964).

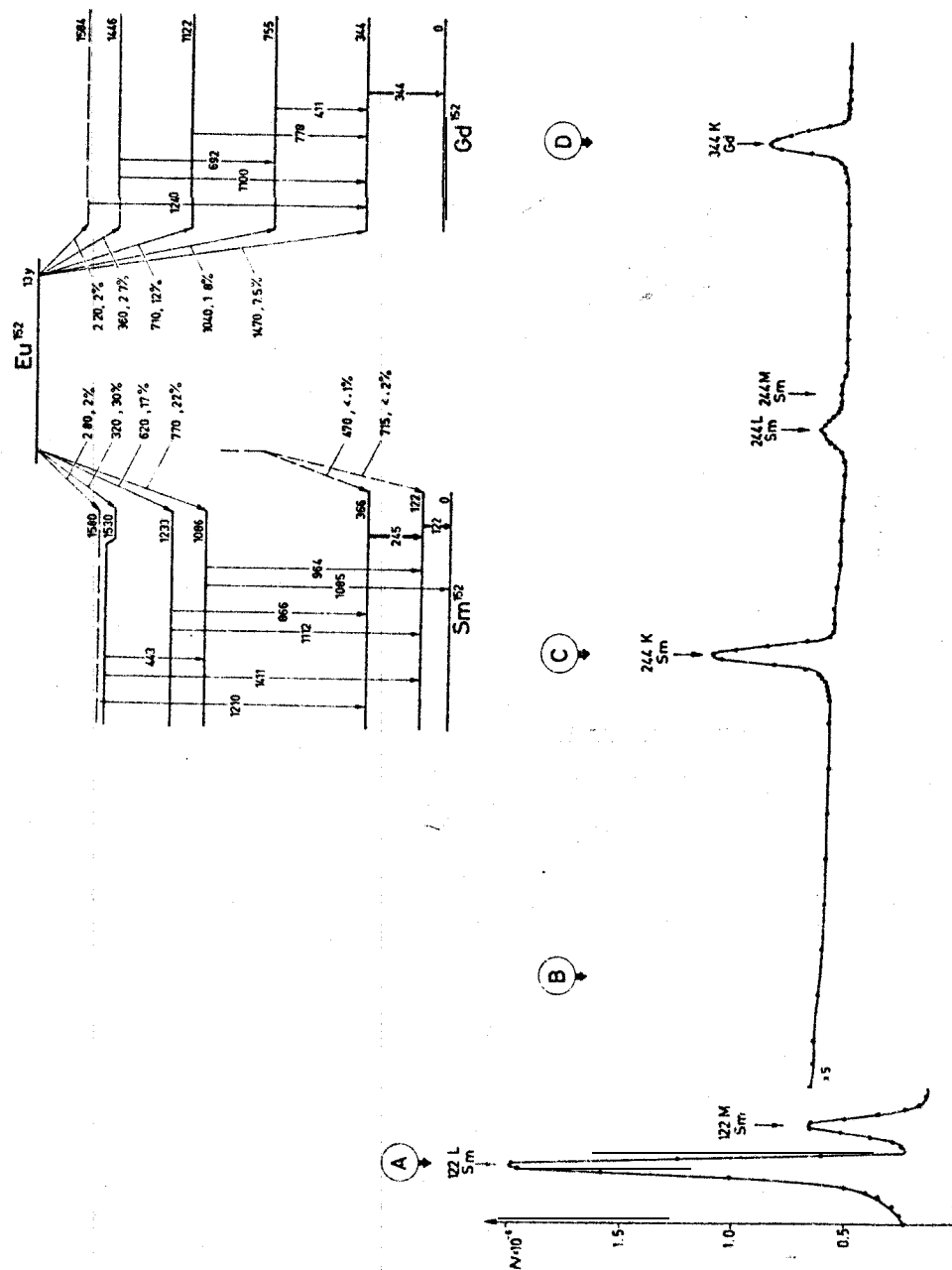
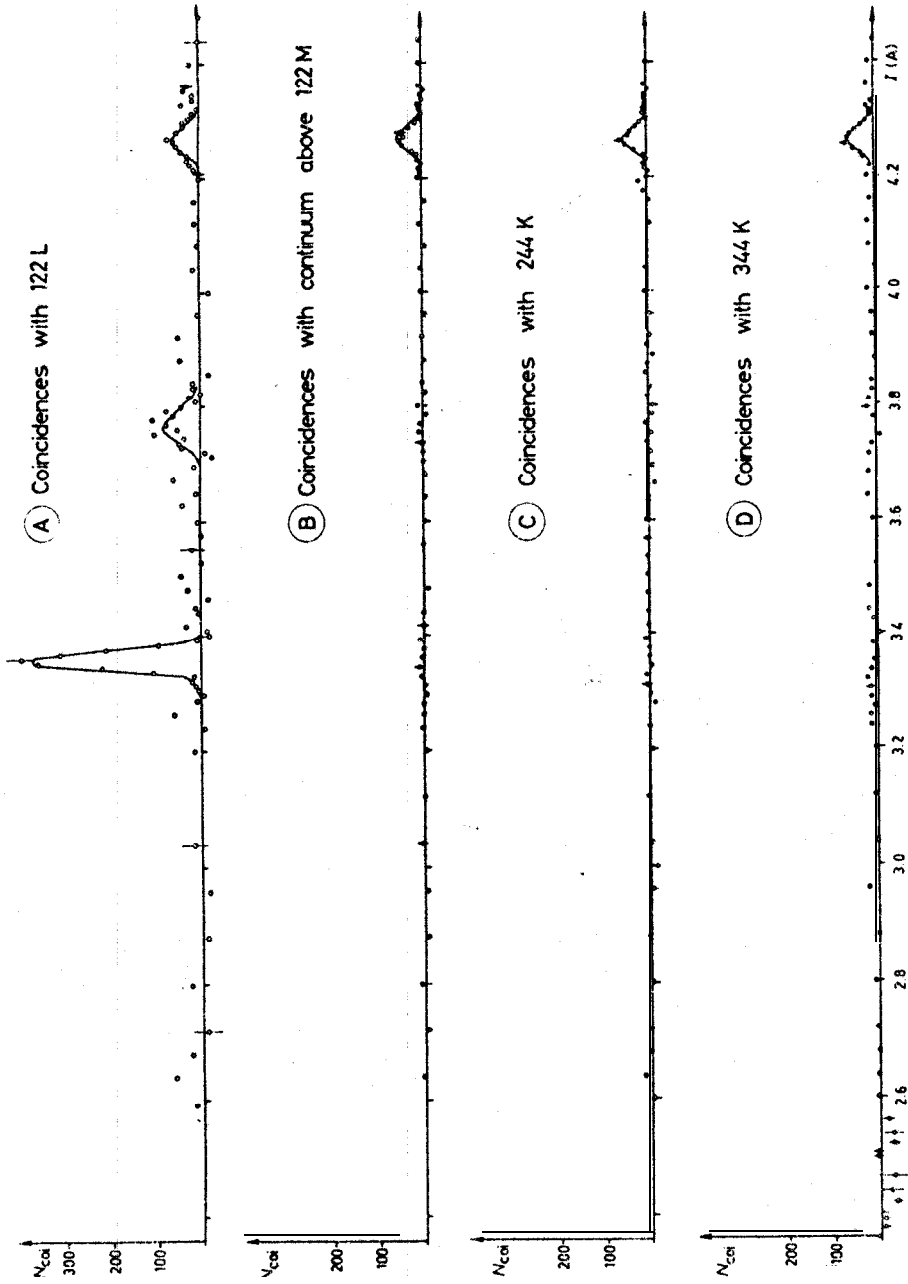


Fig. 62a. e-e-coincidence study of the decay of Eu¹⁵² obtained with the instrument shown in Fig. 61. In the upper curve a single spectrum is shown together with the settings of the fixed spectrometer for the four coincidence runs A to D. The coincidence spectra are corrected for background coincidences. Results:

- (1) The 122 keV and 244 keV transitions are coincident (shown in run A). The 122 keV transition



is not in coincidence with the continuous -distribution (D) nor with the 344 keV transition (D, comparison of A and B).

(2) The 244 keV transition is not coincident with the -continuum (B, C) and the 344 keV transition (D, comparison of B and C).

(3) The 344 keV transition is coincident with the -continuum (comparison of A to D).

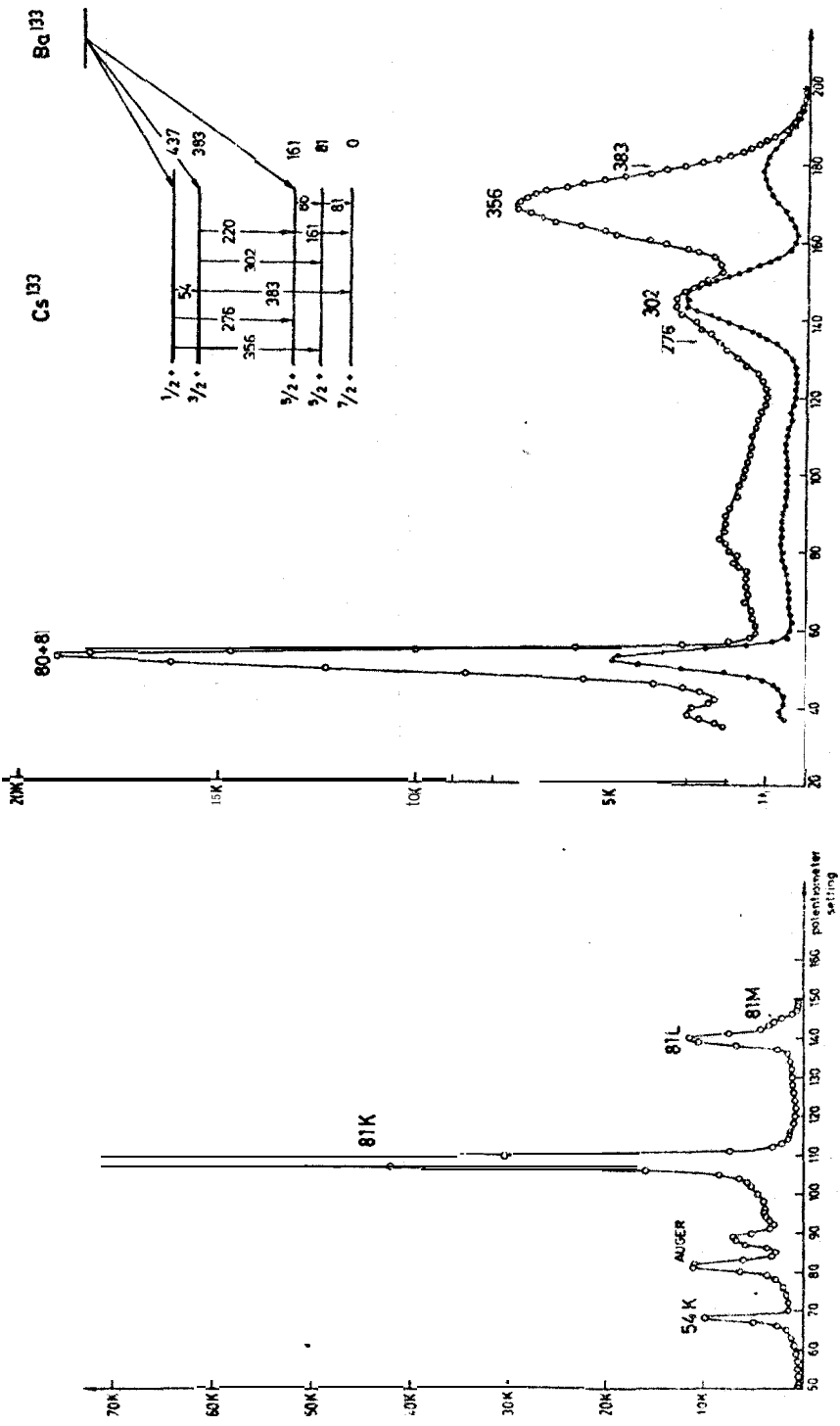


Fig. 62b. The part on the right shows the gamma spectrum of Cs^{133} (open circles) and the same spectrum in coincidence with the 54 keV electron line (solid dots) focused in the magnetic lens spectrometer shown in Fig. 64. The coincidence spectrum clearly shows the 383 keV line, which is completely masked in the single spectrum by the presence of the strong 356 keV line, and in addition, the pure 302 keV line which in the single gamma spectrum is broadened by the 276 keV line. To the left is shown the electron spectrum below 50 keV with the lens spectrometer.
insert: The decay scheme of Ba^{133} .

dence spectrum. An example of a simple e-e coincidence study is given in Fig. 62.

Electronically one can arrange the system to collect *simultaneously* the coincidences between the various channels. By employing more than two detectors for angular correlation measurements, not only the solid angle and thus the efficiency increased, but in addition the set-ups have a higher degree of symmetry and therefore are self-normalizing and less sensitive to instrumental drifts (see Fig. 63). Multi-

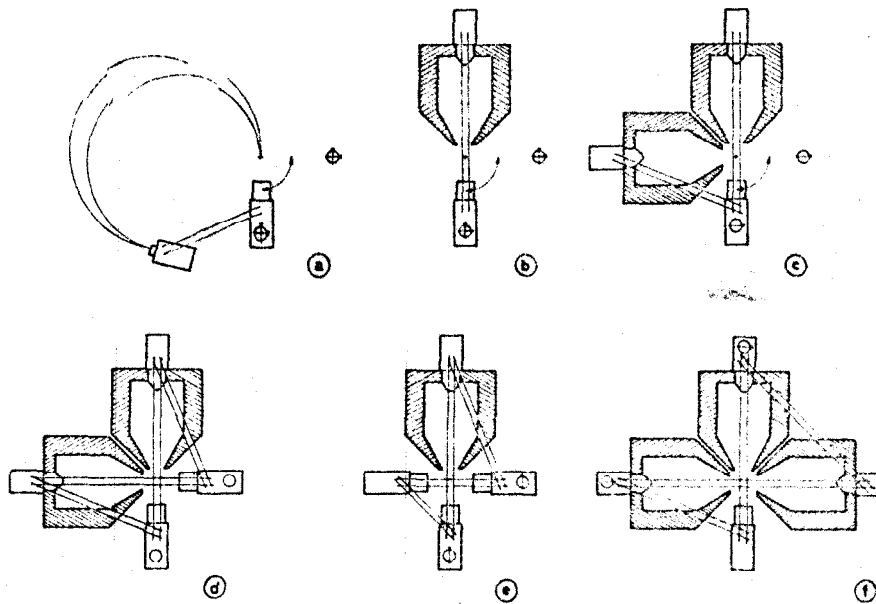


Fig. 63. Different detector geometries and their symmetry properties for measuring angular correlations involving electrons. The double lines connecting two detectors symbolize coincidence circuits. (a) and (b) show conventional two-detector set-ups for a high-resolution double focusing spectrometer and a lens spectrometer, respectively. A frequent change of the angular position of the -detector is required to eliminate fluctuations in both detectors ($\top \cdot \downarrow$) and in the coincidence circuit (\bigcirc). By adding another -detector in (b) in a fixed position, e.g. 90° from the lens, and having the first -detector movable, one obtains a simple system for reproducing e- as well as - angular correlations. This scheme is, due to its simplicity, perhaps that most commonly used. (c) By employing two electron spectrometers in 90° position not only the solid angle is improved by a factor of two, but also the set-up is insensitive to fluctuations in the -detector, as the -signals simultaneously contribute to the 90° and 180° coincidence rates. As in a two detector set-up the imperfections in the electron counters and in the coincidence circuits are eliminated by changing the -detector angular position (\ominus). (d) Four-detector geometry with optimal symmetry properties. The detector fluctuations cancel out as each detector simultaneously contributes to the 90° and 180° coincidence rates. Differences and drifts in the coincidence circuits are eliminated by interchanging the position of two detectors accepting the same radiation (\leftrightarrow). (e) and (f) By combining three plus one detectors in a four-detector set-up it becomes possible to simultaneously measure two different angular correlations of the same decay cascade. The symmetry properties of these set-ups are identical to those of the geometry shown in (c).

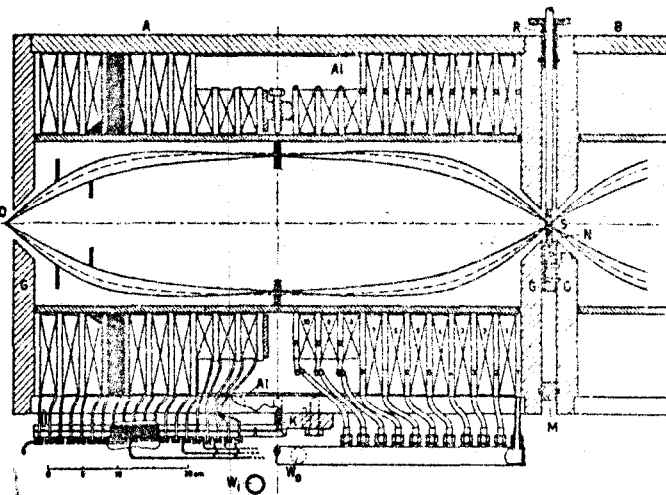
For a detailed discussion see ref.

channel analyzers are incorporated in the system for e- studies and in combination with time-to-pulse-height converters for measurement of very short-lived states. Fig. 64 is a photograph of the two-lens plus two -detectors alternative. When only one lens and two -scintillation detectors are used, one of the latter can automatically be moved around the source, stepwise scanning both the e- γ and γ - γ angular correlations.

Previously, a two-lens arrangement for e-e angular correlations was used by Siegbahn¹⁶¹ (β -spectrogoniometer). Coincidence arrangements between electrons and -rays, registered by means of one lens and one -detector, are easier to build since interference between two focusing fields is not encountered. Such arrangements have been used by Stevenson and Deutsch¹⁶², Goldberg and Frankel^{162a}, Gerholm, and Pettersson¹⁶³, and several others.

If one is not interested in the angular distribution but only in obtaining coincidence data a number of other lens arrangements can be used. One high efficiency system is the intermediate image spectrometer, provided with a scintillation crystal behind the source for coincidences^{164, 165, 165a}, or two such spectrometers placed end-to-end for e-e (see Fig. 65)¹⁶⁶.

The formation of the image is well demonstrated in Fig. 66. The fact that a well-defined small image is formed at the axis outside the lens makes it possible to use



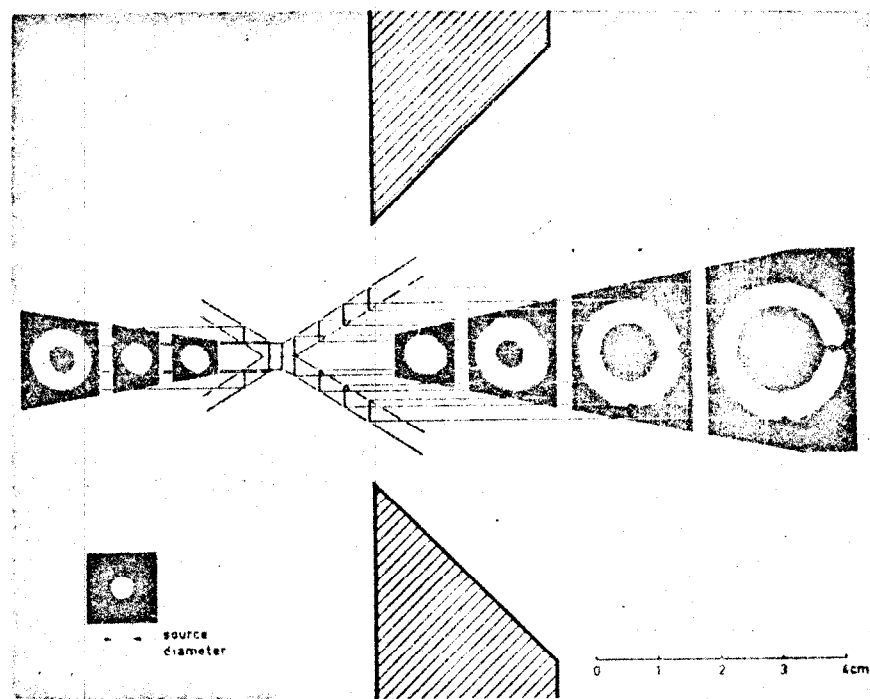


Fig. 66. Image formation in the two-lens spectrometer of Fig. 65, yielding a point focus which enables tandem action.

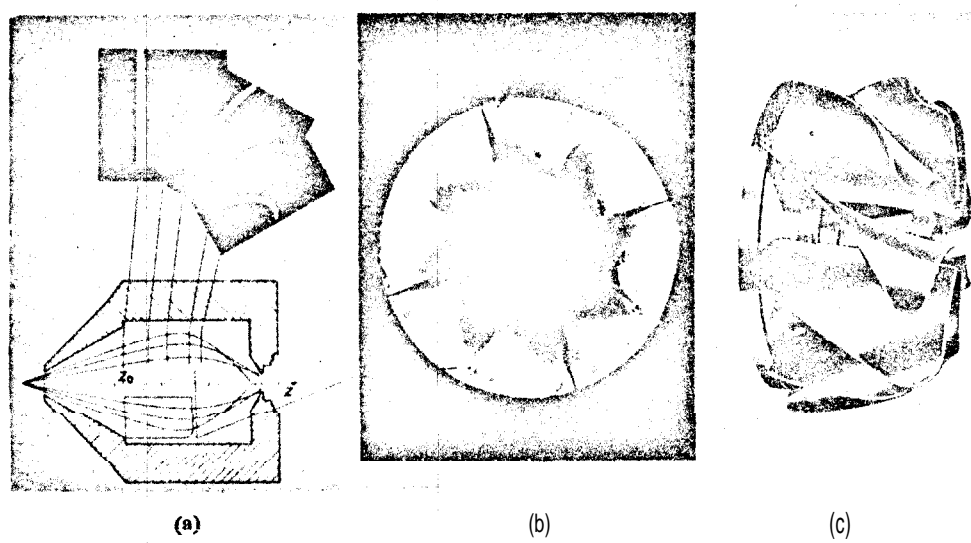


Fig. 70. Twisted positron baffle (c) belonging to lens according to Fig. 58, ray tracing for shape determination (a) and check of the fit of the baffle blades (b).

this two-lens system in a tandem fashion. This was tried by Slatis and Herrlander¹⁶⁶ who found improved resolution. The performance data of one lens used for coincidence are given in Fig. 67. The transmission is reduced from the maximum value of 10% when the source and detector are inside the field. The strong dependence on the source size is noticed.

Several similar arrangements of other lenses have been used. Bell and Graham¹⁶⁷ introduced the combination of two magnetic lenses end-to-end for life-time measurements by means of the delayed coincidence technique. Gerholm and Lindskog¹⁶⁸ have used this technique with two iron shielded lenses with ring focus. Sergienko¹⁶⁹ has described another end-to-end arrangement. A long lens with concave fieldform has been used by de Waard¹⁷⁰ as an e- coincidence spectrometer, etc.

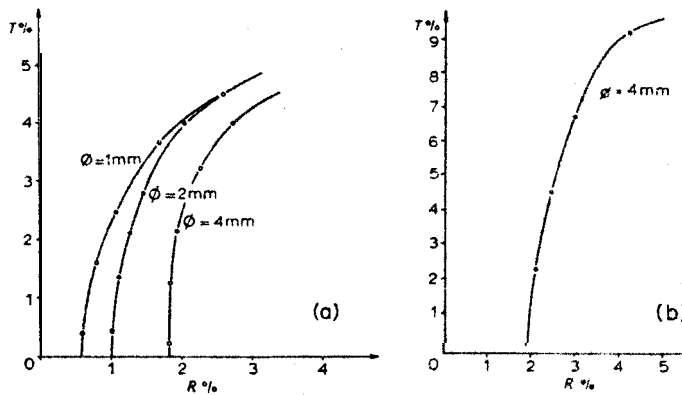


Fig. 67. Transmission versus resolution in intermediate image spectrometer. (a) Source and detector outside the field¹⁶⁵. (b) Source and detector inside the field^{165a}. The spectrometers have been adapted for high transmission e-e and e-γ coincidence measurements, respectively.

Obviously the lens method has many practical advantages, e.g. simplicity and flexibility, and also symmetry in electron-optical geometry, etc. Quite good solid angles of up to 10 % can be obtained, which are adequate for most coincidence experiments if moderate resolution is sufficient. At very good resolution (say below 0.5%) the lens method is not so convenient because of the mentioned difficulty with the small sources which have to be used (low luminosity). At higher transmission (2-5%) on the other hand, spherical aberration becomes increasingly disturbing. Envelope shutters improve the situation and also the use of special fieldforms, such as the strongly concave type giving intermediate image focusing. The future of the lens

¹⁶⁷ R. E. Bell and R. L. Graham, Phys. Rev. 86 (1952) 212.

¹⁶⁸ T. R. Gerholm, Rev. Sci. Instr. 26 (1955) 1069; Ark. f. Fysik 11 (1956) 55;

T. R. Gerholm and J. Lindskog, Ark. f. Fysik 24 (1963) 171.

¹⁶⁹ V. A. Sergienko, Izv. Akad. Nauk SSSR Ser. Fiz. 22 (1958) 198 (Engl. transl. Bull. Acad. Sci. USSR ser. phys. 22, 195.)

¹⁷⁰ G. de Waard, Thesis, Groningen University (1954).

method will depend to some extent on the possibilities of reducing aberration errors. A systematic theoretical study of the focusing properties of a whole variety of fields (34 altogether), bell-shaped, triangular, and concave ones, has recently been carried out by Lindgren and Schneider¹⁷¹. Using a computer they accurately mapped the trajectories by numerically solving the equations of motion (116) for different take-off angles α and from points on the periphery of disk sources of different radius. In this way it is possible to calculate for each fieldform the spherical aberration at ring focus and the so-called 'image width'. The previous quantity is defined by the radial spread r for a point source (see Fig. 68). As previously mentioned (p. 148), the position of the ring focus is obtained from

$$(\partial r / \partial \alpha)_{z,p} = 0. \quad (129)$$

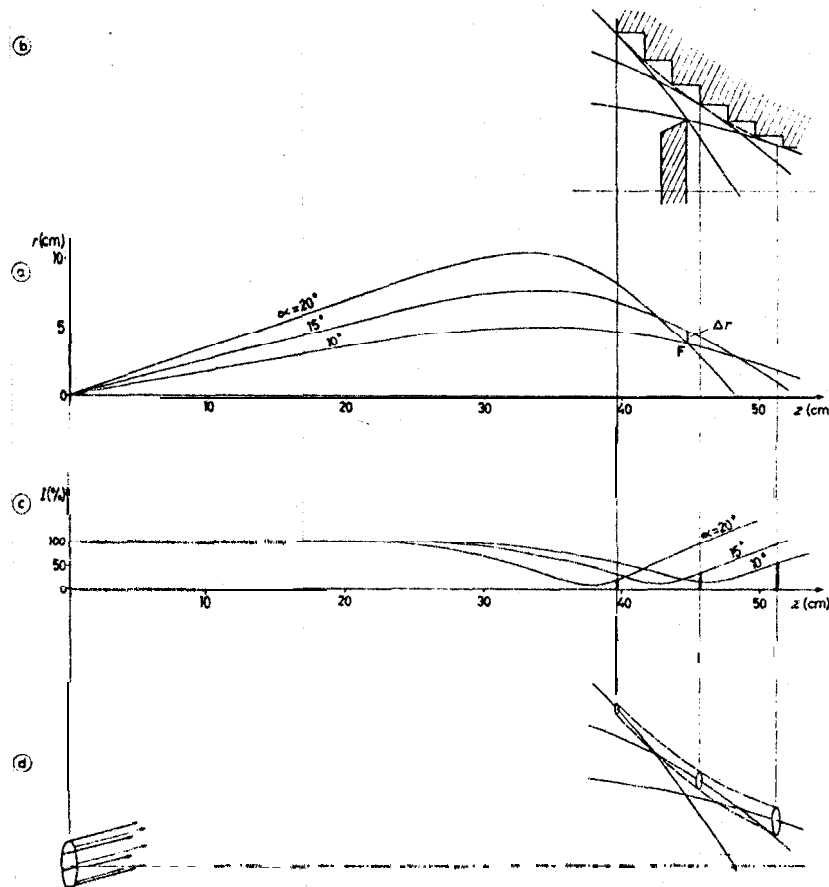


Fig. 68. Spherical aberration (a) and 'image width' (c) of the lens according to Fig. 58. For more detailed discussion see text and ref. 159.

¹⁷¹ I. Lindgren and W. Schneider, Nucl. Instr. and Methods 22 (1963) 48;
I. Lindgren, G. Pettersson and W. Schneider, Nucl. Instr. and Methods 22 (1963) 61.

The focus width Δr , caused by spherical aberration, is approximately

$$\Delta r \approx \frac{1}{2} (\partial^2 r / \partial \alpha^2)_{z,p} (\Delta \alpha)^2. \quad (130)$$

Since the transmission $T \approx \Delta \alpha \sin \alpha$ we get for a point source

$$\Delta r \approx \frac{(\partial^2 r / \partial \alpha^2)_{z,p} T^2}{2 \sin^2 \alpha}. \quad (131)$$

The line profile using the envelope baffle in Fig. 68b can be derived by recalling that particles with momentum $p > p_0$ cannot pass through the system. For $p < p_0$ one gets the following transmission if d is the slit width:

$$T(p) = \sin \alpha \left[d + \frac{(\partial r / \partial p)_{z,\alpha} (p - p_0)}{\frac{1}{2} (\partial^2 r / \partial \alpha^2)_{z,p}} \right]^{\frac{1}{2}} \quad (132)$$

$(\partial r / \partial p)_{z,\alpha}$ is the momentum dispersion. Figure 69 shows the transmission curve. This

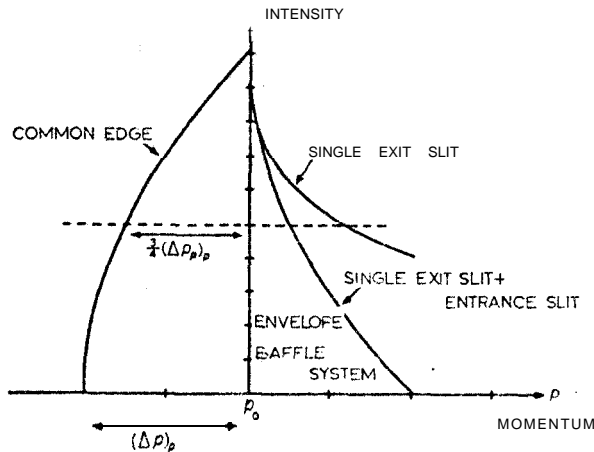


Fig. 69. Theoretical transmission curve for a point source for different baffle arrangements.

transmission curve is, for obvious reasons, reversed to an actual monokinetic conversion line profile as shown in Fig. 59. In order to obtain in practice the advantageous steep edge it is necessary to carefully design the external shutter to follow accurately the photographically traced trajectory envelope along the whole region concerned. The base width of the resolution curve is

$$(\Delta p)_p = \frac{d}{(\partial r / \partial p)_{z,\alpha}}. \quad (133)$$

The base resolution R_p^0 for a point source is then:

$$R_p^0 = \frac{(\Delta p)_p}{p_0} = \frac{d}{p_0 (\partial r / \partial p)_{z,\alpha}} \quad (134)$$

From eq. (131) it follows that the half-width is $\frac{3}{4}$ of the base width. For other instru-

ments we have previously assumed that this factor is $\approx \frac{1}{2}$. As pointed out in discussing Fig. 59, the actual resolving power towards the steep edge is actually not given by the half-width but rather by the slope of this edge. The quantity R_p^0 is the contribution of spherical aberration to the line width for a point source.

If the source has a certain extension I , this will contribute to the image width as well. Analogously, one may therefore define the *disk source resolution* as

$$R_d = \frac{I}{p_0(\partial r/\partial p)_{z,\alpha}}. \quad (135)$$

According to Fig. 68d, the rays from a disk source with a certain emission angle α will form a trajectory tube, the width of which varies along the path. This width is plotted in Fig. 68c for the actual fieldform obtained in the magnetic lens in Fig. 58. Evidently the width connected with each emission angle α has a strong minimum, the position z of which is a function of α . Furthermore, these minima do not coincide with the position of the ring focus. Fortunately, in the present case, a good compromise between the different minima is obtained by placing the ring focus slit at the correct ring focus position. The fact that minima in the trajectory tubes occur means that the source dimensions contribute much less to the line width than one might anticipate, since the total line width can be written as the sum of the two contributions.

The calculations referred to show conclusively that both the spherical aberration and the source image width are quite dependent on the fieldform. In agreement with experiments it is found that concave fields show less spherical aberration than others. The best field in this respect seems to be a field ratio between minimum and maximum of about $\frac{1}{4}$. This is indeed quite close to the empirically found value for intermediate focusing known to have particularly small spherical aberration.

The results concerning the source image width, on the other hand, favour those fieldforms that have the largest spherical aberrations. From this point of view, intermediate image focusing is not so favourable and consequently large sources should not be used in this case. This is in accordance with the first focusing experiments using this method and by the recent measurements performed by Slatis and Herrlander¹⁶⁶. In the ironfree version by Alburger¹⁵⁵ the contribution due to source size has been measured to be 0.3% per mm of diameter.

The calculations by Lindgren and Schneider thus give a complete answer to the lens field problem. Shaping of the fieldform alone is not sufficient to reduce both contributions to the resolution.

One further possibility still remains, namely to start from a fieldform which may be compatible with large sources, and then try to reduce the spherical aberration by means of an additional 'corrector'.

Some preliminary attempts have been made to use such correctors for magnetic lenses, which look fairly encouraging, although more experience is needed before one can judge the feasibility of such systems. In principle, one could either try an electrostatic corrector, similar to that successfully applied to the double focusing spectrometer by Bergkvist [see p. 108], but a two-dimensional version, i.e. a ring-

formed one, or a magnetic corrector, which should take the form of a toroid coil. One form of the latter system has been tried by Dolmatova and Kelman¹⁷² for a homogeneous field and by Dzhelepov *et al.*¹⁷³ for a short lens and used by Scrgienko¹⁶⁹ in his end-to-end coincidence spectrometer. One form of the toroid coil can easily be calculated for a homogeneous focusing field as was done by Kelman *et al.* and then tried experimentally. At an effective transmission of 6.5% ($\Omega = 8.7\%$ of 4π) the line width for a 1 mm source was found to be 1.9% with the corrector in operation. The width of the annular image was found to be reduced 2.5-3 times when the corrector was applied.

Positrons and electrons can effectively be separated from each other in a lens due to their different signs of rotation. A twisted baffle system was already designed by Deutsch *et al.*¹⁴² for this purpose.

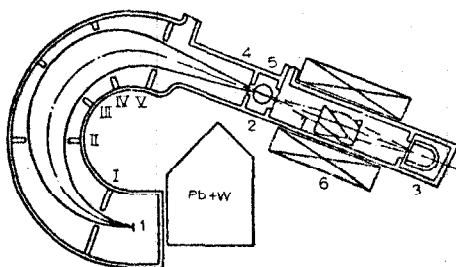


Fig. 71. Positron separating system consisting of one sector spectrometer followed by a magnetic lens provided with twisted positron baffle. Counters 2 and 3 are in coincidence.

The twist angles can be calculated from eq. (116c). As seen, this angle contains t and consequently the angle of rotation at a certain z-value is dependent on the emission angle α of each trajectory. The twisted system may thus take a rather complicated screwed form if an ultimate high transmission efficiency is aimed at by using many blades. Again, the form of these blades can be determined very accurately by the photographic trace method. The loss in transmission for the lens depicted in Fig. 58, with a positron baffle (see Fig. 70) consisting of 8 blades, was found to be less than 8% which is very nearly the geometrical cross-section of the blades themselves.

Recently, an efficient separating baffle system was used by Wu *et al.*¹⁷⁴ in a solenoidal spectrometer in the study of a possible positron 'line' effect in ^{81}Br .

An extremely powerful positron separating combination consisting of one double focusing sector spectrometer of the $1/\sqrt{\rho}$ type and one lens (see Fig. 71) has been used by Vasilenko *et al.*¹⁷⁵. The sector spectrometer is set to focus positrons and these

¹⁷² K. A. Dolmatova and V. M. Kelman, Dokl. Akad. Nauk SSSR 113 (1957) 1244; Nucl. Instr. and Methods 5 (1959) 269.

¹⁷³ B. S. Dzhlepov, N. S. Chan and P. A. Tischkin Izv. Akad. Nauk SSSR Ser. Fiz. 20 (1956) 947. (Engl. transl. Bull. Acad. Sci. USSR phys. ser. 20, 857.)

¹⁷⁴ R. Wiener, C. Chasman, P. Hanhar and C. S. Wu, Phys. Rev. 130 (1963) 1069.

¹⁷⁵ S. S. Vasilenko, M. G. Kaganskii and D. L. Kaminskii, PTE (1961) No. 5, 42. (Engl. transl. Instr. Exp. Techn. 1961, 864.)

are allowed to pass through thin windows in the detector into a magnetic lens with a twisted shutter system. The lens detector and the sector spectrometer detector are coupled in coincidence. The momentum resolution is set by the sector spectrometer and the lens will transmit more than 60% of the double focused beam. Without any spiral baffle, this system was found to have a small background of 70 coincidences per hour. It was thus possible to investigate positron spectra with an intensity of 10^{-7} positrons per disintegration. Inserting the spiral baffle the background was reduced to 0.3 coincidence per hour. Figure 72 shows the positron spectra in the decay of Ag^{110m} . With the twisted baffle inserted it was possible to measure the two components at high energies (transitions at 1750 and 1900 keV) The total number of

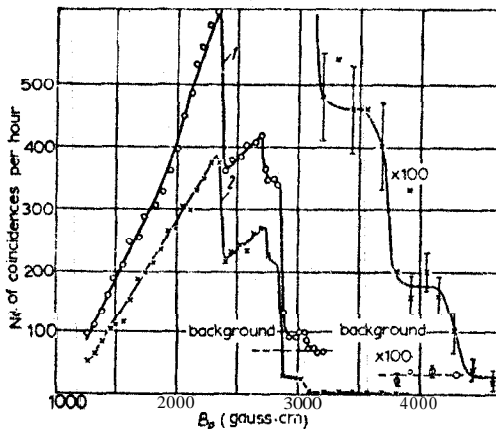


Fig. 72. Spectrum of positrons formed in the decay of Ag^{110m} ; 1) measurements without spiral baffle; 2) measurements with baffle.

positrons in the whole spectrum is very small ($\approx 10^{-5}$ per decay). The intensities of the two high energy components discovered in this way have intensities of only 10^{-7} to 10^{-8} positrons per decay. The limit of positron detection with this set-up is estimated to be about 10^{-8} - 10^{-9} positrons per decay.

It is tempting to consider the possibility of using the tandem arrangement in intermediate image focusing (see Fig. 65) for low intensity positron studies. At the position of the first small image between the lenses a double window counter could be placed and coincidences between this and the counter of the second lens registered. The resolution should be set higher for the first lens. The observed fact that only electrons originating from the position of the source have good detection probability also favours a discrimination against scattered radiation.

A multi-mode charged particle analyzer with interesting and flexible focusing and spin precession properties has been suggested by L. Page¹⁷⁶ and J. Brimhall. It consists of one long, uniform solenoidal field and a radial electric field superimposed over a portion of the magnetic field region. The focusing calculations have been

¹⁷⁶ L. Page, private communication (1963).

carried out for the first order for a point source on the axis. The electrons travel through a length of the magnetic field, through the crossed electric and magnetic field region, and enter again into a magnetic field region where the particles may be focused in a ring. The longitudinal position and radius of this ring focus is extremely flexible. The electrons can alternatively be focused to some *point* back on the axis. If the spacing of the two cylindrical tubes forming the electric field is $\approx 15\%$ of their mean radius, the particle transmission can be about 1% with $\alpha \approx 20^\circ$ and about 3.5 % for $\approx 45^\circ$. The analyzer can be used in several focusing 'modes': as a momentum spectrometer, or as a point or ring focusing device independent of particle energies. Further, the spin precession relative to the velocity precession from source point to final focus has been calculated and it is possible to obtain complete transverse polarization for a given longitudinal polarized input at the source.

§ 9. Magnetic -ray spectrometers

The field of α -spectroscopy is treated in Chapter XI. Although detection methods such as the semiconductor techniques, etc. [see Chapters VIA and VIB] are in many cases quite adequate and simple to apply, magnetic spectroscopy is still the method which yields the most accurate results. The present resolution is such that line widths of the order of 2-4 keV can be obtained, provided that extreme care is taken in preparing the source. In spite of the small solid angles that are usually employed the sensitivity of a magnetic spectrograph can be considerably enhanced by combining magnetic, high dispersion analysis with a background-reducing detector, like a photographic emulsion. This can be carefully examined after a long accumulation of tracks as to the directions and lengths of the observed events, which greatly reduces the background.

Contrary to the analysis of β -particles, α -spectroscopy is greatly hampered by the high values of $B\rho$ which necessitate fields of the order of 10000 gauss at $\rho \approx 50$ cm. Ironfree designs are therefore more or less excluded, which greatly limits the possibilities. With a few exceptions, there are only two types of α -spectrographs in existence, the semicircular and the $1/\sqrt{\rho}$ double focusing ones. Also, higher order focusing in the latter case is limited to the 'wide aperture' choice ($\beta = \frac{1}{2}$), since a high aperture would require too much power.

In principle, there is nothing particular separating α -spectroscopes from the corresponding B -instruments, except dimensions and practical design features.

The early history of α -spectroscopy is described in the book by Rutherford et al.¹², and more recently by Rosenblum¹⁷⁷ who pioneered this field and discovered the fine structure of α -lines in 1929¹⁷⁸. The semicircular spectrographs using the magnets at Bellevue together with appropriate measuring techniques are described by e.g. Bastin-Scoffice¹⁷⁹. Two devices are used, one a conventional α -spectrograph and one

¹⁷⁷ S. Rosenblum, Beiträge zur Physik und Chemie des 20. Jahrhunderts, M. von Laue zum 80. Geburtstag (Verlag F. Vieweg & Sohn).

¹⁷⁸ S. Rosenblum, J. Phys. Radium 1 (1930) 438.

¹⁷⁹ G. Bastin-Scoffice, These, Univ. Paris (1961).

which has been modified to correct for radial aberration of the second order¹⁸⁰. According to this scheme a correcting 'lens' of the type shown in Fig. 73 is introduced symmetrically between the source and the middle of the photographic plate. Within certain limits one will still be able to retain a focal plane (see Fig. 74). There is no axial focusing.

More recently a permanent magnet has been built at Orsay with a pole surface of $1.6 \times 1.0 \text{ m}^2$ and a pole gap of 48 mm. $\rho_{\max} = 50 \text{ cm}$ and $B = 8545 \text{ gauss}$. The usual focusing is adapted, but special care has been taken to allow high precision 'absolute' measurements of Q-values to be made. Thus, the magnetic field is measured along the different trajectories by means of a proton resonance probe. A series of extremely

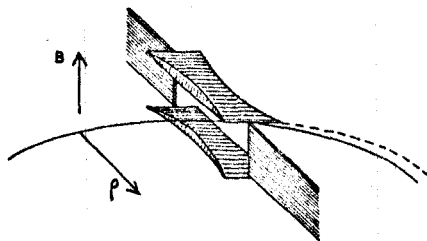


Fig. 73. Cylindrical magnetic lens corrector for semicircular focusing.

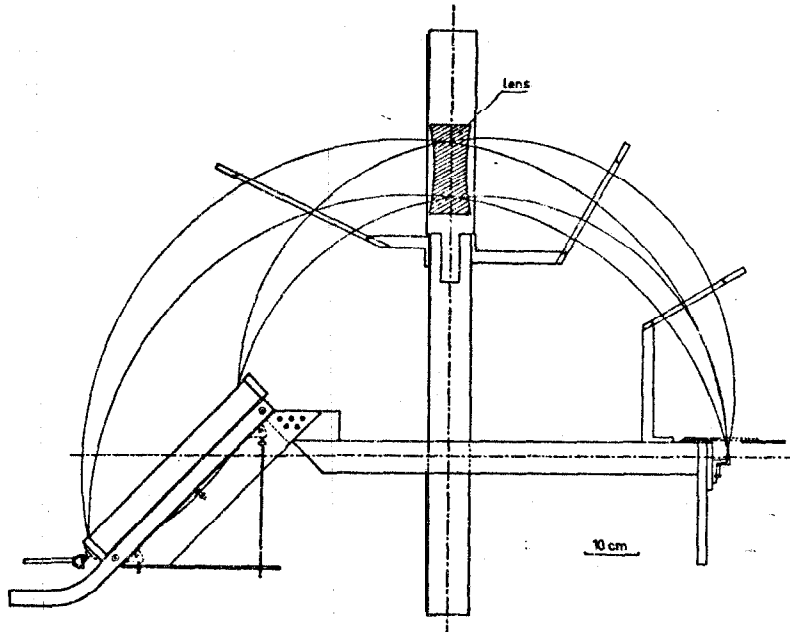


Fig. 74. Trajectories adjusted by means of a magnetic corrector in semicircular focusing.

¹⁸⁰ R. J. Walen, Nucl. Instr. and Methods 1 (1957) 242.

TABLE 4
Standard lines for β -spectroscopy

Nuclide	$B\rho$ (kgauss · cm)	$B'\rho$ (MHz · cm)	E (MeV)
Po²¹⁰	331.774	1412.561	5.304 81 \pm 0.000 62
Bi²¹² α_0	354.346	1508.665	6.050 60 66
	355.492	1513.545	6.089 77 66
Bi²¹¹ α_0	370.720	1578.380	6.622 19 69
	360.936	1536.720	6.277 52 68
Po²¹⁴	399.442	1700.663	7.686 95 75
Po²¹²	427.060 ± 0.020	1818.254 ± 0.085	8.785 40 80
Ra²²³ α_4	345.29	1470.11	5.745 5
	344.35	1466.11	5.714 3
	341.05	1452.05	5.605 3
	338.96	1443.18	5.537 1
Rn²¹⁸ α_0	376.16	1601.52	6.817 6
	368.72	1569.85	6.550 9
	365.12	1554.55	6.423 9
Po²¹⁵	391.49 ± 0.028	1666.79 ± 0.12	7.384 1 ~ 0.0010

accurately measured 'standard' lines has been reported by Rytz¹⁸¹, using this instrument. It is found that the preparation of the sources is of quite decisive importance regarding peak profiles, i.e. line widths and peak positions and consequently also for the results of the energy measurements. Even presumably 'weightless' sources can easily give line shifts of one or several keV. It is consequently understandable that high precision energy determinations performed by different workers may show deviations between themselves which are far outside the quoted limits of error, if the source problem has not been adequately taken into consideration. At the moment it seems reasonable to give particular weight to Rytz' measurements in view of the detailed examinations he has made of possible sources of error, including the source conditions. Table 4 shows Rytz' results. As can be seen the errors amount to 0.6-0.7 keV, corresponding to a relative accuracy in the absolute energies of $\approx 10 \times 10^{-5}$. A critical discussion of the new situation concerning absolute energy standards in β -spectroscopy is found in a paper by Asaro¹⁸², where it is pointed out that if the new set of energy standards is accepted the previously accepted standard energy line of RaC' (7.6804 MeV) has to be corrected upwards as much as 6 keV, which is considerably outside the previously given probable error of that line (7×10^{-5}). In view of the recognized importance of the source conditions Asaro suggested as an

¹⁸¹ A. Rytz, Helv. Phys. Acta 34 (1961) 240.

¹⁸² F. Asaro, Proc. Int. Conf. Nucl. Masses, Hamilton (1960).

alternative to the widely used Po^{210} as a standard source, that Ra^{224} ($\text{Thx}; \tau = 3.6 \text{ d}$) be used. This can be prepared by the well-known recoil technique from mass free Th^{228} ($\tau = 1.9 \text{ y}$).

There are three a-spectrographs in Russia, all of which are double focusing with $\beta = \frac{1}{8}$ ¹⁸³⁻¹⁸⁶. Goldin's et al. instrument has $p_0 = 50 \text{ cm}$, $R = 7.5 \text{ keV}$ and $T \approx 2 \times 10^{-4}$ (of 4π). Magnet weight is approximately equal to 4.5 tons.

Baranov et al. have designed their field to have the field parameter $= \frac{3}{16}$. The reason for this is as follows. If a good *focal plane* is required, i.e. one wishes to have good focusing for a large range of energies simultaneously (which is particularly important when a photographic plate is used as the detector), one can show¹⁸⁷ that the β -value of $\frac{1}{8}$ combined with $\gamma = -\frac{5}{16}$ yields this property together with higher order focusing in the vertical plane. Since $\beta = \frac{1}{8}$ is excluded for a-spectrographs, because of limitation in the field gap, the value corresponding to $\beta = \frac{1}{8}$ has to be evaluated. As was shown by Verster¹⁸⁷ and others^{74, 188, 189}, $\gamma = \frac{1}{16}$ will give third order focusing in φ for particles with a given momentum $p_0 = (B\rho)_0$. As is shown by Zelenkov¹⁸⁵ the alternative choice of $\gamma = \frac{3}{16}$ will give second order focusing in φ , but for particles with different energies. The focal surface is slightly curved with an angle of 42° relative

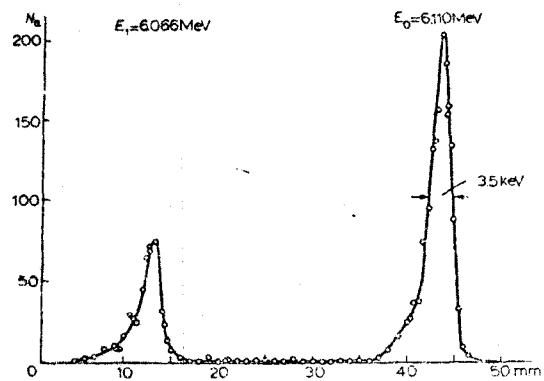


Fig. 75. Alpha-spectrum of Cm^{242} recorded in a double focusing a-spectrograph with $\rho_0 = 155 \text{ cm}$. Dispersion $2.28 \times 10^{-4} E_0/\text{min}$.

¹⁸³ L. Goldin, E. Tretyakov and G. Novikova, Proc. USSR Acad. Sci. July 1 (1955) 226.

¹⁸⁴ S. A. Baranov, A. G. Zelenkov, G. Ia. Schepkin, V. V. Beruchko and A. F. Malov, Izv. Akad. Nauk SSSR Ser. Fiz. 23 (1959) 1402 (Engl. transl. Bull. Acad. Sci. IJSSR phys. ser. 23, 1389.)

¹⁸⁵ A. G. Zelenkov, Izv. Akad. Nauk SSSR Ser. Fiz. 23 (1959) 1411. (Engl. transl. Bull. Acad. Sci. USSR phys. ser. 23, 1396.)

¹⁸⁶ B. S. Dzhelepov, R. B. Ivanov, N. G. Nedovesov and V. G. Chumin, Izv. Akad. Nauk SSSR Ser. Fiz. 23 (1959) 782. (Engl. transl. Bull. Acad. Sci. USSR phys. ser. 23, 780.)

¹⁸⁷ N. F. Verster, Physica 16 (1950) 815.

¹⁸⁸ P. P. Pavinskii, Izv. Akad. Nauk SSSR Ser. Fiz. 18 (1954) 175.

¹⁸⁹ S. Baranov, A. Malov and K. Shlyagin, PTE 1 (1956) 3.

to the radius vector. The energy range for simultaneous photographic detection is 10%. The instrument of Baranov et al., having ρ_0 as large as 155 cm, has a very high dispersion $\approx 2.28 \times 10^{-4} E_0$ per mm, corresponding to 1.2 keV/mm for Po^{210} -particles. The maximum solid angle is 8×10^{-4} (of 4π). The resolution is 3.5 keV ($A(B\rho)/B\rho = 0.028\%$) as shown in Fig. 75 for the γ -spectrum of Cm^{242} ($E = 6.066$ MeV). Because of the large dimensions of this instrument one can use samples with up to 100 μg active material for investigating particle groups with a partial period of up to 2×10^{10} years at high resolution. Figure 76 shows the instrument, having a total weight of 90 tons.

The instrument of Dzhelepov et al. has a higher maximum transmission, namely 0.3% at a resolution of 6 keV ($A(B\rho)/B\rho = 0.05\%$). In this case it was found that the line width along the focal surface, tilted 45° to the radius vector, was constant over 300 keV. The sensitivity is such that an exposure time of 100 hours will require an activity of only $10^{-5} \mu\text{Cur}$ per γ -line.

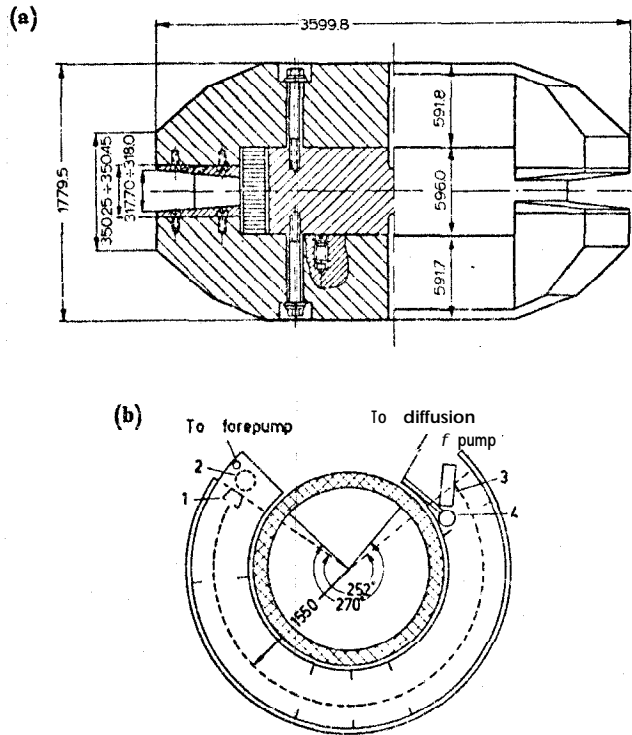


Fig. 76. Cross sections of the $\rho_0 = 155$ cm α -spectrograph according to Baranov et al. (a) Magnet (weight 90 tons); (b) spectrometer, (1) entrance aperture, (2) device for changing sources, (3) photographic cassette, (4) magnetic field probe.

The spectrograph used at Berkeley⁸⁸ has been mentioned (§ 6). It is a double focusing sector instrument with $r_0 = 35$ cm. We may recall that the fringing field had been taken into account in determining the field coefficients. In this case the tilting of the focal plane can be calculated to be $\approx 60^\circ$. Maximum solid angle is 5×10^{-4} (of 4π). The spectrometer is provided with a multi-array of semiconductor detectors in the focal plane, simultaneously accumulating the data in a multichannel analyzer. Provision is also made for γ -coincidences with a γ -scintillation detector that is movable around the source. A large amount of information on γ -spectra has been obtained by the Berkeley group, which is described in more detail in thesis works¹⁹⁰ and in Chapter XI.

If weightless sources can be prepared an interesting possibility of studying the Spectra of α -recoiling nuclei in an γ -spectrograph presents itself. The momentum of the recoiling nucleus is the same as the emitted γ -particle and depending on the charge, its Bp -value will be related to that of the γ -particle by a simple multiple. The charge spectrum of the ions can then be studied. Such studies are under way¹⁹¹.

Another point of interest for high resolution magnetic spectroscopy would be to see if γ -line widths of less than 1 keV can be reached. The extreme source requirements may eventually limit such efforts.

§ 10. Electrostatic spectrometers

So far, only very little work has been done with electrostatic focusing β -ray spectrometers. In the low energy region it seems very probable, however, that such focusing devices will become much more frequently used in the future. In fact the figures of merit concerning resolution and transmission can be made very favourable. Two cases can be distinguished, one using the field between two concentric cylinders¹⁹² (focusing after 127°), and the other using the field between two concentric spherical conductors (focusing after 180°). The latter case seems to offer advantages. It was shown by Purcell¹⁹³ that the focusing in this case shows a remarkable similarity to the magnetic semicircular case with the additional advantage that it is space-focusing because of the spherical symmetry. In both arrangements sector fields can be used. Contrary to the magnetic prisms, the electric fringing fields can be controlled to a high degree. Unfortunately, at higher energies the relativistic mass increase of electrons starts to adversely affect the focusing properties. Cavanagh³ has considered the case of a spherical energy analyzer for electrons, having a mean diameter of 1 m and a gap between the spheres of 1.5 cm. The ratio between transmission and resolving power at 0.2 MeV is then 1.6, whereas at 0.7 MeV it is 0.7.

¹⁹⁰ R. Pilger, UCRL-3877 (July 1957);
M. Hill, UCRL-8423 (Aug. 1958);
C. Ruiz, UCRL-9511 (April 1961).

¹⁹¹ F. Asaro, private communication.

¹⁹² A. L. Hughes and V. Rojansky, Phys. Rev. 34 (1929) 234. (See also R. O. Bondclid and C. A. Kennedy, Phys. Rev. 115 (1959) 1601.)

¹⁹³ E. M. Purcell, Phys. Rev. (1938) 818.

A spherical electrostatic spectrometer, primarily intended for analyzing heavy particles, has been designed by Allison and Weyl¹⁹⁴. At a calculated transmission of 0.8%, the expected energy resolving power was 0.5 %. Experimental data so far obtained for a B-line are 0.4% and 1.2%. Because of relativity, the maximum energy limit of the instrument for electrons is 1.7 MeV.

Electrostatic focusing spectrometers have also been investigated by Rogers¹⁹⁵ and Ashby¹⁹⁶ (relativistic effects) and Kobayashi¹⁹⁷. Brosi et al.¹⁹⁸ have used a spherical electrostatic spectrometer especially adapted for precision measurement of the longitudinal polarization of P-particles following P^{32} -decay.

Some recent theoretical work has been done by Ritchie et al.¹⁹⁹. They treated the case when the source is placed *inside* the field, which naturally limits the practicability of an electrostatic device. The particles are allowed to emerge through a slit into a fieldfree region where post-acceleration occurs. For a point source they got a theoretical resolution of 6 % at a transmission of 25 %. A particular case presents itself if the electron-emitting source is distributed on the surface of the inner sphere. If the radius of this source is allowed to be as much as 30% of the inner radius, a resolution of 7.7% at a transmission of 16% is obtained. It is likely, however, that sector focusing at high resolution, which corresponds more to the case originally treated by Purcell, will be of more interest in the future.

A brief review of the theory of the spherical electrostatic spectrometer may be useful as a starting point for further attempts in this direction.

In the inverse square field of a spherical condenser the electron trajectories are ellipses with the same major axis $2a$, where a is the radius of the 'central' orbit. Focusing after π occurs in close analogy to the homogeneous magnetic field with the important additional advantage of double focusing. Let us now consider the sector case (see Fig. 77). We start by considering a point source on the axis AF. The regions I and II are fieldfree. At the borders between the regions we neglect the fringing field. In the field III we have as a condition for a circular orbit with radius a (velocity and energy of the electron are v_0 and E):

$$\frac{V_t R_1 R_2}{r^2(R_2 - R_1)} = \frac{amv_0^2}{er^2} \quad (136)$$

$$Ee = \frac{1}{2} mv_0^2. \quad (137)$$

If we put $a = \frac{1}{2}(R_1 + R_2)$ we get for the focusing potential V_t

$$V_t = E \left(\frac{R_2}{R_1} - \frac{R_1}{R_2} \right) \quad (138)$$

¹⁹⁴ S. Allison and P. Weyl, personal communication (1954).

¹⁹⁵ F. T. Rogers Jr., Rev. Sci. Instr. 8 (1937) 22; 11 (1939) 19: 14 (1943) 216.

¹⁹⁶ N. Ashby, Nucl. Instr. and Methods 3 (1958) 90.

¹⁹⁷ Y. Kobayashi, J. Phys. Soc. Japan 8 (1953) 135, 440, 648.

¹⁹⁸ A. R. Brosi, A. I. Galonsky, B. H. Ketelle and H. B. Willard, Nucl. Phys. 33 (1962) 353.

¹⁹⁹ R. H. Ritchie, J. S. Chcka and R. D. Birkhoff, Nucl. Instr. and Methods 6 (1960) 157.

Using Binet's formula for the trajectory in an inverse square field (region III) we get the differential equation :

$$\frac{d^2}{d\varphi^2} \left(\frac{1}{r} \right) + \frac{1}{r} = \frac{k^2}{A^2} \quad (139)$$

where $k^2 = av_0^2$ and $A = r^2\dot{\varphi}$. The solution is

$$\frac{1}{r} = P \cos \varphi + Q \sin \varphi + \frac{k^2}{A^2}. \quad (140)$$

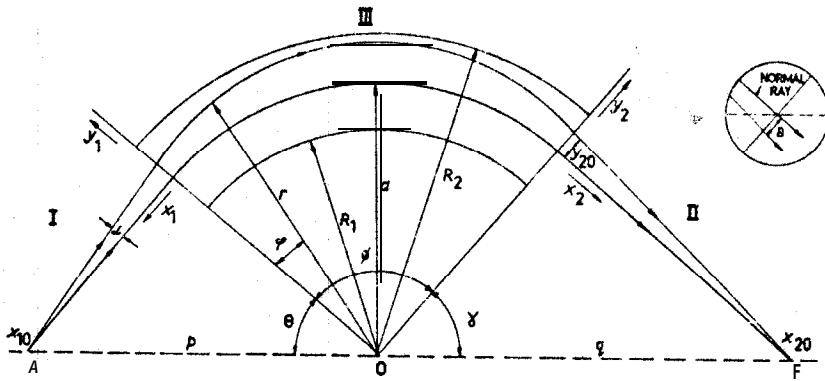


Fig. 77. Trajectories in an electrostatic sector field. Calculations show that Barber's rule is valid for the spherical sector field, forming the basis for space focusing.

The boundary conditions, requiring a focus at x_{20} (the source being situated at x_{10}) independent of small α (neglecting second order terms) and a smooth trajectory through the regions, determine P and Q and yield:

$$a(x_{10} + x_{20}) = \operatorname{tg} \phi (x_{10} x_{20} - a^2). \quad (141)$$

It can now be shown that the conjugate points, i.e. the 'source' and 'slit', lie on a line through O. According to Fig. 77 $\operatorname{tg} \gamma = x_{20}/a$ and $\operatorname{tg} \theta = x_{10}/a$. We then have:

$$\operatorname{tg} (\theta + \gamma) = \frac{a(x_{20} + x_{10})}{a^2 - x_{10}x_{20}}. \quad (142)$$

If this expression is compared with eq. (141) we get

$$\operatorname{tg} \phi = -\operatorname{tg} (\theta + \gamma) \quad (143)$$

giving :

$$\phi + \theta + \gamma = 180^\circ. \quad (144)$$

This is the well-known property valid for a homogeneous magnetic sector field found by Barber. In § 6 it was discussed how Barber's rule could also be applied to the

magnetic double focusing sector field ($1/\sqrt{\rho}$ -field) although in that case Barber's 'modified' rule was of a formal nature. In the case of a spherical electric sector field Purcell's extension of Barber's rule will, however, form the basis of a three-dimensional spectrometer using the whole gap between the spherical shells for focusing and yielding a point image on the axis.

The dispersion is obtained if one calculates the distance y_2 by which a particle with velocity $v_0(1+\beta)$ misses the focal point for particles of velocity v_0 . It is found to be

$$y_2 = 2\beta a[1 - \cos \phi + (x_{20}/a)\sin \phi]. \quad (145)$$

If the distance from the source to $r=0$ is p and from the slit to $r=0$ is q one simply gets:

$$y_2 = 2\beta a(1 + p^{-1}q). \quad (146)$$

The velocity dispersion D_v is defined as y_2/β :

$$D_v = 2a(1 + p^{-1}q). \quad (147)$$

This is twice the dispersion found for the case of the homogeneous magnetic field and equal to the magnetic double focusing $1/\sqrt{\rho}$ field. The energy dispersion is $\frac{1}{2}D_v$.

In order to find the resolving power one has to calculate the distance B by which a ray starting at a small angle α to the central ray will miss the focus, i.e. one has to take the previous calculations to the second order in α . B will then be a measure of the spherical aberration. One first calculates the quantity (see Fig. 77),

$$\frac{y_{20}}{a} = \alpha \sin \gamma / \cos \theta + \alpha^2 \sin^2 \gamma / \cos^2 \theta + \alpha^2 (\sin \theta \sin \gamma - \cos \theta \cos \gamma - \sec^2 \gamma). \quad (148)$$

One finally arrives at:

$$B = -\alpha^2 a(p^2 q^{-2} + p^{-1}q) \quad (149)$$

which is just twice the corresponding expression for the homogeneous magnetic field. The velocity base resolving power is identical in both cases, namely:

$$R_v = BD_v^{-1} = \frac{1}{2} \alpha^2 (1 - pq^{-1} + p^2 q^{-2}). \quad (150)$$

The energy base resolving power R_E is perhaps a more appropriate quantity since an electrostatic device is an *energy* dispersive instrument [E is proportional to the applied voltage V_f according to eq. (138)]. The energy resolving power is:

$$R_E = \alpha^2 (1 - pq^{-1} + p^2 q^{-2}). \quad (151)$$

This has a minimum for $q=2p$ for which case one gets:

$$(R_E)_{\min} = \frac{3}{4} \alpha^2. \quad (152)$$

For the symmetrical case $p=q$, $R_E = \frac{1}{2}\alpha^2$. For comparison, R_E for the cylindrical case is $\frac{1}{4}\alpha^2$.

The effect of finite source dimensions on the resolving power can be obtained if one uses expressions (148) and (149) and the fact that the conjugate points are

on a line through O. One can, however, get an approximate estimate of the effect by recalling that any given trajectory is reversible. Consequently, if the source width is made smaller than $\approx \alpha^2 a$, the spreading of the trace due to source-width will be smaller than the contribution due to aberration according to eq. (149).

There are two main problems left that may seriously influence the *validity* of the above results: (a) The aberration due to the fringing fields and (b) the effects of relativity. (a) can be reduced by using grounded guard-diaphragms as suggested by Herzog²⁰⁰. The relativity correction may at first sight be supposed to be small because of the small changes in energy as the electrons transverse the condenser. The spread in focus will unfortunately be of the order of αa even when v/c is a few tenths. The situation is actually similar to that of the precession of the relativistic Kepler orbits in the atomic quantum theory leading to fine structure. Let y_r be the distance by which a relativistic trajectory misses the non-relativistic focus. y_r/a can then be developed into $k_1\alpha + k_2\alpha^2 + \dots$. Purcell has calculated k_1 for different values of v/c and geometrical quantities. In the general symmetrical case, k_1 was calculated numerically for $E = 100$ keV for several values of ϕ , including 90° and 180° . It turns out that k_1 changes sign between these limits. For $\phi = 90^\circ$, $k_1 = -0.48$ and for $\phi = 180^\circ$ $k_1 = 0.60$. k_1 is equal to zero for $\phi = 131^\circ$. For this angle k_1 is small also for $E \geq 500$ keV. The parameter p/q could probably also be adjusted to minimize y_r . For a more complete treatment of the relativistic effects the reader is referred to Ashby's paper¹⁹⁶.

Purcell emphasizes the technical difficulties of constructing a three-dimensional spectrograph under optimum conditions. His actual design, which so far has not been seriously followed up by others, exhibits encouraging figures. For simplicity he chose $\phi = 90^\circ$, $p = q = a\sqrt{2}$, $R_1 = 8.61$ cm and $R_2 = 10.16$ cm, which means a total source-to-slit distance of 21.65 cm. One then gets $V_t/E = 0.315$. He furthermore used Herzog guard-diaphragms. The spectrometer was tested with an electron pun. Due to asymmetries of the condenser (≈ 1 mm) maximum resolving power was not quite reached but experiments indicated that the solid angle of $\approx 2\%$ used probably could have been further increased at the theoretically calculated resolving power $R_E \approx 0.2\%$. It will be interesting to see further attempts in this direction, since it would permit high resolution in high transmission coincidence work, etc., at least in the low energy region. The main problem to be solved is the influence of the fringing fields which still seems to be easier to handle than in the magnetic case. A spectrograph with only a sector in the lateral direction would also be convenient for many types of investigations using low energy electrons. Such an instrument would perhaps be easier to handle and one could make use of narrow and extended sources. The introduction of new fringing fields in the lateral direction would be a possible source of complication.

§ 11. Precision spectroscopy

Among the lighter elements the spacing of levels is often such that a moderate resolution may be regarded as satisfactory. The situation changes, however, rather quickly

²⁰⁰ R. Herzog, Z. Physik 97 (1935) 596; Phys. Zeitschr. 41 (1940) 18.

at higher Z's. Most interesting and decisive problems are to be found among the heavier elements, where many closely spaced levels are frequently excited in radioactive decay. A typical example is the decay of Bi^{206} studied by Alburger²⁰¹. This case exhibits a fairly normal level spacing in this region and 28 -lines are emitted. These lines are converted in several atomic shells and the resulting -line spectrum is very line-rich and complicated to interpret. An example studied by Mihelich et al.²⁹, is given in Fig. 8 in this chapter. The above 'moderate' resolution then turns out to be entirely inadequate. The situation is well illustrated by Fig. 78, showing a line group

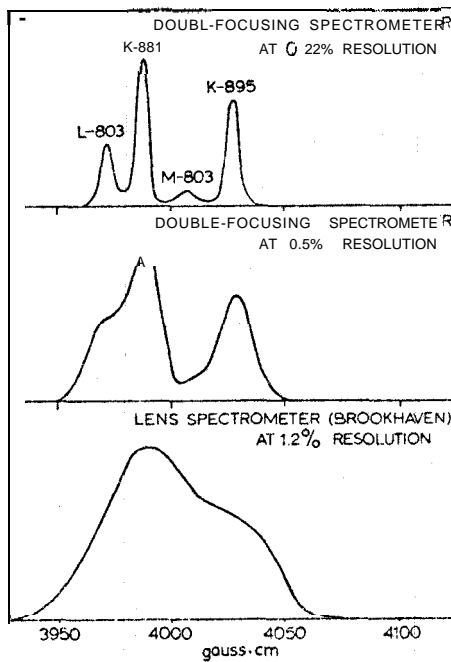


Fig. 78. A portion of the $\text{Bi}^{206}(K)\text{Pb}^{206}$ internal conversion spectrum showing the need for high resolution.

in the spectrum of Bi^{206} . The structure is completely unresolved with a resolution of 1.2% taken in a lens spectrometer. With the double focusing spectrometer a resolution of 0.5% is still insufficient to separate the components. At 0.22% resolution the group is completely resolved.

Another example is given in Fig. 79, where the conversion spectrum of the neutron deficient Au-isotopes produced in the reaction $\text{Pt}(p,xn)\text{Au}$ was studied²⁰² by means of an automatically scanning double focusing spectrometer (see page 102). The spectrum was run at a resolution of 0.35% and it is noted that this resolution is not quite enough to get a complete separation of all the lines. Compare Fig. 12 which is the same spectrum recorded photographically.

²⁰¹ D. E. Alburger and M. H. L. Pryce, Phys. Rev. 92 (1953) 514; Phys. Rev. 95 (1954) 1482.

²⁰² I. Marklund, E. Karlsson and K. Korkman, Ark. f. Fysik 22 (1962) 289.

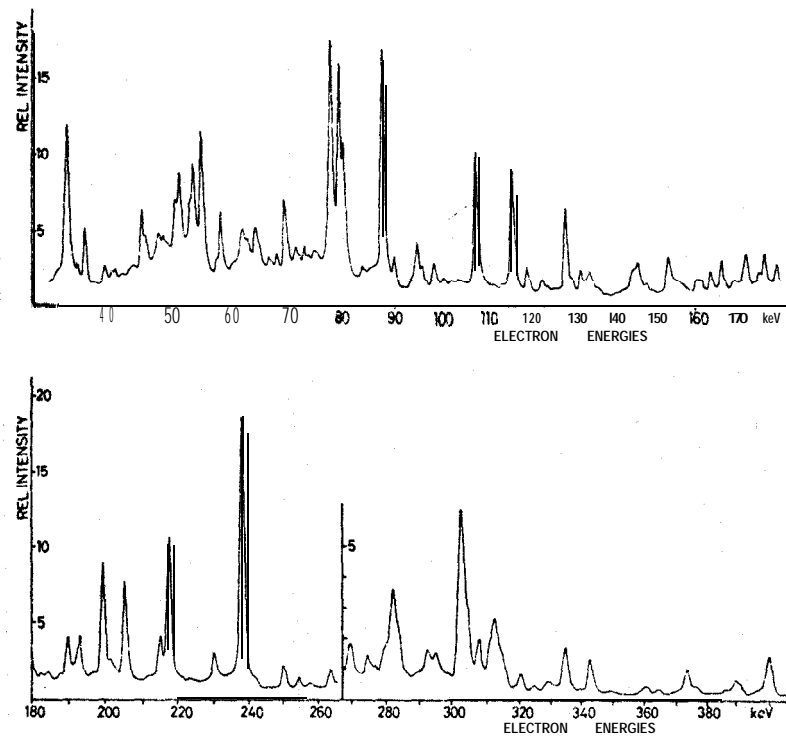


Fig. 79. Conversion spectrum of neutron-deficient Au isotopes produced in the reaction $\text{Pt}(\text{p},\text{xn})\text{Au}$ and automatically scanned in a double focusing instrument at a resolution of 0.35%. This resolution is not quite enough to resolve the spectrum. Compare the photographically recorded spectrum in Fig. 12.

A particularly instructive case²⁰³ for a high resolution decay scheme study is that of Au^{194} . This decay contains more than 100 γ -transitions and the conversion spectrum, containing some 350 detectable lines, is probably the most line-rich one that has been studied and analyzed so far. Figure 80 shows part of the spectrum, from $B\rho=6200$ to $B\rho=8400$, the complexity being roughly equal from the very lowest $B\rho$ -values up to $B\rho=13000$. It was studied using the 50 cm radius iron yoke instrument shown in Fig. 20 set at a resolution of 0.17 %. By means of a double counter operated in coincidence it was possible to detect lines of an intensity 10^{-5} times that of the strongest lines. The accuracy of $B\rho$ measurements was 2 parts in 10^4 . When all conversion lines had been measured and attributed to K, L_I, . . . lines of specified γ -energies, a large matrix was made up containing all γ -lines and their sum energies, altogether 2700 sums. Each of these energy sums was compared to the transition energies and the values that coincided to within $\pm 1:10^3$ were marked to form the material for a detailed analysis. A few 'cross-over' transitions which were quite reliably established were used to get approximate energy doubling for consistent reference

²⁰³ G. Backstrom, O. Bergman, J. Burde and J. Lindskog, Nucl. Phys. 15

566.

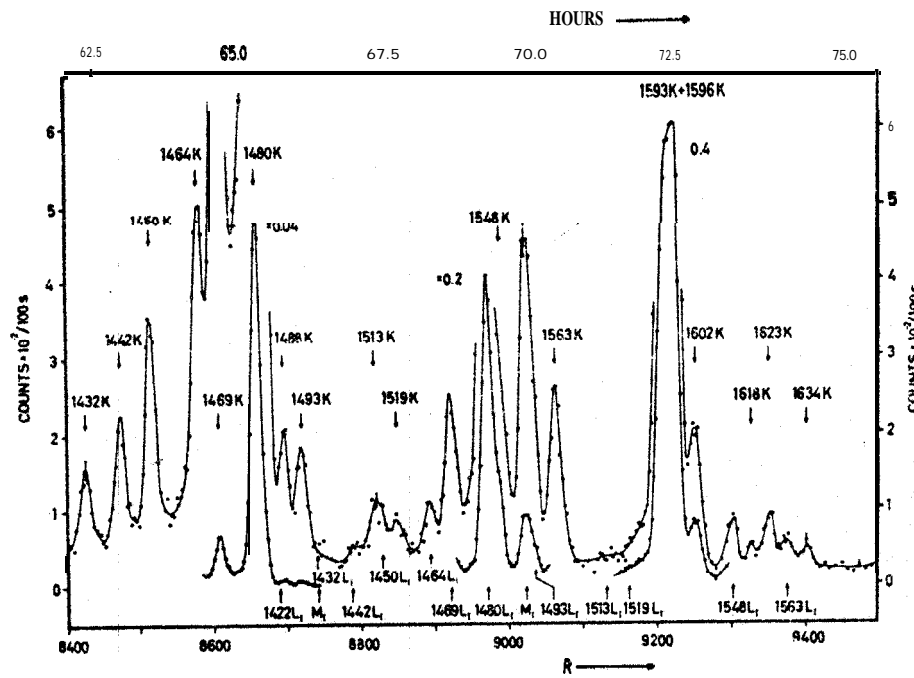


Fig. 80. Part of Au^{194} spectrum recorded in the 50 cm iron yoke double focusing instrument shown in Fig. 20. Resolution set at 0.17 %.

energy purposes over the entire very extended spectrum. In this way reference lines around 300 keV were directly connected to lines of 2 MeV. The number of accidental sum relationships in the matrix can easily be calculated, the formula being closely analogous to that used in time coincidences: The probability that an energy value ε coincides with the energy of a γ -ray, within its limits of error $\pm \Delta\varepsilon$, is $2\delta\varepsilon\rho(\varepsilon)$, where $(\)$ is the line density (number of lines per keV). The density of energy sums $\rho_s(\varepsilon)$ may be taken directly from the matrix. The total number N_{acc} of accidental relationships contained in the matrix then becomes:

$$N_{\text{acc}} = 2 \sum \Delta\varepsilon \rho(\varepsilon) \rho_s(\varepsilon) \delta\varepsilon, \quad (153)$$

where the sum is taken over all energies and the energy span is subdivided into intervals of length $\delta\varepsilon$. In the actual case, allowing for a deviation of 0.1%, N_{acc} was calculated to be 420, whereas the number found from the matrix was 526. Evidently only some 20% of the sum relationships can be expected to be true if the energy measurements are not better than 0.1 %. For complicated decay scheme studies it is therefore essential to reduce the error to something like $\approx 1 : 10^4$. The scheme finally arrived at is shown in Fig. 81, where most of the transitions can be fitted in. This scheme was further tested by $e^- - e^-$ coincidence studies of selected lines using a two-lens coincidence spectrometer. Further support and additional information concerning the decay scheme was obtained from a similar study of Ir^{194} , decaying to the same daughter nuclide.

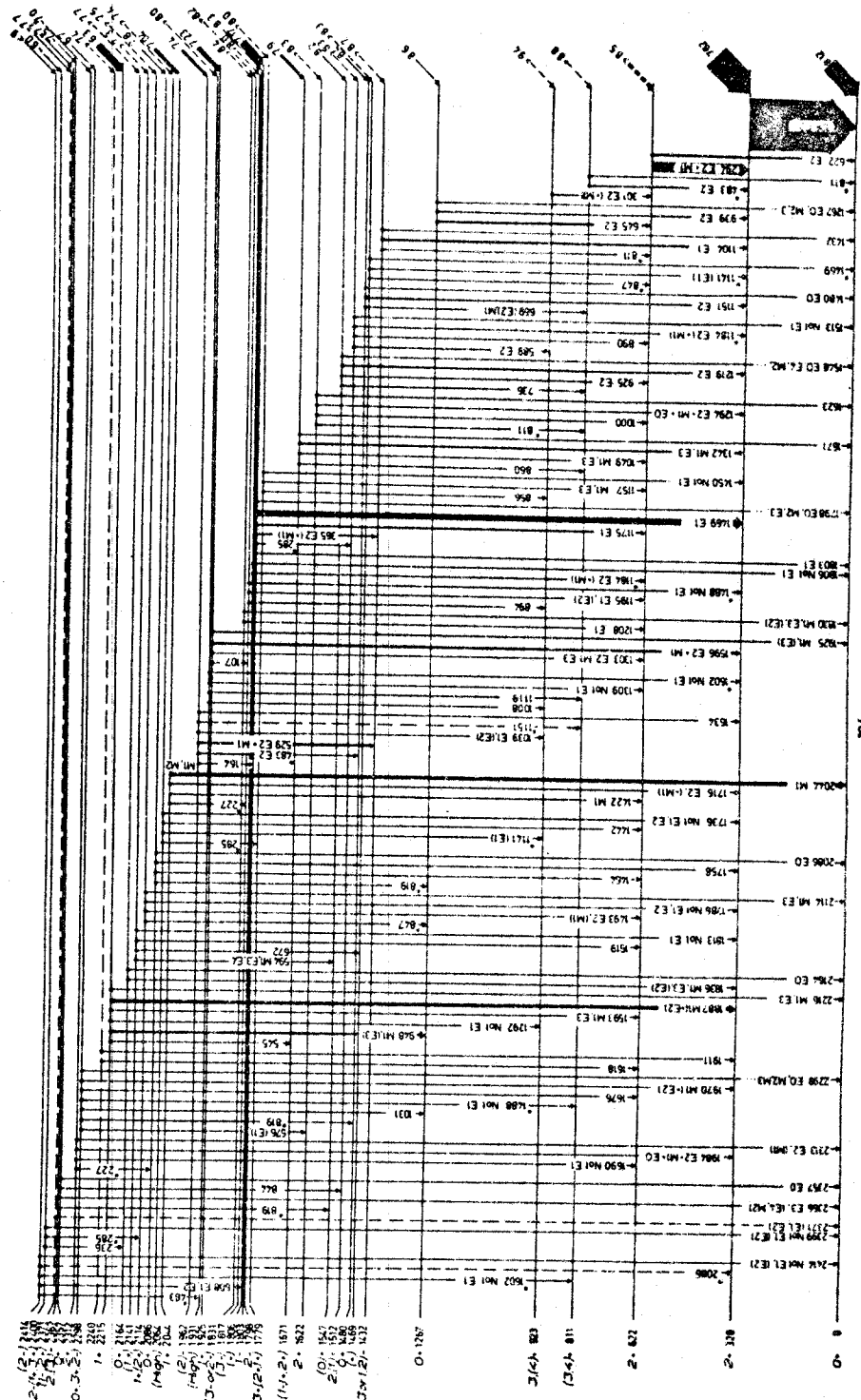


Fig. 81. Nuclear level scheme of Pt^{194} obtained from the studies of Au^{194} and Ir^{194} radioactive decays, using both internal and external photo-electron spectra.

Pt^{194}

A high resolution study of the intensity of the separate conversion lines yields the fundamental quantum-mechanical properties of the nuclear levels, namely spins, parities, mixing ratios of the various transitions, and transition probabilities. The *absolute* values of the conversion coefficients are mostly somewhat difficult to measure accurately. Several methods can in principle be applied, the most universal one being the 'internal-external photo-electron' method, described in Chapter VIIIA, which in complex spectra also calls for high resolution.

It is interesting to note that it is not necessary to determine the absolute values of the conversion coefficients in order to get the information listed above. In Fig. 82 are given the calculated values of the ratios of the conversion coefficients in the K, L_I, L_{II}, L_{III} shells for Z=78 and, for completeness, also the absolute K conversion coefficients. The K/L ratio will evidently determine some of the mentioned entities fairly uniquely. It is obvious, however, that a very much better and more detailed picture of the transition is obtained from an additional knowledge of the ratios of the various L subshells. These ratios are quite sensitive to the multipolarity of the transitions and very accurate values for the mixing ratios, etc. can be obtained from them.

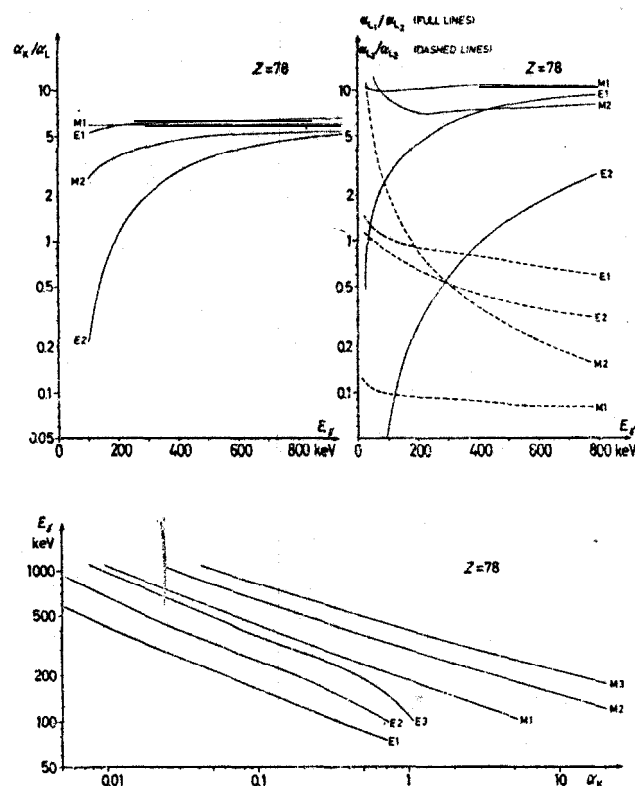


Fig. 82. Theoretical K conversion coefficient (lower figure) for Z=78 and K/L, L₁/L₂ and L₃/L₂ figures).

It is interesting to note that with present high precision instruments the L subshell intensities can be measured with higher accuracy than they can be *interpreted* by use of existing conversion coefficient theory. Although the theory obviously demands that the same value of the M1-E2 mixing ratio be obtained from the observed values of the L_I/L_{II} , L_I/L_{III} , and L_{II}/L_{III} intensity ratios, measurements with double focusing ironfree instruments have shown that this is not always the case^{204, 205, 208}. In one example, that of the 103-keV transition²⁰⁵ in Eu^{153} , the E2 percentages inferred from the observed L_I/L_{II} and L_{II}/L_{III} intensity ratios were $2.02 \pm 0.08\%$ and $1.44 \pm 0.06\%$, respectively, with use of the Sliv theoretical coefficients. Differences of this magnitude can be of consequence when use is made of the E2 transition probabilities in nuclear-model correlations or in interpretation of angular distribution experiments with mixed transitions. The situation is further complicated by the fact that the theoretical L shell M1 and E2 conversion coefficients of Rose²⁰⁶ and of Sliv and Band²⁰⁷ differ by as much as 50%, especially in the L_I and L_{II} subshells.

Since the atomic binding energy differences (see Appendix 2) between the L_I , L_{II} , and L_{III} levels are small very good resolution is needed in order to resolve the triplets. Figure 83 shows the L_I , L_{II} , L_{III} triplet from the 279 keV γ -ray transition²⁰⁸ in Hg^{203} taken with the 30 cm ironfree double focusing spectrometer (see p. 109). The relative line width (including the natural line width) was 0.07%. The triplet is completely resolved. A resolution of 0.2% would give a very inexact value for the $L_I : L_{II}$ ratio whereas a resolution of somewhat about 1% (indicated in the figure) would give no information at all about the triplet structure. The situation would be better at lower

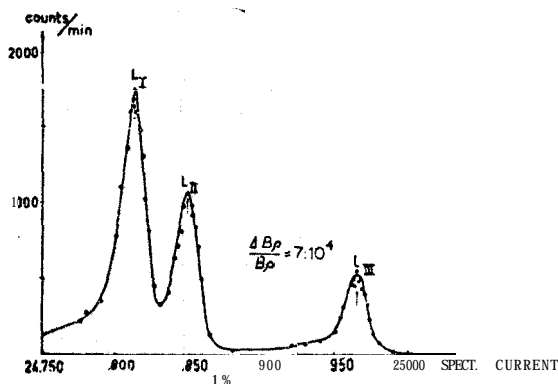


Fig. 83. L_I , L_{II} , L_{III} triplet from the 279 keV γ -line of Hg^{203} taken with 30 cm ironfree double focusing spectrometer (Fig. 24). Instrumental resolution set at $\approx 0.05\%$.

²⁰⁴ T. Novakov and R. Stepic, Physics Letters 3 (1962) 82.

²⁰⁵ T. Novakov, R. L. Graham and J. M. Hollander, unpublished data (July, 1963).

²⁰⁶ M. E. Rose, Internal Conversion Coefficients (North-Holland Publ. Co., Amsterdam, 1958).

²⁰⁷ L. A. Sliv and I. M. Rand, Tables of Internal Conversion Coefficients. Appendix 5.

²⁰⁸ C. Nordling, K. Siegbahn, E. Sokolowski and A. H. Wapstra, Nucl. Phys. 1 (1956) 326.

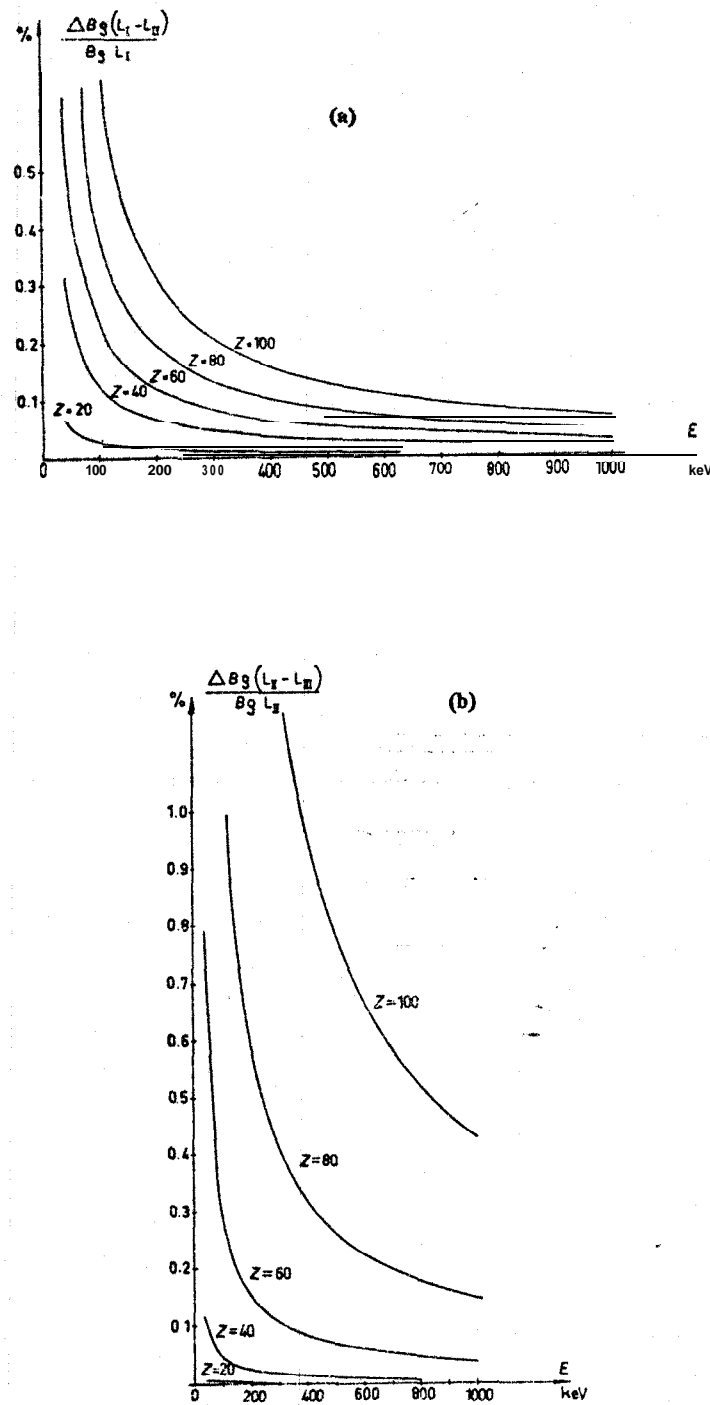


Fig. 84. Relative momentum separation versus energy for (a) $L_1-L_{2\text{II}}$ and (b) $L_1-L_{3\text{III}}$ at different values.

REFERENCE ONLY PHYSICS-111-LAB. DO NOT REMOVE

184

K. SIEGBAHN

CH. III

energies, but on the other hand worse at smaller Z-values. The recorded spectrum of Hg^{203} shown above is of some historical interest since it was the first experimental indication, obtained by Wapstra et al., of the effect of finite nuclear size on internal conversion (the transition is M1) and is further discussed in Chapter XVIIC.

The momentum resolution needed in order to resolve L_I from L_{II} and L_{III} from L_{IV} is plotted in Fig. 84. For -energies ≥ 400 keV and $Z \leq 80$, one has to have a resolution of better than 0.1% in order to obtain a complete separation of the triplet.

The possibilities of using M subshell conversion lines for similar purposes have not yet been explored. High resolution is needed. The applicabilities are probably less general, and would be of particular interest for low energies and high Z-values.

Coincidence or angular correlation experiments usually require large solid angles in order to collect the data at a high speed. This demand should, however, not be overestimated, and in fact many such experiments are also quite feasibly performed at small solid angles, i.e. one might run such experiments at high resolution, too. The recording time only will become correspondingly longer. When only one of the two channels needs high resolution this disadvantage may sometimes be trivial. Coincidences and angular correlations between well-resolved lines (e.g. K and L sublines) in a high resolution spectrometer, and -lines or conversion lines registered by a scintillation or a semiconductor detector using a multichannel analyzer are procedures that will become more extensively used in future work.

As an illustrative example we may quote a recently performed study²⁰⁹ of the electron emission from cl-recoiling ions. This investigation concerned the possibilities of using the recoil effect for measuring life-times of nuclear states from which conversion electrons are subsequently emitted. The ironfree 50 cm radius double focusing instrument at Berkeley⁶³ was used and Cm^{244} , decaying by α -emission to Pu^{240} , was investigated. It is known that a conversionline which is emitted from a recoiling ion in flight is broadened because of the Doppler effect. The well-known A line in the spectrum of ThC(Bi^{212}) of the 40 keV transition has e.g. such a Doppler broadened shape (this line is reproduced in Fig. 7) and Burde and Cohen²¹⁰ and Siekman and de Waard²¹¹ have used this hct to determine the lifetime of the 40 keV excited state in Tl^{208} , following the α -decay in Bi^{212} (see Chapter XVII). The new Berkeley method consists in principle of accurately measuring, by means of an applied electric field over the source, the time of flight of the ion before the electron is emitted, the conversion line being studied at high resolution ($\approx 0.1\%$). Figure 85 shows the arrangement. The source was on grounded thin Al foil and, a few millimeters from this, a fine mesh metal grid was placed at a negative potential V_0 of ≤ 12 kV. A few millimeters further away another mesh metal grid at ground potential was situated. An -scintillation detector was placed behind the source and another scintillation detector was used as a -detector in the spectrometer. The detectors could be coupled

²⁰⁹ T. Novakov, J. M. Hollander and R. L. Graham, Nucl. Instr. and Methods 26 (1964) 189.

²¹⁰ J. Burde and S. G. Cohen, Phys. Rev. 104 (1956) 1093.

²¹¹ J. G. Siekman and H. de Waard, Phys. 8 (1958) 402.

in a conventional fast-slow coincidence arrangement according to the figure. In the simple case when the α -particle is emitted rearwards, it is easy to see that the following relation holds:

$$t = \frac{\epsilon}{(V_0/L)v_r}, \quad (154)$$

where t is the time of flight of the ion before the electron is emitted (which is equal to the nuclear lifetime of that ion), ϵ is the net energy gain of the ion in the decelerating and accelerating electric fields, V_0/L is the electric field, and v_r is the velocity of the recoil ion. The latter is accurately known (for $A \sim 240$ and $E_\alpha = 6$ MeV, $v_r = 2.8 \times 10^7$ cm/sec, corresponding to 100 keV) and V_0/L can be accurately measured. When the field is applied, the high energy side of the line will be transformed into an exponential decay curve and from the slope of this one immediately gets

$$T_1 = \frac{\epsilon_t}{(V_0/L)v_r}. \quad (155)$$

The electrons emitted from ions travelling in the forward direction can be identified

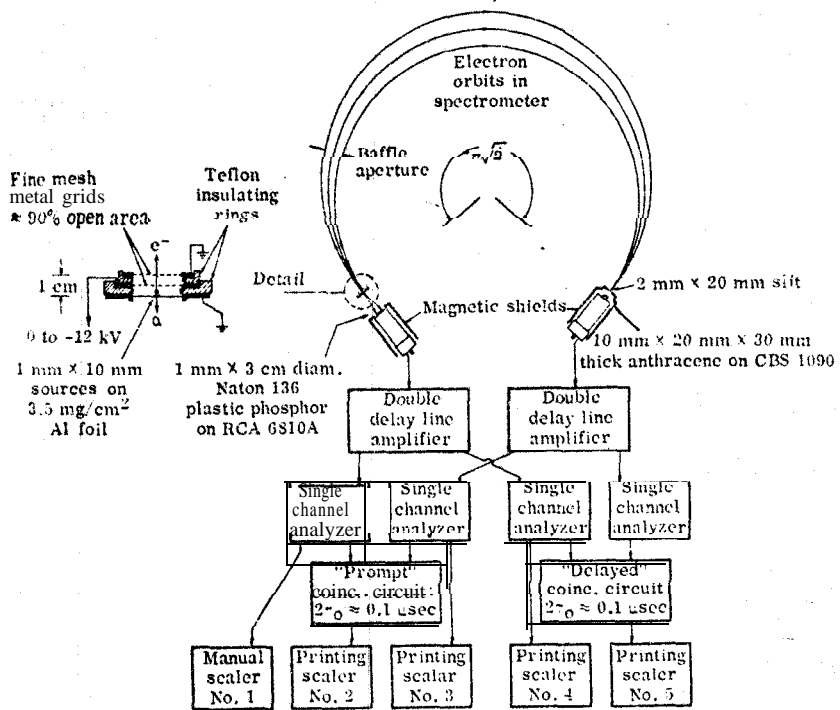


Fig. 85. Determination of nuclear life times by means of high-resolution studies ($\approx 0.1\%$) of Doppler-broadened conversion-lines after α -decay. The time of flight of the recoiling ion before the electrons emitted is measured accurately by applying a decelerating-accelerating electric field at the source.

by a coincident γ -particle being emitted in the backward direction. The method does not necessarily require this condition, but the interpretation becomes more clear-cut and accurate. One can, however, calculate the shape of the 'decay' curve when the field is applied by taking into consideration all different angles. The result is a slightly curved slope which asymptotically approaches the correct slope.

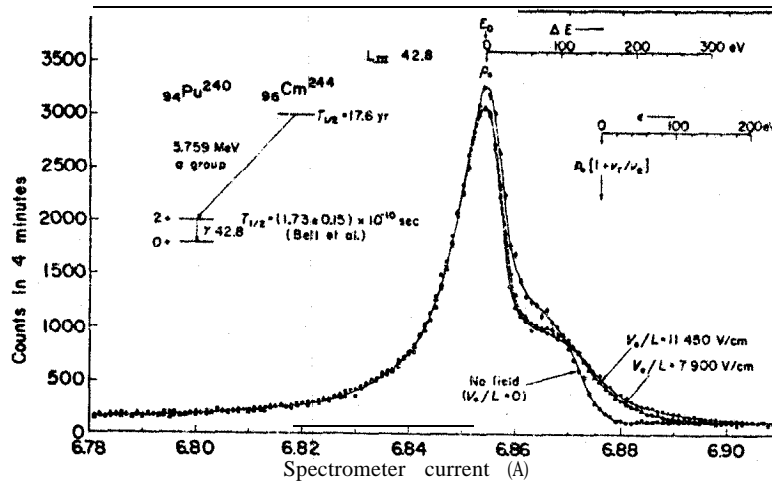
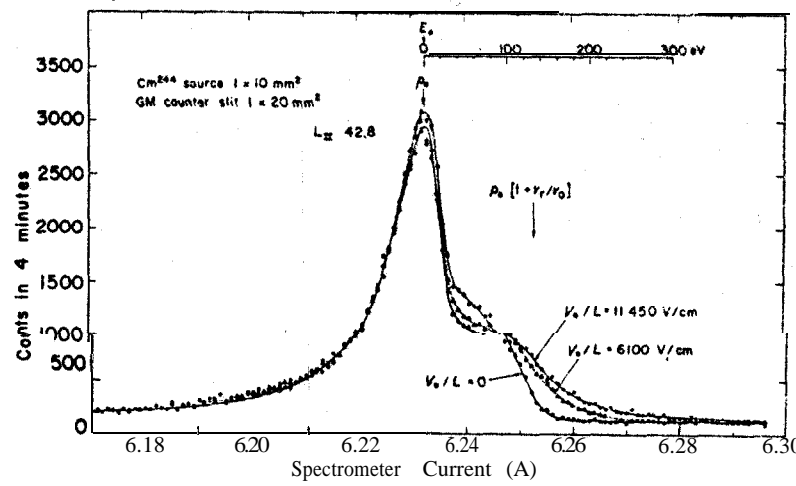


Fig. 86. L_{II} and L_{III} conversion lines of the 42.8 keV transition in Pu^{240} . The lines are recorded without the coincidence condition, both with and without an electric field applied at the source according to Fig. 85. The Doppler shoulder is strongly affected by the field.

One evidently has to distinguish between two shifts: one from the Doppler effect and the other from the electrostatic field. The new method is related to the latter shift.

The first shift is obtained from

$$p = p_0 + \Delta p = p_0 [1 + (v_r/v) \cos \theta]$$

where θ is the emission angle of the electron with respect to the recoil direction. Under idealized conditions with an infinitely thin source and ultra-high resolution, one would expect from an integration of the previous equation to get a rectangular shoulder momentum distribution extending from p_0 to $p_0 + \Delta p$. In practice, however, the ideal distribution of a sharp line at p_0 plus a rectangular high momentum shoulder is smoothed by the finite instrumental resolution and source thickness effects.

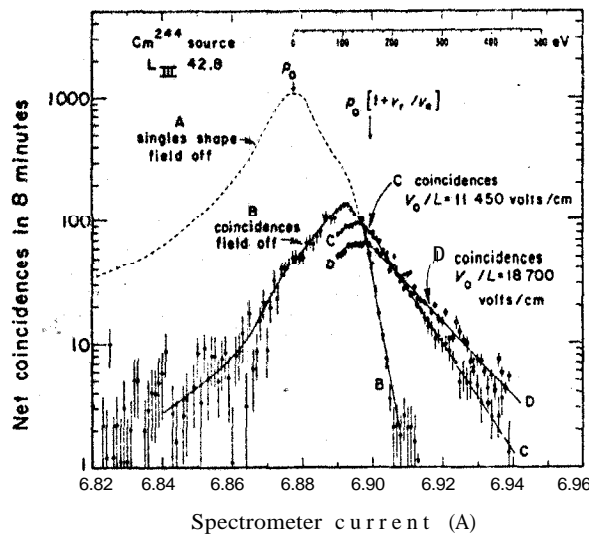


Fig. 87. The same L_{III} line as in Fig. 86 but taken in coincidence with α -particles emitted rearwards. With electric fields 11450 and 18710 V/cm two well-defined 'decay' curves are obtained enabling an accurate determination of the life time ($1.6 \pm 0.2 \times 10^{-10}$ sec).

Figure 86 shows the L_{II} and L_{III} conversion lines of the 42.8 keV transition in Pu^{240} without the coincidence condition, both with and without an electric field. The expected Doppler shoulder at $p_0(1 + v_r/v_e)$ is indicated in the figure. With the electric field on, the electrons are extended towards higher momenta.

Figure 87 shows the corresponding coincidence line plotted logarithmically after the background is subtracted. There are two well-defined exponential 'decay' curves, shown for $V_0/L = 11450$ and 18710 V/cm. Fields of more than 40000 V/cm can be handled without too much difficulty. From the figure one can easily calculate a half-life of $(1.6 \pm 0.2) \times 10^{-10}$ sec without correction for absorption in the sources. This correction can be measured separately in future experiments and it seems likely that further experiments will allow much more accurate results to be obtained. A discussion of the potentialities of the method shows that it should be possible to measure lifetimes as short as $\approx 3 \times 10^{-12}$ sec following cc-decay and as short as 3×10^{-13} sec following reactions involving heavy ions.

The previous experiment is an example of how an accurate line profile study under high resolution can be performed with and without coincidence arrangements. In this particular case the source conditions were varied by means of an electric field. Atomic and other effects may also be studied under high resolution. One example is the natural or inherent line widths of conversion lines, which is treated in more detail in Chapter XVIIIB. Such an effect is demonstrated in Fig. 25.

A similar line broadening effect is observed when the annihilation -line at ≈ 511 keV is studied by means of an external converter such as a thin U foil. This was first done by Lind and Hedgran²¹² when they investigated the Doppler width of

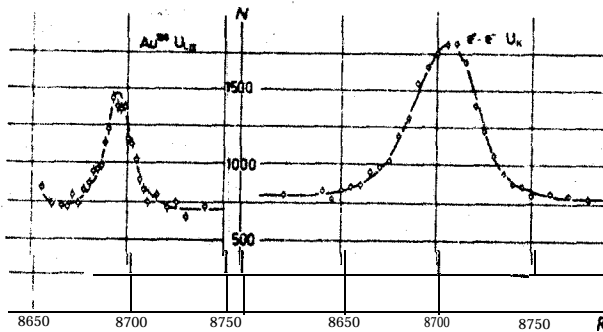


Fig. 88. Doppler width of annihilation radiation according to Lind and Hedgran. Left curve: L_{III} external photoline expelled from a 0.7 mg/cm^2 U converter by the 412 keV -ray of Au^{198} . Right curve: K external photoline from the same converter expelled by the annihilation radiation.

annihilation radiation produced by positrons trapped in copper. In liquids and solids positrons rapidly loose their kinetic energy forming either positronium (or a positronium molecule) or annihilate at rest with an electron. In metals the latter process is the dominant (see Chapter XXVI). Since the electrons in a metal have a momentum distribution, there will be a Doppler broadening of the annihilation curve. A particularly sensitive test of this phenomenon is the angular spread of the quantum pairs around 180° . Lind and Hedgran were able to observe and quantitatively measure this Doppler width in the 50 cm double focusing instrument by comparing the 412 keV -radiation of Au^{198} and the annihilation radiation from copper using the same U converter. The thickness of this was 0.7 mg/cm^2 , which will contribute fairly little to the line width for energies around 0.5 MeV as can be calculated from the probability for inelastic electron scattering. To minimize this energy-dependent effect, comparisons were made between the UL_{III} photo-line for the Au^{198} radiation and the UK photo-line for the annihilation radiation, which happen to have almost the same energies (see Fig. 88). There remains the difference in the inherent widths of the K and L_{III} levels in U to consider. From the form of the Au photo-line one can construct

²¹² D. Lind and A. Hcdgran, Ark. f. Fysik S (1952) 29.

a window curve, and by means of a folding procedure the energy spread due to Doppler effect in copper was determined. The result was 975 eV.

These investigations have been extended to other metals by Bäckström²¹³. He studied in more detail the momentum distribution in Cu, Al and CuO. and was able to show that the spectroscopic momentum analysis could in principle yield the same picture of the annihilation mechanism as the angular fine structure distribution. These phenomena are related through the relation

$$\varphi = p_z/mc \quad (156)$$

where p_z is the momentum component of the electron-pairs perpendicular to the direction of observation and φ the deviation from the 180° emission angle. According to angular correlation measurements²¹⁴ the expectation value for Cu is $\bar{p} = 1.15$ ($mc/137$). Using an iteration process in the folding procedure of the spectrometric results the p_z distribution in Cu could be deduced by Backstrom and \bar{p} determined to be 1.3 ($mc/137$). Figure 89 shows the resultant momentum distribution of annihi-

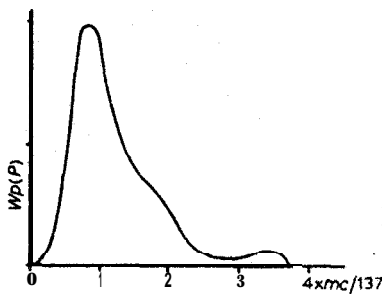


Fig. 89. The momentum distribution of the annihilation pairs in Cu due to Backstrom using spectrometer data of the annihilation line width. The small high energy tail is due to positrons penetrating into the region of bound electrons. The main contribution is from conduction electrons.

lating pairs in Cu. The high energy tail is due to positrons penetrating into the region of bound electrons, whereas most of the annihilations occur with the conduction electrons.

Apart from the Doppler effect the main purpose of the investigation by Lind and Hegran was to obtain a precision measurement of the Au¹⁹⁸ 412 keV line related to the annihilation radiation, which in turn is related to accurately known atomic constants, namely

$$m_0 c^2 = \pi e^2 R/\alpha^3 = 510.976 \pm 0.007 \text{ keV}$$

(least-squares adjusted value by Cohen et al.¹⁴). The result of their measurement was: -energy of Au¹⁹⁸ = 411.809 ± 0.041 keV. The reasonable assumption that the rest mass of the positron coincides with that of the electron has been checked to within $7 : 10^5$ by Page et al.²¹⁵.

²¹³ G. Backstrom, Ark. f. Fysik 11 (19%) 361.

²¹⁴ G. Lang, S. de Benedetti and R. Smoluchowski, Phys. Rev. 99 (1955) 596.

²¹⁵ L. A. Page, P. Stehlé and S. B. Gunst, Phys. Rev. 89 (1953) 1273.

Although this investigation could link together a commonly used reference line with atomic constants and furthermore give conclusive information about positron annihilation in metals, the Doppler broadening of the annihilation line puts a severe limit to the ultimate accuracy of the energy comparison. The momentum spread caused by this effect is around 0.5 %. The instrumental line width was only 0.2 % and the accuracy in the energy comparison ($10 : 10^5$) was mainly determined by the uncertainty in the folding procedure. This is complicated by the fact that the exact momentum distribution of the annihilating electron-positron pairs is not simple gaussian. A possibility to refine the experiment offered itself when it was found by de Zafra and Joyner²¹⁶ that the angular distribution of annihilation quanta from ice showed a narrow momentum component in the usual broad distribution. From the width and intensity of the narrow component its existence was attributed to annihilation of

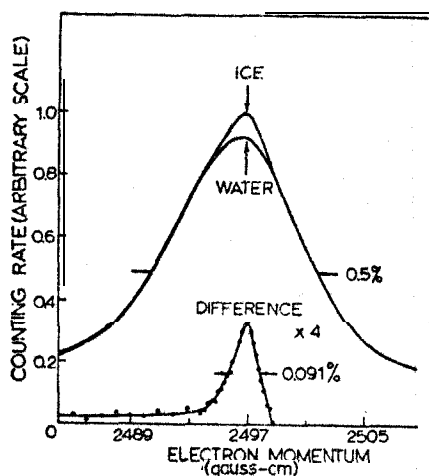


Fig. 90. Annihilation line in water and ice due to Murray et al. Subtraction of the lines yields the small peak (multiplied by a factor of 4). This line is monoenergetic and corresponds to annihilation of completely thermalized singlet positronium.

completely thermalized *singlet positronium*. Consequently, these quanta should be *monoenergetic*, which would remove the complication in the energy comparison measurement. Murray *et al.*²¹⁷ used the ironfree 100 cm radius instrument at Chalk River to make this investigation. The U converter thickness was the same as in the previous experiment and the same photo-lines were also compared (K and L_{III}). Figure 90 shows the annihilation UK photoline for ice and water and the difference between the two curves. This is definitely much narrower than the water curve and corresponds actually to a monoenergetic line (taking into consideration the inherent width of the UK level and of the window curve). By a careful folding procedure Murray *et al.* were able to give a very accurate value of the energy of the gold line. The binding energy for free $1S_0$ positronium is only 6.8 eV and has been corrected for. The new value is: -energy of Au¹⁹⁸ = 411.770 ± 0.010 keV.

²¹⁶ R. L. de Zafra and W. T. Joyner, Phys. Rev. 112 (1958) 19.

²¹⁷ G. Murray, R. L. Graham and J. S. Geiger, Nucl. Phys. 45 (1963) 177.

TABLE 5

Results of the four most accurate determinations of the Hg^{198} 412 keV γ -ray energy deduced using the 1955 and 1961 (preliminary) sets of fundamental constants

Group	1954 Constants	1961 Constants
Lind and Hedgran ²¹²	411.809 ± 0.041	411.838 ± 0.041
Muller <i>et al.</i> ²¹⁸	411.803 ± 0.036	411.806 ± 0.036
P. Bergvall ²¹⁹	411.770 ± 0.033	I 411.773 ± 0.033
Murray <i>et al.</i> ²¹⁷	411.770 ± 0.010	411.799 ± 0.007

The results obtained by four groups, as quoted from Murray *et al.*, are summarized in Table 5. Muller *et al.* and Bergvall both made crystal wavelength measurements. Within the limits of error the four values are consistent with each other. In the table are also listed the values obtained if the latest 1961 (preliminary) set of atomic constants are used²²⁰. According to the latter, the rest mass of the positron is 511.0058 ± 0.0014 keV. The difference in rest mass between the 1955 and 1961 values is disturbingly high (29.8 eV). It is mainly caused by a change of 21 ppm in the electronic charge and 12 ppm in the fine structure constant. In this book we are consequently using the 1955 values and any new generally accepted convention regarding atomic constants can easily be used to recalculate the values presented here.

The source conditions are of decisive importance for precision measurements. In the above investigation this problem did not enter because the energy comparison could be made at almost the same energy. Under favourable conditions β -sources can be made carrier-free [see Chapter VII B]. By far the best technique for ultra-resolution spectroscopy is that of electromagnetic isotope separation (preferably retarded ions). In the case of external converters it is necessary to make compromises in the choice of radiator thickness for obvious intensity reasons. These problems have recently been further studied by Goudsmit²²¹ and Murray *et al.*²²². Figures 91 and 92 from Goudsmit's paper show some typical line shifts [see also Chapter SVII B].

The magnitude of these effects and the pronounced energy dependence encountered here makes it necessary to have available a set of conveniently distributed reference lines that have been measured with high precision under reliable source conditions.

These 'standard' lines may be classified as either *primary*, in the sense that their values are not dependent on any other γ -ray energy, or *secondary*, if they are measured

²¹⁸ D. E. Muller, H. C. Hoyt, D. J. Klein and J. W. M. DuMond, Phys. Rev. 88 (1952) 775.

²¹⁹ P. Bergvall, Ark. f. Fysik 17 (1960) 125.

²²⁰ E. R. Cohen, J. W. M. DuMond, A. McNish, APS Meeting, Washington (1962).

²²¹ P. F. A. Goudsmit, Nucl. Instr. and Methods 23 (1963) 203.

²²² G. Murray, R. L. Graham and J. S. Geiger, to be published.

relative to some well-established γ -line. In order to be able to check the internal consistency of the whole set of standard lines, it is of course valuable to measure several of them in a more or less independent and absolute way.

In magnetic spectroscopy two quantities have in principle to be measured, namely B and ρ . Both quantities are generally difficult to measure accurately. A direct measurement of B requires a uniform field spectrometer, so that the nuclear magnetic resonance method is applicable. In order to eliminate errors due to magnetic inhomogeneities one has to measure the field along the different electron paths, and then to

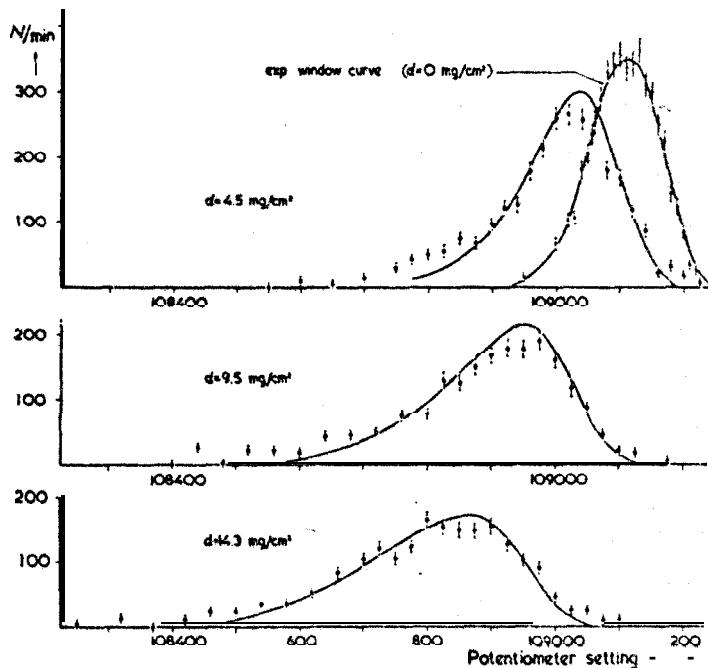


Fig. 91. Experimental and theoretical line shapes of the ThX line with lead absorbers of different thicknesses in front of the source (acc. to Goudsmit).

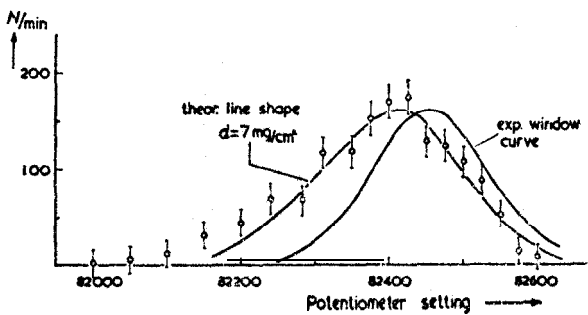


Fig. 92. Line shape of the 2754 keV γ -ray in Na^{24} converted in a 7 mg/cm^2 Pb converter, compared with a theoretical line shape (acc. to Goudsmit).

Th B+C"

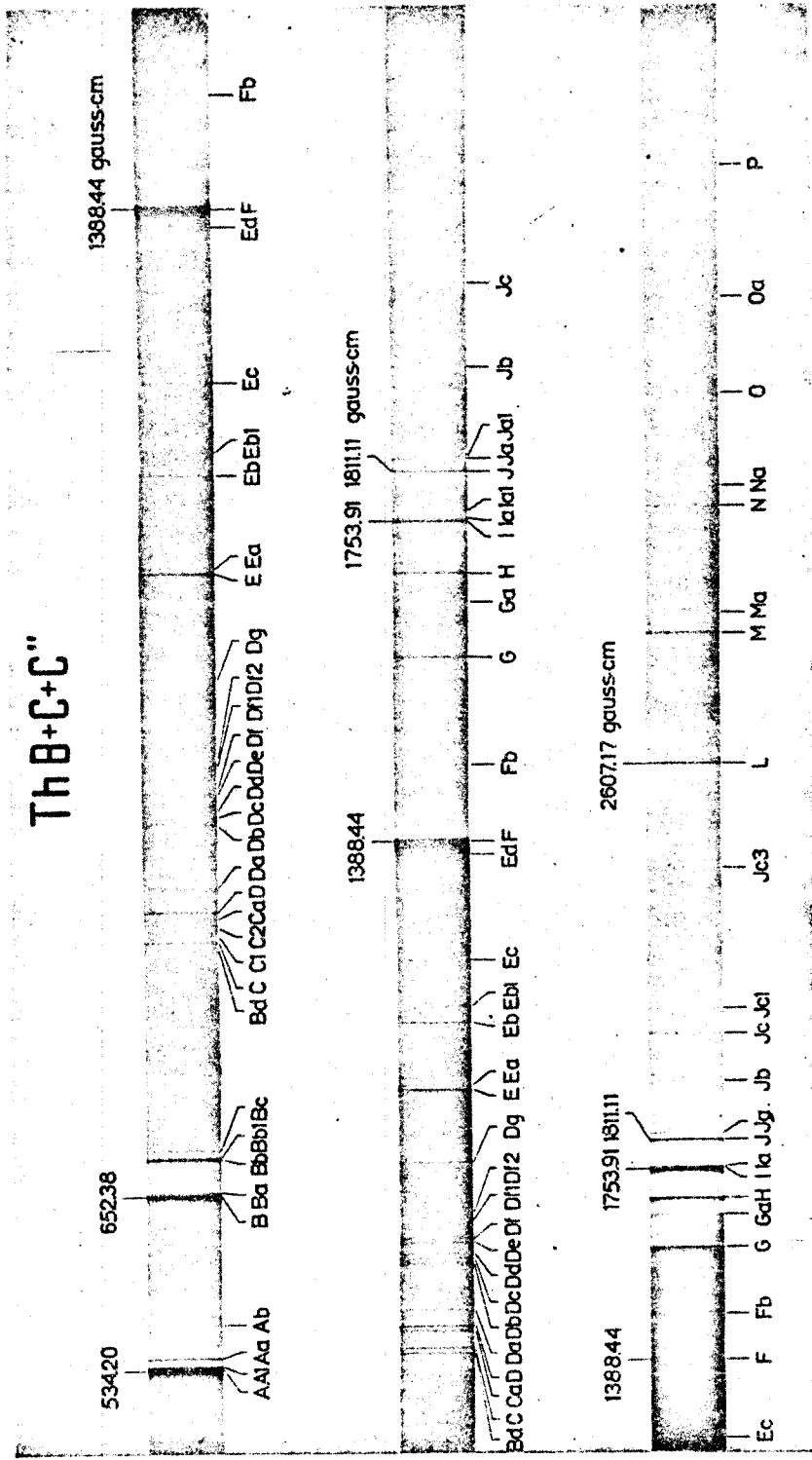


Fig. 94. The β -spectrum of Th(B+C+C'') recorded in a high resolution permanent-magnet spectrograph by H. Slatis.

correct for the departures from homogeneity by means of the previously quoted formula due to Hartree (see page 114). The exact source-image distance = 2ρ is unfortunately experimentally found to be subject to more uncertainties than the theoretical treatment of the image formation would indicate. (This is true in both β - and γ -spectroscopy.)

Lindstrom measured the well-known F, I, L lines²⁵ and X line²²³ in the spectrum of Th(B+C+C'') in a semicircular spectrograph employing the proton resonance, and more recently Jungerman *et al.*¹⁵² measured some of the same lines in their large solenoid spectrometer. Around these lines and the previously discussed Au¹⁹⁸ line a number of secondary standards were measured at high precision, e.g. the Cs¹³⁷ line, the two Co⁶⁰ lines, the two Na²⁴ lines, etc., first by Lindstrom and later by several others.

The situation up to 1956 concerning the precision measurements of primary standards was summarized in a paper by Siegbahn and Edvarson⁶¹. In that paper an attempt was made to reach the precision region of $\approx 1: 10^5$, at least in relative measurements. Absolute measurements of line positions, e.g. the quantity 2ρ , in that range of precision must be regarded as unattainable so far. It is possible, however, to overcome many of these difficulties by using a simple method^{18, 224} which does not require separate B and ρ measurements but only a determination of the ratio between two lines, both originating from the same γ -transition but from different atomic shells. The energy differences between a pair of such β -lines can be expressed by hv , where v is the frequency corresponding to the X-ray transition between the two levels. If $B_2/B_1 = a$ is the ratio of the two fields corresponding to equivalent points on the lines (based on some folding procedure taking into consideration the difference in natural line widths), one can show that:

$$(B\rho)_1^2 = U + \sqrt{U^2 + V}, \quad (157)$$

$$U = \frac{a^2 + 1}{(a^2 - 1)^2} \left(\frac{\hbar}{e} \right)^2 \left(\frac{v}{c} \right)^2, \quad (158)$$

$$V = \frac{4 - s^2}{(a^2 - 1)^2} \left(\frac{\hbar}{e} \right)^2 \left(\frac{e}{m_0} \right)^{-2} v^2, \quad (159)$$

$$s = \frac{hv}{m_0 c^2} \ll 1. \quad (160)$$

This method has the advantage that the less well-defined source-image distance need not be known, but only equivalent points on the two lines. The absolute value of B

²²³ G. Lindstrom, Phys. Rev. 87 (1952) 678.

²²⁴ K. Siegbahn, Ark. Mat. Astr. Fys. 28B (1941) No. 6.

need not be measured at all and further the spectrometer field need not be homogeneous but may have any prescribed form. The experimental conditions are particularly favourable when an ironfree spectrometer is used with the average external field (earth field etc.) along the path completely compensated for. In this case the field ratio $B_2/B_1=a$ is simplified to a ratio between two currents through the spectrometer coils, which with standard procedures can be measured with an accuracy of better than $1:10^5$. If this ratio can be determined to that accuracy, the remaining error is largely due to the errors in the X-ray data, which will influence the $B\rho$ -values for the F and I lines in ThB to the extent of $\lesssim 5:10^5$.

It is of interest to note that the accuracy of the measurements of β -lines permits the evaluation of atomic constants. If one combines the results from two line pairs, e.g. the I : F ratio and the B : A ratio [in the Th(B+C) spectrum], respectively, one can calculate the atomic constant h/m_ec , which agrees well with the result obtained from the wave-length determination of annihilation radiation by DuMond et al.²¹⁸.

By applying an accurately known potential to the source, surrounded by a grounded electrode, it is possible to measure β -lines directly in eV. Meyer and Schmidt²²⁵ have tried this method using an ironfree lens spectrometer. The $B\rho$ -value obtained by them for the ThB F-line was estimated to have an error of $\approx 15:10^5$. This method can presumably be developed still further.

If two electron lines with a known energy difference, obtained from X-ray data, are made to coincide in the spectrometer by means of an electric field around the source, one can get a direct measurement of the atomic constant h/e that is free from the objections raised against the so-called isochromate method using the continuous short wavelength X-ray limit, since such a measurement is related to equivalent points on two lines²²⁶. Such an investigation has recently been performed²²⁷ and will be developed to higher accuracy in the future.

It is possible to apply similar methods that utilize the fact that relative line measurements are sufficient in order to determine unknown transition energies. As an example, Backstrom et al.²²⁸ considered the case of three transitions, two of which form a cascade and the third is the 'cross-over' transition. One then has

$$E_1 + B_{E_1} + E_2 + B_{E_2} = E_3 + B_{E_3} \quad (161)$$

where E_n is the conversion electron energy and B_{E_n} the corresponding electronic binding energy. If $B_{E_2}=B_{E_3}$, i.e. one of the cascade transitions and the 'cross-over' are observed as conversion lines from the same atomic shell, one gets:

$$B_{E_1} = E_3 - E_2 - E_1. \quad (162)$$

One furthermore has $B\rho=cI$, where c is the calibration constant of the spectrometer.

²²⁵ D. I. Meyer and F. H. Schmidt, Phys. Rev. 94 (1954) 927.

²²⁶ K. Siegbahn, Appl. Sci. Res. 4B (1954) 25.

²²⁷ S. Hagstrom, O. Hornfeldt, C. Nordling and K. Siegbahn, Ark. f. Fysik 23 (1962) 145.

²²⁸ G. Backstrom, O. Bergman and J. Burde, Nucl. Phys. 7 (1958) 263.

Using the relation between energy and momentum, this equation (and other similar ones) can be solved explicitly for c , or, more simply, by an iteration procedure using the **Bp-keV** tables (see Appendix 2).

Backstrom *et al.* used the above cross-over relationship to determine the L_1 binding energy in Hg since this was considered to be somewhat uncertain at that time. Using the 50 keV, 158 keV and 208 keV transitions (as represented by the L_1 , K, and K conversion lines, respectively) in the decay of Au^{199} it was found that the Lr binding energy was very insensitive to the value of the calibration constant c . With the conversion line energies obtained B_{L_1} for Hg was calculated to be 14.846 ± 0.010 keV. This should be compared to the value given in Appendix 2 from a compilation of X-ray and photo-electron data, namely 14.836 keV. (This appendix gives an account of another branch of high-resolution low-energy electron spectroscopy.)

Recently Bartlett²²⁹ surveyed the relevant explicit formulas that might provide 'absolute' energy determinations without recourse to the usual comparisons with electron lines of known energy.

Apart from special cases when ‘absolute’ measurements of β -lines are performed without relation to other lines (e.g. by measuring B and ρ separately), high precision and other investigations are usually performed as *relative* line measurements either as self-consistent ones or by comparing to standard lines. These are simplified if all

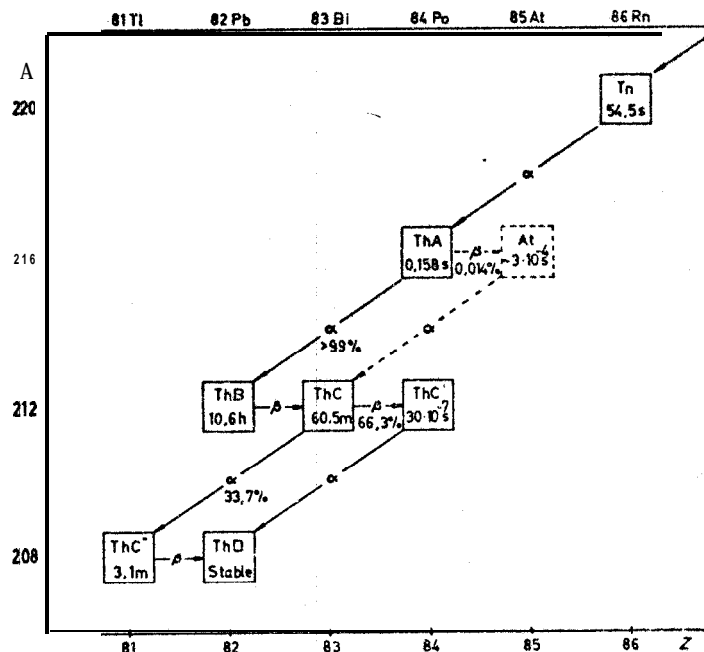


Fig. 93. Genetic relationships between members in the Th-series.

the lines studied belong to the same radioactive source, and if the source is perfectly carrier-free and is situated on the surface of the backing (like ThB deposit). In all other cases one has to face certain problems:

If an *external converter* is used, this is usually placed a few millimeters from the γ -sources and if these are reasonably accurately placed in a reproducible standard position, the radiator foil will act identically when the two sources are interchanged. In this case one has only to consider the energy dependence of the electron straggling effect due to the finite thickness of the converter. If different atomic shells of the converter are used, the differences in natural line width has to be considered when employing the folding procedure. The difference in angular distribution of the emitted photo-electrons of different shells does not seem to cause any shifts (although the intensities may be affected).

The most common case is, however, when two ordinary P-sources are used, one containing the isotope under study and the other containing one or several reference lines in the appropriate energy region. It is easy to see that even the smallest radial displacement of one of the sources or a slight non-uniformity of the active layer of one of the sources will make accurate energy comparisons meaningless. In order to overcome this difficulty a simple method has been used²³⁰, which may be described

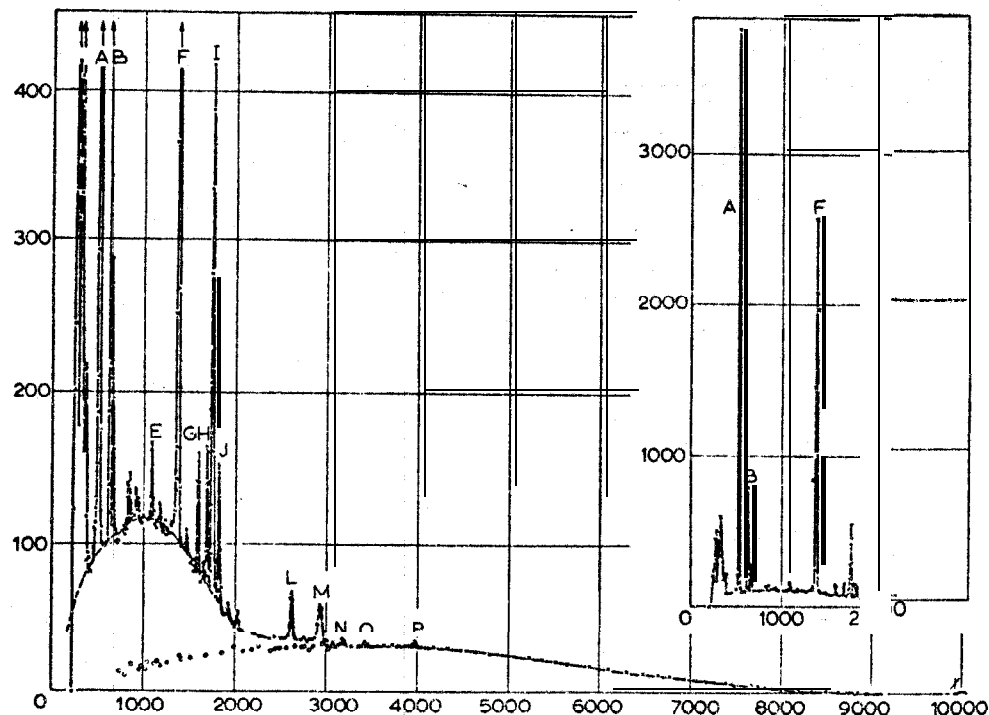


Fig. 95. The γ -spectrum of $\text{Th}(\text{B}+\text{C}+\text{C}'')$ showing the most commonly used β -lines and the continuous β -spectrum as a background (acc. to Flammersfeld²⁵⁷).

²³⁰ M. de Croes and G. Backstrom, Ark. F. Fysik 16 (1960) 567.

as the 'turn-around' procedure. The sources are mounted on metal rings, which fit with high precision into a circular indentation in the spectrometer. The position and internal distribution of the radioactive source (usually a 'line' source near the center of each ring) need not be accurately known. Instead one records the line twice, the source being turned through 180° between the runs. The same procedure is also done for the source containing the reference line. If the mean of the two runs is used as the energy comparison, the above difficulty is eliminated to a high order of approximation.

There are now available a large number of accurately measured reference lines. A particularly useful source is the deposit containing $\text{Th}(\text{B}+\text{C}+\text{C}'')$ in approximate equilibrium. New, fresh, and strong sources can be easily made from highly emanating RdTh and the spectrum exhibits reference lines from 24 keV (A line) up to 2.5 MeV (X line). Figure 93 illustrates the genetic relationships between the different members in the series. Figure 94 is a photographic recording of the whole spectrum up to the P line (at 773 keV) due to Slatis and Fig. 95 is a spectrometric recording showing the main lines and the continuous spectrum forming the background. Table 6a gives the precision-measured strong standard lines in this spectrum and Table 8 a complete list of all existing lines in the spectra of $\text{Th}(\text{B}+\text{C}+\text{C}'')$ together with their $B\rho$ -values, energies, intensities, origin, etc., relative to the standard lines in the spectrum.

Table 6b and Table 7 contain a list of other convenient standard lines that are measured with the highest precision.

The set of tables is a rather complicated compilation since so many different methods of variable accuracy have been used (see list of references). Weighted mean values have been calculated, however, together with estimates of the probable errors. These errors are only to serve as a guide for the user of the tables and if one intends to make a new precision measurement of a certain line a critical study of the probable errors should be made by going directly to the reference quoted in the tables. The latter are based on the 1955 set of fundamental constants.

- 231 H. Craig, Phys. Rev. 85 (1952) 688.
- 232 A. I. Zhernovoi, E. M. Krisiuk, G. D. Latyshev, A. S. Remennyi, A. G. Sergeev and V. I. Fadeev, Zhur. Exp. Teor. Fiz. 32 (1957) 682. (Engl. transl. Soviet Phys. JETP 5, 563.)
- 233 C. de Vries, Nucl. Phys. 18 (1960) 428.
- 234 R. L. Graham, G. Murray and J. S. Geiger, to be published.
- 235 A. Hedgran, Phys. Rev. 82 (1951) 128.
- 236 E. M. Krisiuk, A. D. Vitman, V. D. Vorobev, G. D. Latyshev and A. G. Sergeev, Izv. Akad. Nauk SSSR Ser. Fiz. 20 (1956) 877. (Engl. transl. Bull. Acad. Sci. USSR phys. ser. 20, 797.)
- 237 G. Murray, R. L. Graham and J. S. Geiger, to be published.
- 238 J. L. Wolfson, Can. J. Phys. 39 (1961) 468.
- 239 W. L. Brown, Phys. Rev. 83 (1951) 271.
- 240 H. C. Hoyt, J. W. M. DuMond, Phys. Rev. 91 (1953) 1027.
- 241 C. de Vries and J. H. Dijkstra, Nucl. Phys. 18 (1960) 446.
- 242 M. P. Avotina and O. I. Sumbaev, Izv. Akad. Nauk SSSR, Ser. Fiz. 22 (1958) 879. (Engl. transl. Bull. Acad. Sci. USSR phys. ser. 22, 5739.)
- 243 B. Hamermesh and R. K. Smither, Ann. Phys. (N.Y.) 13 (1961) 307.

TABLE 6a
Standard lines. Th (B + C + C')

<i>Line</i>	<i>Conv. shell</i>	<i>Daughter nuclide</i>	<i>Bp</i> (gauss-cm)	<i>Electron energy</i> (keV)	<i>Binding energy</i> (keV)	<i>Transition energy</i> (keV)	<i>Methods and references*</i>
A	L ₁	81Tl ²⁰⁸	534.21 ± 0.03	24.510 ± 0.003	15.348	39.858 ± 0.004	ce 61, 225, 231
B	M ₁	81Tl ²⁰⁸	652.43 ± 0.04	36.155 ± 0.004	3.704	39.859 ± 0.004	ce 61
E	L ₁	83Bi ²¹²	1109.85 ± 0.06	98.780 ± 0.010	16.389	115.169 ± 0.010	ce 152, 232
F	K	83Bi ²¹²	1388.49 ± 0.05	148.089 ± 0.009	90.531	238.620 ± 0.010	ce 23, 61, 152, 225, 231, 233, 234 cr 218, 219
I	L ₁	83Bi ²¹²	1753.95 ± 0.06	222.224 ± 0.013	16.389	238.613 ± 0.013	ce 25, 61, 152, 225, 231, 233, 234 cr 218, 219
I _a	L ₁₁	83Bi ²¹²	1757.08 ± 0.09	222.898 ± 0.019	15.712	238.610 ± 0.019	ce 61, cr 218, 219
J	M ₁	83Bi ²¹²	1811.09 ± 0.07	234.603 ± 0.015	4.003	238.606 ± 0.015	ce 61, 152, 233, cr 218, 219
L	K	83Pb ²⁰⁸	2606.68 ± 0.13	422.715 ± 0.033	88.006	510.72 ± 0.03	ce 25, 152, 225, 233, 234 cr 218
M	K	83Pb ²⁰⁸	2890.94 ± 0.08	495.120 ± 0.021	88.006	583.126 ± 0.021	ce 226, 237, 238
O	K	84Po ²¹²	3418.17 ± 0.18	634.09 ± 0.05	93.111	727.20 ± 0.05	ce 152, 236
P	K	83Pb ²⁰⁸	3927.17 ± 0.21	772.46 ± 0.06	88.006	860.47 ± 0.06	ce 152, 236
X	K	83Pb ²⁰⁸	9986.83 ± 0.32	2526.29 ± 0.09	88.006	2614.30 ± 0.09	ce 152, 223, 225, 233, 236, 237, 239

* See Table 6b.

TABLE 6b
Other standard lines

<i>Parent nuclide</i>	<i>Conv. shell</i>	<i>Daughter nuclide</i>	<i>Bp</i> (gauss-cm)	<i>Electron energy</i> (keV)	<i>Binding energy</i> (keV)	<i>Transition energy</i> (keV)	<i>Methods and references*</i>
Au ¹⁹⁹	L ₁	80Hg ¹⁹⁹	641.32 ± 0.14	34.974 ± 0.015	14.850	49.824 ± 0.015	ce 228
I ¹³¹	K	84Xe ¹³¹	735.80 ± 0.11	45.580 ± 0.013	34.586	80.166 ± 0.009	cr 240
Au ¹⁹⁹	K	80Hg ¹⁹⁹	958.36 ± 0.08	75.234 ± 0.012	83.107	158.341 ± 0.012	ce 228, 241, 242, cr 243
Au ¹⁹⁹	K	80Hg ¹⁹⁹	1263.28 ± 0.12	125.048 ± 0.021	83.107	208.155 ± 0.021	ce 228, 242, cr 243
Hg ²⁰³	K	81Tl ²⁰³	1618.10 ± 0.24	193.59 ± 0.05	85.531	279.12 ± 0.05	ce 244
I ¹³¹	K	84Xe ¹³¹	1879.72 ± 0.23	249.72 ± 0.05	34.586	284.31 ± 0.05	cr 240
I ¹³¹	K	84Xe ¹³¹	2227.51 ± 0.21	329.88 ± 0.05	34.586	364.47 ± 0.05	cr 240
Au ¹⁹⁸	K	80Hg ¹⁹⁸	2222.42 ± 0.04	328.669 ± 0.010	83.107	411.776 ± 0.010	ce 212, 217, 241, cr 218, 219, 243
Ann. line						\$10.976 ± 0.007	computed 14
Bi ²⁰⁷	K	82Pb ²⁰⁷	2838.6 ± 0.4	481.64 ± 0.10	88.006	569.65 ± 0.10	ce 245, 246, pe 247
Cs ¹³⁷	K	83Ba ¹³⁷	3381.03 ± 0.26	624.14 ± 0.07	37.445	661.59 ± 0.07	ce 51, 248, cr 218
Bi ²⁰⁷	K	82Pb ²⁰⁷	4657.3 ± 1.0	975.81 ± 0.28	88.006	1063.82 ± 0.28	ce 249, pe 247
RaC (R line)	K	84Po ²¹⁴	4839.7 ± 0.8	1027.28 ± 0.23	93.111	1120.39 ± 0.23	ce 250
Co ⁶⁰	K	82Ni ⁶⁰	5323.57 ± 0.14	1164.79 ± 0.04	8.337	1173.13 ± 0.04	ce 250, ce pe 237, cr 242
Co ⁶⁰	K	82Ni ⁶⁰	5878.90 ± 0.17	1324.05 ± 0.05	8.337	1332.39 ± 0.05	ce 250, ce pe 237, cr 242
Na ²⁴	UK	12Mg ²⁴	5631.00 ± 0.14	1252.79 ± 0.04	115.607	1368.40 ± 0.04	pe 237
RaC (T line)	K	84Po ²¹⁴	5874.2 ± 0.6	1322.70 ± 0.17	93.111	1415.81 ± 0.17	ce 250
Na ²⁴	UK	12Mg ²⁴	10364.8 ± 0.4	2638.03 ± 0.12	115.607	2753.64 ± 0.12	pe 237

*ce = conversion electrons; pe = photo-electrons; cr = crystal diffraction.

TABLE 7
Some transitions in the decay of Ir^{192*}

<i>Daughter nuclide</i>	<i>Bp</i> (gauss · cm)	<i>Electron energy</i> (keV)	<i>K-electron binding energy</i> (keV)	<i>Transition energy</i> (keV)	<i>References</i>
⁷⁸ Pt ¹⁹²	834.38 ± 0.11	57.940 ± 0.014	78.399	136.339 ± 0.014	218, 251, 252
⁷⁶ Os ¹⁹²	1276.54 ± 0.11	127.423 ± 0.020	73.876	201.299 ± 0.019	218, 219, 251, 252
⁷⁶ Os ¹⁹²	1301.33 ± 0.11	131.906 ± 0.020	73.876	205.782 ± 0.019	218, 219, 251, 252
⁷⁸ Pt ¹⁹²	1732.04 ± 0.04	217.526 ± 0.009	78.399	295.925 ± 0.009	218, 219, 237, 251, 252, 253, 254
⁷⁸ Pt ¹⁹²	1790.05 ± 0.05	230.021 ± 0.010	78.399	308.420 ± 0.010	218, 219, 237, 251, 252, 253, 254
⁷⁸ Pt ¹⁹²	1826.96 ± 0.05	238.076 ± 0.010	78.399	316.475 ± 0.010	218, 219, 237, 251, 252, 253, 254
⁷⁶ Os ¹⁹²	2103.03 ± 0.17	300.56 ± 0.04	73.876	374.44 ± 0.04	251, 252, 253
⁷⁸ Pt ¹⁹²	2473.73 ± 0.05	389.620 ± 0.013	78.399	468.019 ± 0.013	218, 219, 237, 251, 252, 254
⁷⁸ Pt ¹⁹²	2948.87 ± 0.07	510.118 ± 0.017	78.399	588.517 ± 0.017	218, 219, 237, 251, 252
⁷⁸ Pt ¹⁹²	3009.67 ± 0.07	525.941 ± 0.017	78.399	604.340 ± 0.017	218, 219, 237, 251, 252
⁷⁸ Pt ¹⁹²	3040.50 ± 0.06	533.994 ± 0.017	78.399	612.393 ± 0.017	218, 219, 237, 251, 252

* For the determinations crystal diffraction^{218, 219, 252}, photo-electrons^{237, 251, 252} and conversion electrons^{237, 253} are used. The most accurate measurements are due to ref. 237.

²⁴⁴ K. Edvarson, K. Siegbahn and A. H. Wapstra - quoted in G. J. Nijgh, A. H. Wapstra, L. T. M. Ornstein, N. Salomons-Grobben, J. R. Huizinga and O. Almén, Nucl. Phys. 9 (1958), 528.

²⁴⁵ G. Bäckström, Ark. f. Fysik 10 (1956) 393.

²⁴⁶ P. Marmier and F. Boehm - quoted in D. E. Alburger and A. W. Sunyar, Phys. Rev. 99 (1955) 695.

²⁴⁷ A. I. Yavin and F. H. Schmidt, Phys. Rev. 100 (1955) 171.

²⁴⁸ G. Lindström, K. Siegbahn and A. H. Wapstra, Proc. Phys. Soc. 66B (1953) 54.

²⁴⁹ D. E. Alburger, Phys. Rev. 92 (1953) 1257.

²⁵⁰ G. Lindström, A. Hedgran and D. E. Alburger, Phys. Rev. 89 (1953) 1303.

²⁵¹ M. W. Johns and S. V. Nablo, Phys. Rev. 96 (1954) 1599.

²⁵² L. L. Baggerly, P. Marmier, F. Boehm and J. W. M. DuMond, Phys. Rev. 100 (1955) 1364.

²⁵³ V. A. Romanov, Izv. Akad. Nauk SSSR Ser. Fiz. 22 (1958) 191. (Engl. transl. Bull. Acad. Sci. USSR phys. ser. 22, 188.)

²⁵⁴ N. Ryde and B. Andersson, Proc. Phys. Soc. 68B (1955) 1117.

TABLE 8

 β -ray spectrum of Th (B+C+C')*

Line	B _p (gauss·cm)	E _e (keV)	Rel. int. 256	Rel. int. (counting) 233, 237, 255	Origin	Shell	γ -line	E _y (keV)
A	534.21	24.510	6.0	94.8	C → C'	L _I	A	39.858
A1	536	24.7	0.2		B → C	K	A ₁	115.2
Aa	541.40	25.158	0.6	8.69	C → C'	L _{II}	A	39.860
Ab	563.51	27.202	0.1	0.755	C → C'	L _{III}	A	39.863
B	652.43	36.155	4.0	21.9	C → C'	M _I	A	39.859
Ba	655	36.4	0.1		C → C'	M _{II}	A	39.8
Bb	678.65	39.015	1.0	5.37	C → C'	N _I	A	39.865
Bb1	680	39.2	< 0.1		C → C'	K	Bb1	124.7
Bc	685.09	39.732	0.2	1.192	C → C'	O _I	A	39.869
Bd	829	57.2	0.6		B → C			
C	835	58.0	1.4		B → C			
C1	840	58.7	—					
C2	845.54	59.419	0.2	0.064	C → C'	K	C2	144.950
Ca	851	60.1	0.6		B → C			
D	857	61.0	1.4		B → C			
Da	873	63.1	0.8		B → C			
Dal	881	64.2	< 0.1		—			
Db	920	69.7	0.3		B → C			
Dc	922	70.0	0.2		B → C			
Dd	929	71.0	0.2		B → C			
De	941	72.7	0.4		B → C			
Df	948	73.7	0.3		B → C	K	Df	164.2
Df1	964	76.1	0.1		B → C			
Df2	972	77.2	0.1		C → C'	K	Df2	162.7
Dg	1030.75	86.171	0.6	0.405	B → C	K	Dg	176.702
Dh	1096	96.5	0.1		B → C	L _I	Dh	112.9
E	1109.85	98.780	3.4	2.21	B → C	L _I	E	115.169
Ea	1113.97	99.454	0.2	0.271	B → C	L _{II}	E	115.165
Ea1	1170	108.8	0.1		C → C'	L _I	Bb1	124.1
Eb	1183.84	111.160	0.6	0.493	B → C	M _I	E	115.163
Eb1	1201.66	114.224	0.2	0.154	B → C	N _I	E	115.167
	1206.19	115.007		0.059	B → C	O _I	E	115.175

* The B_p-values in this table are taken from Krisiuk *et al.*^{233, 237, 255} and Surugue²⁵⁶.

All the values have, however, been adjusted to match the standard lines given in Table 6a.

²³⁵ V. D. Vorobev, K. I. Ilin, T. I. Kolchinskaia, G. D. Latyshev, A. G. Sergeev, Iu. N. Trofimov and V. I. Faleev, Izv. Akad. Nauk SSSR Ser. Fiz. **21** (1957) 954. (Engl. transl. Bull. Acad. Sci. USSR phys. ser. **21**, 956.)

²³⁶ J. Surugue, Ann. phys. **8** (1937) 484.

S. P. Choong and J. Surugue, J. Phys. Radium **9** (1938) 437.

²³⁷ A. Flammersfeld, Z. Physik **114** (1939) 227.

TABLE 8 (continued)

Line	B _p (gauss·cm)	E _e (keV)	Rel. int. (photometric) 256	Rel. int. (counting) 233, 237, 255	Origin	Shell	γ-line	E _γ (keV)
Eb2	1226	118.5	0.1		B → C	K	Eb2	209.0
Ec	1254.01	123.396	0.4	0.275	C' → D	K	Ec	211.402
Ecl	1295	130.8	0.1		—			
Ec2	1323	135.9	<0.1		—			
Ed	1374	145.4	0.2	0.20	C' → D	K	Ed	233.4
F	1388.49	148.089	200.0	139.0	B → C	K	F	238.620
						L _I	Df	164.5
F1	1436	157.2	0.1	0.023				
F2	1439	157.8	<0.1	<0.02	B → C			
Fa	1453.02	160.48	0.4	0.079	B → C	L _I	Dg	176.87
Fa1	1458	161.4		0.035				
Fb	1473.8	164.53	0.6	0.725	C' → D	K	Fb	252.54
Fb1	1476	165.0	0.1		C' → D			
G	1597.5	189.35	4.0	4.66	C' → D	K	G	277.36
G1	1599	189.7	0.1		—			
G2	1628	195.6	0.1	0.05	C' → D	L _I	Ec	211.5
Ga	1661.8	202.67	0.4	0.54	C → C'	K	Ga	288.20
H	1694.7	209.59	6.0	5.24	B → C	K	H	300.12
H1	1721	215.2	0.1	<0.02	C' → D	K	H1	303.2
H2	1732	217.5	0.1	0.06	C' → D	L _I	Ed	233.4
I	1753.95	222.224	22.0	20.97	B → C	L _I	F	238.613
Ia	1757.08	222.898	1.4	2.43	B → C	L _{II}	F	238.610
Ia1	1766.86	225.00	0.1	0.14	B → C	L _{III}	F	238.42
Ia2	1787	229.4	0.1	<0.05	—			
J	1811.09	234.603	6.0	4.98	B → C	M _I	F	238.606
J1	1812.6	234.93	<0.1	0.58	B → C	M _{II}	F	238.63
J2	1821	236.8	<0.1	0.16	C' → D	L _I	Fb	252.7
Ja	1825.5	237.76	1.8	1.71	B → C	N _I	F	238.70
Ja1	1829.4	238.61	<0.1	0.35	B → C	O	F	238.78
Ja2	1847.1	242.50	0.1	0.16	C → C'	K	Ja2	328.03
Ja3	1909	256.2	<0.1	<0.01	—			
Ja4	1916	257.9	<0.1	0.01	—			
Jb	1932.5	261.51	0.6	0.87	C' → D	L _I	G	277.37
Jb1	1985	273.4	0.2	0.11	C → C'	L _I	Ga	288.7
Jb2			0.2	0.20	C' → D	M _I	G	277.3
Jb3	1998.3	276.42	<0.1	0.054	C' → D	N _I	G	277.33
Jb4	2009	278.8	<0.1	0.01	—			
Jc	2030.39	283.76	0.6	0.91	B → C	L _I	H	300.15
Jc1	2034.8	284.8	<0.1	0.07	—			
Jc2	2084.3	296.21	0.2	0.20	B → C	M _I	H	300.21
Jc3	2097.8	299.34	<0.1	0.059	B → C	N	H	300.28
Jc3a	2154	312.5	—	0.021	C → C'	L _I	Ja2	327.8
Jc3b	2206	324.8	—	0.014	B → C	K	Jc3b	415.3
Jc4	2304	348.2	<0.1	0.009	C → C'	K	Jc4	433.7